Coordination Chemistry of Sb (III) and Sb (V) Cations

by

Christopher Frazee
BSc., University of New Brunswick, 2014

A Dissertation Submitted in Partial Fulfillment
of the Requirements for the Degree of

DOCTOR OF PHILOSOPHY

in the Department of Chemistry

Supervisory Committee

Coordination Chemistry of Sb (III) and Sb (V) Cations

by

Christopher Frazee
BSc., University of New Brunswick, 2014

Supervisory Committee

Dr. Neil Burford, Supervisor
(Department of Chemistry, University of Victoria)

Dr. Robin G. Hicks, Departmental Member
(Department of Chemistry, University of Victoria)

Dr. David J. Berg, Departmental Member
(Department of Chemistry, University of Victoria)

Dr. Christopher J. Bose, Outside Member
(Department of Mathematics, University of Victoria)

Abstract

Supervisory Committee

Dr. Neil Burford, Supervisor
(Department of Chemistry, University of Victoria)

Dr. Robin G. Hicks, Departmental Member
(Department of Chemistry, University of Victoria)

Dr. David J. Berg, Departmental Member
(Department of Chemistry, University of Victoria)

Dr. Christopher J. Bose, Outside Member
(Department of Mathematics, University of Victoria)

The coordination chemistry of antimony(III) and antimony(V) have been investigated to reveal fundamental structural and electronic features. The limited scope of known cationic antimony(V) complexes was greatly expanded, including the first examples of pnictogen(V) trications. The systematic nature of these investigations led to the observation of redox chemistry, determined to be the result of reductive elimination of chlorobenzene and biphenyl from an antimony center. The reactivity of $[Ph_2Sb(OPyrMe)_4][OTf]_3$ was investigated and it was found that the OPyrMe ligands are sufficiently labile to perform ligand substitution chemistry. However, when exposed to phosphines, ligand-centered reactivity prevails and phosphonium salts of the form $[R_3P(2\text{-}4\text{-methylpyridine})][OTf]$ which may be useful reagents in the field of medicinal chemistry and drug design. While attempts were made to synthesise antimony(V) tetra- and penta-cations have been unsuccessful, the methodologies reported here will serve as a foundation to future endeavors.

Table of Contents

List of Tables

List of Figures

List of Schemes

Acknowledgments

First and foremost, I am greatly indebted to Dr. Neil Burford for my graduate experience over the last four years. The freedom he provided to independently design and manage research projects has greatly enhanced my feeling of control and ownership over the work presented in this thesis. Neil has granted me the opportunity to be involved in all aspects of running a research lab, including installation, maintenance, and decommission. Additionally, he has been extremely helpful and interactive in the process of writing manuscripts. He has also given me the opportunity to act as Senior Lab Instructor for two summers when I previously expressed interest in teaching. I hope to continue benefiting from his mentorship in the future.

I would also like to acknowledge the vital collaboration with the many crystallographers I have worked with: Dr. Brian Patrick from the University of British Columbia, Dr. Andreas Decken from the University of New Brunswick, and Dr. Bob McDonald and Dr. Mike Ferguson from the University of Alberta. This thesis is reliant on them and I greatly appreciate the care that went into handling my sensitive samples.

I would like to thank the friends I have made over the last four years including past and present members of the Burford group, the Hicks group, and the Berg group. Particular mention goes to Nick Richard, Dillon Hofsommer, and Leah Gajecki for the invaluable distraction of morning coffee.

Finally, I would like to thank my partner, Jessica Dobson, for her unwavering support from across a continent and two oceans for far too long. She makes me a better person everyday. I can’t wait until eventually.

List of Abbreviations and Symbols

° : degree

Å : angstrom

acac: acetylacetonate

AN: acceptor number

Ar : generic aromatic substituent

avg. : average

BIMEt$_3$: tris((1-ethyl-benzoimidazol-2-yl) -methyl)amine

bipy : 2,2'-bipyridine

bipy-O$_2$: 2,2'-dipyridyl N,N'-dioxide

Bu : n-butyl

C : Celsius

***Ca.* :** approximately

Cy : cyclohexyl

DCM : dichloromethane

DFT : density functional theory

dmap : 4-dimethylaminopyridine

dt : doublet of triplets (in NMR)

e.g. : for example

Et : ethyl

Et$_2$O : diethyl ether

FLP : frustrated Lewis pair

mL : millilitre

µL : microlitre

m : multiplet (in NMR)

Me : methyl

MeCN : acetonitrile

Mes : mesityl (2,4,6,-trimethylphenyl)

MO: molecular orbital

M.P. : melting point

J$_{XY}$: coupling between nuclei X and Y

NMR : nuclear magnetic resonance

***n*Pr :** propyl

OPyrMe : 4-methylpyridine-N-oxide

OTf : triflate (trifluoromethanesulfonate)

Ph : phenyl

Phen : phenanthroline

Pn : Pnictogen

ppm : parts per million

q : quartet (in NMR)

R : generic organic substituent

r$_{(cov)}$: covalent radius

r$_{(vdW)}$: van der Waals radius

g : grams

HOMO : highest occupied molecular orbital

Hz : hertz

i.e. : that is

% : per cent

***i*Pr** : isopropyl

p : pentet (in NMR)

LUMO : lowest unoccupied molecular Orbital

Δ : difference or change in a quantity

Σ : sum of

s : singlet (in NMR)

***t*Bubipy** : 4,4'-*t*Bu_2-2,2'-bipyridine

t : triplet (in NMR)

***t*Bu** : tert-butyl

td : triplet of doublets (in NMR)

TMS: trimethylsilyl

K : Kelvin ***vs.*** : versus

VSEPR : valence shell electron pair repulsion

Chapter 1: Introduction

1.1. Classical Coordination Chemistry

In 1913, the first Nobel Prize in inorganic chemistry was awarded: Alfred Werner won the Prize for his work on how molecules interact with a metal centre. Werner established many of the concepts and vernacular used to this day, making him widely regarded as the founder of coordination chemistry. Coordination chemistry is the study of a class of molecules dubbed coordination complexes, in which a central 'acceptor' atom or ion, traditionally a metal, is bound to a surrounding array of 'donor' molecules or ions. This acceptor atom or ion is conventionally designated as a Lewis acid, while the donor molecules or ions are Lewis bases or ligands.

Werner's work showed that there were two different environments in a metal complex: a long-distance interaction between the metal and a ligand, which he termed the primary valence, and a shorter interaction called the secondary valence. This secondary valence, known as the coordination number, is defined as the number of substituents directly linked to the metal center. The terminology Werner established has evolved with our understanding of coordination complexes such that the terms primary and secondary valence have been replaced respectively with outer and inner sphere.

Another invaluable contribution Werner provided to the field is the concept of isomerism in coordination complexes. In chemistry, isomerism is the relation of two or more molecules that possess identical chemical formulas but different structural

arrangements in space. Werner was specifically interested in a chemical with the empirical formula $Co(NH_3)_4Cl_3$, as it was known to be either green or purple depending on the environmental factors like pH, solvent, and concentration. He correctly proposed that the complex exists as two different geometric isomers of $[Co(NH_3)_4Cl_2]Cl$: one in which the chlorine atoms are *trans* (Latin: across) to each other, and another in which they are *cis* (Latin: on the same side) (**Figure 1.1.1**).

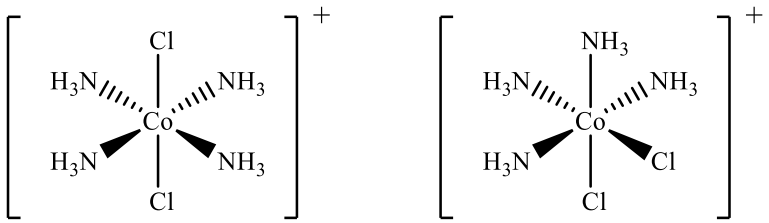

trans-$[Co(NH_3)_4Cl_2]^+$ *cis*-$[Co(NH_3)_4Cl_2]^+$

Figure 1.1.1: Depiction of *trans* and *cis*-$[Co(NH_3)_4Cl_2]^+$ cation.

Building on the foundational principles of coordination chemistry established by Werner, inorganic chemists around the globe began to investigate the plethora of unique structures and bonding environments available to transition metal complexes. This groundwork has allowed chemists to develop a variety of beneficial compounds with applications ranging from use in electronic materials, such as dye-sensitized solar cells, to the production of commercially useful chemicals such as catalysts. Traditionally, it was believed that these properties are distinct to the transition metals; however, more recently, it has been observed that these concepts can be extended to the main group elements.

1.2. Resurgence of Main Group Chemistry

The study of main group chemistry led to the development of a number of fundamental concepts in chemistry. For example, valence shell electron pair repulsion (VSEPR) theory, molecular orbital (MO) theory, and acid-base chemistry all originated from the observations of structural and bonding trends of main group elements. Additionally, even the birth of organometallic chemistry can be attributed to advances in main group chemistry with the discovery of the organo-arsenic compounds $(CH_3)_2As$-$As(CH_3)_2$ and $(CH_3)_2As$-O-$As(CH_3)_2$.[1] After a period of prosperity, interest in main group chemistry began to flounder by the mid 1900s, as it was believed that all major discoveries in the area have been uncovered. This waning interest was exacerbated by the advent of fundamental and applied chemistry of transition metals. Nevertheless, work continued in the area until a series of discoveries led to what the field has colloquially called "The Renaissance of Main Group Chemistry."[2],[3]

This renewed interest can be attributed to the simultaneous discovery of three landmark compounds in 1981 that defied the conventional wisdom of the "double bond rule";[4],[5] which states elements with a principal quantum number greater than two, (*i.e.* Period 3 elements and lower) should not form multiple bonds with themselves or other elements. These compounds were the first examples of multiply bonded species outside the second row elements: $Mes_2Si=SiMes_2$,[6] Mes*P=PMes*,[7] P≡C*t*Bu[8], and $(SiMe_3)_3Si=C(OSiMe_3)(C_{10}H_{15})$[9] (**Figure 1.2.1**). The isolation of these three compounds showed that the scope of main group compounds was much broader than expected.

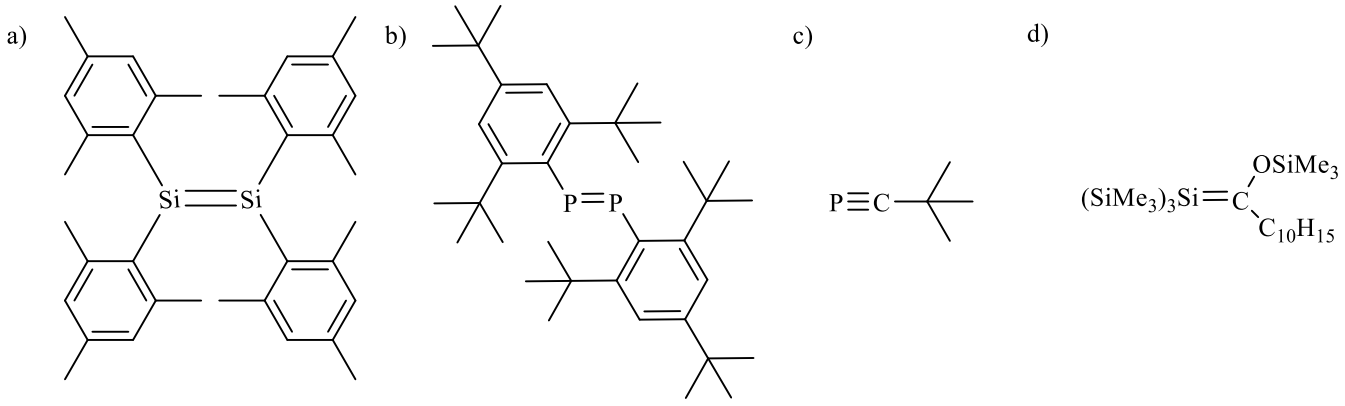

Figure 1.2.1: Reported examples of a) disilene, b) diphosphene, c) phosphaalkyne, and d) silaethene.

This resurgence of main group chemistry led to fundamental advances and the synthesis of many exotic structural and bonding motifs. Examples include: complexes with high molecular charge,[10] coordinately unsaturated main group elements in low oxidation states,[11],[12] multiply bonded element-element fragments,[13] and multi-element clusters and chains.[14] These advances in main group chemistry are fueled by, and help to fuel, advancements in the field of ligand design, where bulky ligands are often required to stabilize reactive species. The nature of these unprecedented bonding situations attracts computational chemists to rationalize them. This leads to new and sometimes controversial theories to describe the nature of these bonding environments, one of which will be discussed in the following section.

Perhaps one of the most significant findings is the observation of the structure and reactivity of main group analogues of transition metal complexes.[15] For example, metal carbonyl complexes are ubiquitous in the realm of coordination chemistry, yet it was not until recently that the first main group center bound by multiple carbonyl ligands, a

borolene dicarbonyl, was reported (**Figure 1.2.2**).[16] Density functional theory (DFT) calculations showed that its highest occupied molecular orbital (HOMO) consisted of a three-centered π bonding interaction between the boron and carbonyl group.[16] This backbonding from the filled p-orbital of the boron atom into the π^* orbital of the carbonyl is directly comparable to metal-to-carbon π backbonding in transition metal chemistry.

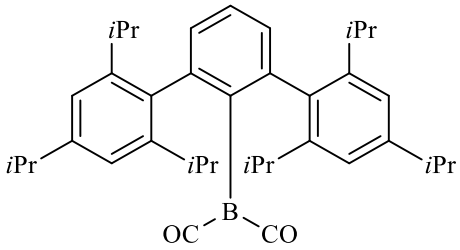

Figure 1.2.2: Reported example of a borolene dicarbonyl.

Furthermore, in the past decade, many examples of reactions previously only possible with transition metals have been performed with main group compounds. The activation of small molecules is one example, the simplest of which is the addition of H_2, a key step in many transition metal-mediated chemical transformations such as hydrogenation. No main group species were known to perform this addition under mild conditions. In 2005, however, it was shown that the Ge alkyne analogue ArGe≡GeAr (Ar = C_6H_3-2,6(C_6H_3-2,6-*i*Pr_2)$_2$) reacted directly with H_2 under ambient conditions, to yield the hydrogenated products Ar(H)Ge=Ge(H)Ar, $Ar(H)_2Ge$-$Ge(H)_2Ar$ and H_3GeAr.[17] This type of reactivity has also been promoted by heavy Ge and Sn carbene analogues[18] as well as monovalent Ga species.[19]

In another major advancement, it was found that H_2 could be bound reversibly to a phosphine-borane system by employing a strategy termed “frustrated Lewis pairs” (FLP). FLP chemistry relies on the high steric demand of the phosphine and borane preventing the

formation of a stable Lewis acid-base adduct hence, ‘frustrated’, while simultaneously promoting the synergistic interaction of H_2 with the lone pair of the phosphine and empty p-orbital of the borane. This polarization of H_2 allows for reversible H-H heterolytic bond cleavage and formation of the phosphonium borate; mild heating allows for the release of H_2 and the regeneration of the phosphine and borane.[20]

1.3. The Coordinate Bond

A distinct difference between coordination chemistry and other purviews of chemistry is in the perceived nature of the bonds involved. Bonds in molecular structures are often interpreted as covalent bonds formed through the sharing of a pair of electrons between two atoms. Conversely, a fundamental concept in coordination chemistry is that of the coordinate or dative bond in which a pair of electrons is donated from one atom to another. While this convention is well accepted in transition metal coordination chemistry, defining a bond as either coordinate or covalent in main group coordination chemistry is a controversial subject.[21],[22],[23] Several criteria attempting to define a coordinate bond have been proposed, but each possesses inherent limitations.

For instance, one proposed criterion is that a coordinate bond is relatively long and weak. This definition is troubling since it assumes a standardization of all bond lengths and strengths between atoms that may serve as reference. It is even more problematic for new bonding motifs for which there are no or insufficient examples to compare to. Additionally, bond strength is greatly affected by the molecular charge of the complex, with cationic species often possessing shorter and stronger bonds than neutral or anionic derivatives. Therefore, it is difficult to classify a bond as long or weak in absolute terms.

A more accurate criterion for defining a coordinate bond is the prevalence of heterolytic versus homolytic bond cleavage. Experimental evidence for a coordinate bond is often demonstrated by performing a ligand exchange reaction in which a neutral Lewis base substituent is replaced by another, stronger Lewis base. This, too, is problematic as it is often unknown whether the substitution is occurring by an associative or dissociative mechanism. An associative pathway involves both the incoming and outgoing ligand in the transition state and, therefore, offers no information on the preference of heterolytic bond cleavage as the transition state is fundamentally different from the compound of interest.

Secondary to all these factors, the use of coordinate bonding model in main group chemistry has come under criticism as seeking to "sell" the chemistry. It is important to remember that any bonding model, be it Lewis or dative, is simply a way for chemists to express the potential reactivity of a compound and, while not fundamentally wrong, can be misleading. In light of this, throughout this thesis a hybrid model will be used that does not distinguish between coordinate or covalent bonds and assigns charge to the overall complex rather than any particular atom (**Figure 1.3.1**).

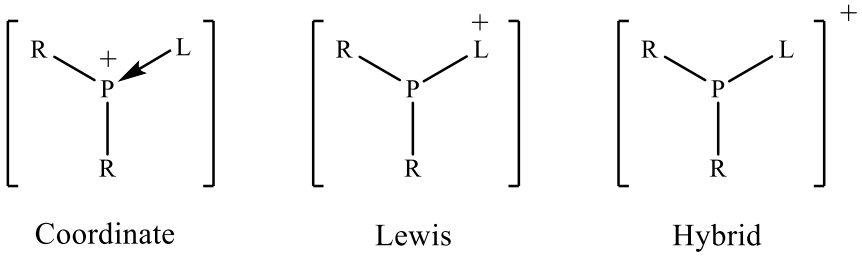

Figure 1.3.1: Example of coordinate, Lewis, and hybrid bonding models for a generic phosphenium cation.

1.4. The Pnictogen Elements

Group 15, consisting of the elements N, P, As, Sb, Bi, and Mc, is also known as the pnictogens (Pn), derived from the ancient Greek term for strangulation or "to choke" due to the suffocation properties of the elements in their gaseous form, particularly nitrogen. Although the term is not recommended by IUPAC, it is the most well established in the main group community and least cumbersome way to collectively identify the Group 15 elements.

The pnictogens have the electron configuration of $ns^2\,np^3$ and possess three common, closed shell, oxidation states (+I, +III, and +V). Selected nuclear properties for the pnictogen elements, with exception of the recently discovered Mc, are highlighted in **Table 1.4.1**. A decrease in Pauling electronegativity and ionization energy is apparent down the group: this signifies an increased metallic character of heavier pnictogen elements, which significantly affects their coordination chemistry. One pertinent implication of this is that lighter elements exhibit more polar covalent bonds, while the heavier elements Pn-X bonds are more ionic. This, for example, allows less energetically demanding abstraction of X^- from a heavy pnictogen than a lighter element.

Another important factor when discussing the coordination chemistry of these elements is the trend of increasing van der Waals radii. Nitrogen, the smallest element, cannot accommodate more than eight valence electrons; on the other extreme, the largest element of the group, bismuth, hypervalency is the norm rather than the exception where coordination number as high as nine are not uncommon. The prototypical hypervalent pnictogen compounds are the pnictogen(V) pentahalides which adopt trigonal bipyramidal geometries and are potent oxidizers and Lewis acids.

Examination of the nuclear spin and natural abundance shows that phosphorus is the most convenient element with respect to analysis by nuclear magnetic resonance NMR spectroscopy techniques. ^{15}N while also possessing a spin integer value of ½, it exists in extremely low natural abundance, making routine NMR analysis impractical without enriched samples. The remaining stable pnictogen nuclides have non-½ nuclear spins, allowing for efficient quadrupolar relaxation of the nucleus such that NMR collection is infeasible if not impossible, in many cases. In terms of organophosphorus compounds, the typical chemical shift range is -100 to 300 ppm. Features affecting ^{31}P chemical shift include electronic properties of the attached substituents, coordination number, and steric encumbrance of the phosphorus center. Generally, like in ^{1}H NMR, phosphorus centers attached to electronegative elements resonate at higher chemical shift compared to less electronegative substituents. Additionally, penta-coordinate phosphorus typically resonates at lower chemical shift than its tri-coordinate counterpart. The large chemical shift window and the high sensitivity to environmental change make phosphorus ideal for investigation *via* NMR techniques.

Table 1.4.1: Selected properties of the pnictogen elements (temperature in °C, energy in kJ/mol, distance in Å).

	N	P	As	Sb	Bi
Atomic Number	7	15	33	51	83
Natural Isotope Abundance	99.6% ^{14}N 0.4% ^{15}N	100% ^{31}P	100% ^{75}As	57.4% ^{121}Sb 42.6% ^{123}Sb	100% ^{209}Bi
Nuclear Spin (I)	+1 ^{14}N -1/2 ^{15}N	+1/2 ^{31}P	-3/2 ^{75}As	+5/2 ^{121}Sb +7/2 ^{123}Sb	-9/2 ^{209}Bi
Melting Point	-210.0	44.15	-	630.6	271.4
Boiling Point	-195.8	280.5	615 (sublimes)	1587	1564
1st Ionization Energy	1402	1012	947	834	703
2nd Ionization Energy	2856	1907	1798	1595	1610
3rd Ionization Energy	4578	2914	2735	2440	2466
4th Ionization Energy	7475	4964	4837	4260	4370
5th Ionization Energy	9445	6274	6043	5400	5400
Electron Affinity	7	72	78	101	91
Pauling Electronegativity	3.04	2.19	2.18	2.05	2.02
Atomic Radius	0.65	1.00	1.25	1.46	1.55
Covalent Radius	0.71	1.11	1.21	1.39	1.48
van der Waals Radius	1.55	1.80	2.00	2.20	2.40

The geometry of pnictogen complexes are discussed in several chapters of this dissertation: structural parameters for prototypical compounds are tabulated in Table 1.4.2 as reference. The trend in bond lengths reflects the larger covalent radii of the heavier group 15 elements. The X-Pn-X angles show a sharp decrease from nitrogen (ca. 107°) to the heavier elements (ca. 90-100°). In valence bond theory terms, this trend is explained by high s-orbital contribution to bonding in the case of amines, and by purely p-orbital bonding for the heavier elements. In other words, the s- and p-orbitals of amines are easily hybridized, forming four sp^3 orbitals, while this hybridization is resisted for the heavier elements. This resistance to hybridization is known as the inert pair effect: this effect implies that the lone pair of heavier pnictogens exhibit greater s-orbital character; moreover, these s-orbitals are more diffuse and polarizable than the hybrid sp^3 orbital of nitrogen which are more directional and less polarizable. Experimentally, these electronic effects on the lone pair are observed in the hard donor characteristics of amines and the soft donor abilities of the heavier analogues.

Table 1.4.2: Structural parameters of prototypical Pn(III) compounds (distances in Å, angles in °).[24]

	NH_3	PH_3	AsH_3	SbH_3	BiH_3
Pn-H	1.012	1.421	1.511	1.700	1.776
H-Pn-H	106.7	93.3	92.1	91.6	90.5
	NCl_3	PCl_3	$AsCl_3$	$SbCl_3$	$BiCl_3$
Pn-Cl	1.759	2.039	2.165	2.334	2.424
Cl-Pn-Cl	107.1	100.3	98.6	97.1	97.5

1.5. Coordination Chemistry of Pnictogen(V) Acceptors

A variety of pnictogen-centered complexes can be envisaged as potential Lewis acceptors, and can be organized by the oxidation state of the pnictogen center and overall charge of the complex (**Figure 1.5.1**). Moving left to right in **Figure 1.5.1**, an anionic substituent, or X-type ligand, is being removed, so a cationic charge is installed on the pnictogen center. Prior to the work of this dissertation, no examples of $[R_2Pn(V)]^{3+}$, $[RPn(V)]^{4+}$, $[Pn(V)]^{5+}$ have been reported in the literature, though the other entries, most notably the pnictogen(III) class and the rarer pnictogen(I).[25],[26],[27] have been reported. However, by no means has a comprehensive list been established, and, in many cases, only isolated examples of a species are reported such that no analysis of trends or understanding of the behaviour of this class of compounds can be undertaken.

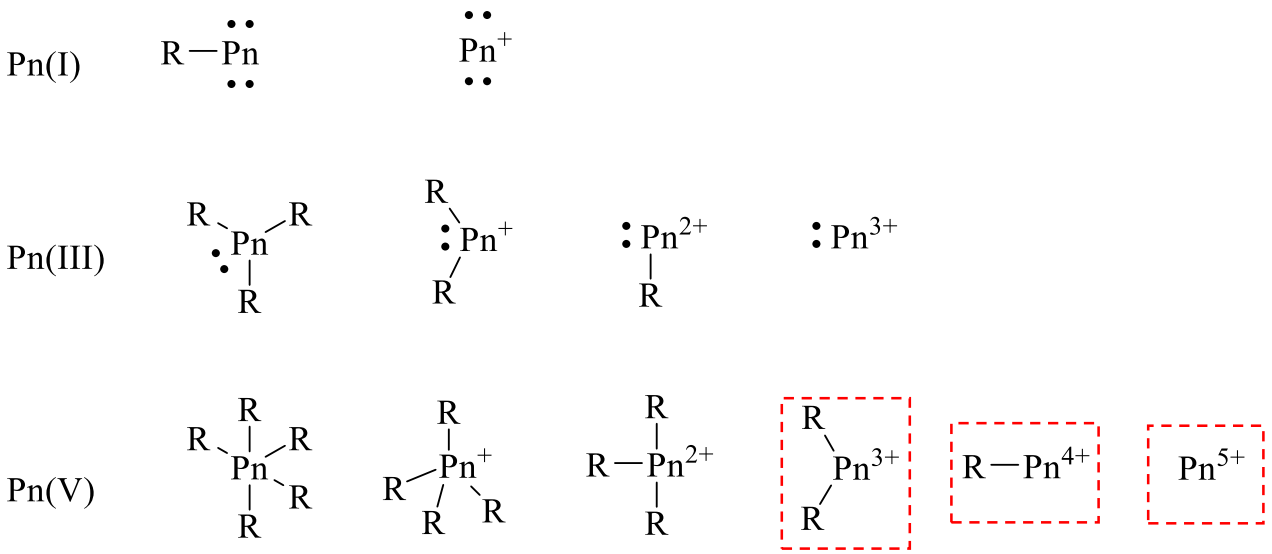

Figure 1.5.1: Potential neutral and cationic pnictogen moieties. Motifs in dashed borders are unreported prior to this dissertation. R = anionic substituent (alkyl, aryl, halogen, *etc*.).

The current scope of pnictogen(V) cation coordination complexes has been recently reviewed.[28] This review discusses the synthesis and structural characteristics of pnictogen(V) coordination complexes. Importantly, it highlights the superficial coverage of species which have been comprehensively characterised and are summarized in **Table 1.5.1**. It can clearly be seen that many structural motifs have yet to be observed, particularly species with a cationic charge greater than 2. These compounds would likely possess interesting chemical reactivity due to their inherently high Lewis acidity.

Table 1.5.1: Generic formulae for potential pnictogen(V) centered coordination complexes prior to the work of this dissertation (X = monovalent susbtituent such as halide or alkyl, Y = divalent substituent such as O, S, or NR, L = neutral ligand, n = number of ligands). * indicates that one or more derivatives of that formula has been isolated and comprehensively characterised. Adapted from reference [27].

Generic formula	n = 1	n = 2	n > 2
$[X_5PnL_n]$	*		
$[X_4PnL_n]^+$	*	*	
$[X_2PnYL_n]^+$	*		
$[PnY_2L_n]^+$	*		
$[X_3PnL_n]^{2+}$	*	*	
$[XPnYL_n]^{2+}$		*	
$[X_2PnL_n]^{3+}$			
$[PnYL_n]^{3+}$			
$[PXnL_n]^{4+}$			
$[PnL_n]^{5+}$			

1.6. Synthetic Methodology

Main group cations are often synthesised from fundamentally simple synthetic routes to target a wide variety of novel compounds. One common methodology, and the one employed through most of this dissertation, is the displacement of a halide substituent by a neutral donor. This approach is versatile and allows for the systematic formation of a broad range of complexes. Recently likened to the Menschutkin S_N2 reaction of amines with alkyl halides to yield ammonium salts,[29] the prototypical reaction of a chlorophosphine with a trialkylphosphine yields the complex $[R_3P\text{-}PR_2][Cl]$ (**Figure 1.6.1**). In cases where the Lewis acidity required to engage the donor is insufficient, abstraction of the halide may be accomplished through a metathesis reaction with a salt of a weakly coordinating anion (OTf^-, PF_6^-, BF_4^-, *etc*), TMSOTf, or Group 13 halide EX_3 (E = Al or Ga, X = Cl, Br, or I). The use of a halide abstractor increases the Lewis acidity of the acceptor and allows interaction with the donor. The use of a weakly coordinating counter-anion ensures that the Lewis acidity of the acceptor center is not quenched, and this counter-anion is easily displaced by a stronger donor.

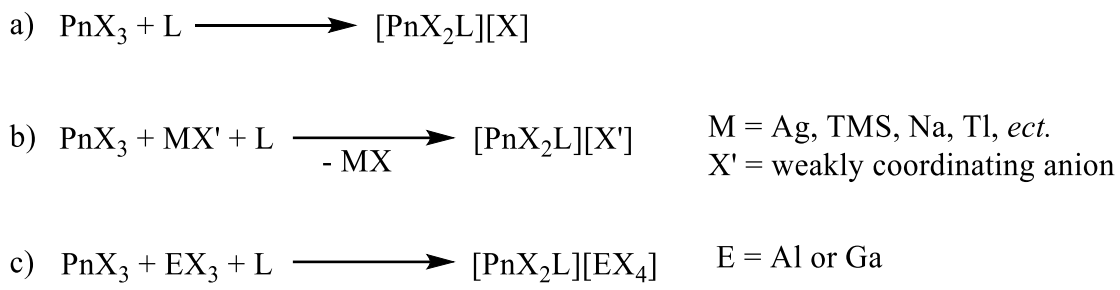

Figure 1.6.1: Generic reaction to form $[PnX_2L]^+$ a) addition of a ligand, b) halide abstraction via salt metathesis, and c) halide abstraction via Group 13 halide. Pn = pnictogen, X = halogen.

1.7. Scope of Thesis

This dissertation investigates the coordination chemistry of neutral and cationic pnictogen acceptors. As outlined above, the development of pnictogen(V) acceptors chemistry is superficial at best. Much of this dissertation focuses on the synthesis and structural characterization of this class of compounds. In the case of highly charged pnictogen(V) cations, subsequent reactivity studies were conducted to investigate the effect of the increased Lewis acidity of the cation.

Chapter 2 begins this investigation with the systematic synthesis and characterization of a series of neutral, mono-, di-, and the first examples of tri-cationic antimony(V) complexes. The discovery and cause of unexpected redox chemistry is also discussed. Chapter 3 details the structural investigation of a series of mono- and bi-dentate pyridine-based donors on antimony(III) acceptors. Focus is given to both the nature of the ligand and the effect of the substituents on the structure and geometry of the cations. Chapter 4 reports several reactivity studies of the novel tricationic antimony(V) synthesised in Chapter 2. Redox reactions with phosphines are of primary interest in this chapter, as is

the applicability of the phosphoniums formed. These reactions are analysed spectroscopically and structurally, where possible. Finally, Chapter 5 reports the attempts and pitfalls in the synthesis of tetra- and penta-cationic pnictogen(V) complexes: the synthetic challenges of forming and isolating these moieties will be discussed as well as potential routes to circumvent these difficulties.

Chapter 2: Coordination Complexes of Antimony(V)

Coordination complexes involving p-block element Lewis acceptor centers offer opportunities for the discovery of new reactivities that are distinct from those of transition metal complexes. In particular, highly electrophilic complexes are of fundamental interest for their bonding and structure, but also for the potential of unique reactivity facilitated by high molecular charge. As previously discussed, the coordination chemistry of pnictogen(III) acceptors has been systematically approached in the past, but investigations of pnictogen(V) acceptors are relatively sparse with many structural motifs yet to be explored. A fundamental understanding of the possible geometric and bonding parameters available to this class of compounds is required before any assessment of their reactivity can be performed.

Antimony(V) is a well known class of Lewis acid compounds, with SbF_5 used to form the strongest superacid, $[H_2F][SbF_6]$. Due to its low electronegativity, antimony can easily engage a Lewis base to form an adduct. The Lewis acidity of antimony(V) can be enhanced by incorporating a cationic charge on the molecule through the substitution of an anionic substituent with a neutral ligand.

The Lewis acidity of antimony(V) cations has been exploited in recent years by the Gabbaï research group to form a variety of anion sensors. Complexation of fluoride anions in protic media is a valuable area of research with applications in drinking water analysis. It was found that 9-anthryltriphenylstibonium, $[(9\text{-ant})Ph_3Sb]^+$, could selectively bind aqueous fluoride at the part-per-million level. Upon binding fluoride, the geometry at antimony changes from tetrahedral to trigonal bipyramidal, inducing a florescence

response allowing for ease of detection.[30] Since this discovery, further tuning of the system allowed for sub-ppm detection of fluoride,[31] use of a sufficiently Lewis acidic neutral antimony species,[32] and improved fluorescence response[33]. Similar approaches have been taken to design detectors for other anions like cyanide and azide.[34]

The following cationic complexes featuring antimony(V) as the Lewis acceptor center have been reported and systematically explored: $[Ph_4SbL]^+$, $[Ph_4SbL(OTf)]$ $[Ph_3SbL_2]^{2+}$, where (L = 4-dimethylaminopyridine (dmap), bipyridine (bipy), phenanthroline (phen) R_3PO (R = Me, Cy, Ph) and 4-methylpyridine-N-oxide (OPyrMe)).[35],[36],[37] Additionally, attempts to form phosphine complexes of $[Ph_3Sb]^{2+}$ have failed and resulted in the oxidative coupling of phosphine to their corresponding diphosphonium salt and reduction of antimony.[35] Based on this finding, redox-resistant donors will need to be used when exploring the coordination chemistry of antimony(V) cations.

Two different approaches can be invoked to access antimony(V) cations. Perhaps the most intuitive of these approaches is to determine a suitable antimony(V) precursor to utilize to investigate its coordination chemistry. Alternatively, previously synthesised antimony(III) complexes can be oxidized to form their corresponding antimony(V) complex. Beginning with an antimony(V) precursor allows for more flexibility and therefore was the route initially chosen for this work.

To that effect, Ph_2SbCl_3, $PhSbCl_4$, and $SbCl_5$ were chosen as suitable precursors for the synthesis of $[Ph_2Sb]^{3+}$, $[PhSb]^{4+}$, and $[Sb]^{5+}$ moieties. $SbCl_5$ is commercially available, and, according to literature,[38] Ph_2SbCl_3 and $PhSbCl_4$ are easily synthesised from

inexpensive starting materials. Moreover, complexes derived from these species would be directly comparable with those previously reported for $[Ph_4Sb]^+$ and $[Ph_3Sb]^{2+}$.[39]

Ph_2SbCl_3 was synthesised by a modified literature preparation as per **Scheme 2.1**.[38] A 2:1 stoichiometric ratio of Ph_3Sb and $SbCl_3$ were combined without solvent to form a viscous melt which was left to stir at ambient temperature for seven days. From this, Ph_2SbCl can be isolated, or the crude mixture can be used to proceed with the reaction *via* dilution in DCM followed by dropwise addition of a 1 M solution of SO_2Cl_2 in DCM; the solution is then left to stir for 24 hours. Crystals of Ph_2SbCl_3 were obtained after recrystallization in DCM at -30 °C. Isolation of Ph_2SbCl offers no benefit in terms of the final isolated yield of Ph_2SbCl_3. Similar methodologies were used to synthesise $PhSbCl_4$. Attempts to isolate $PhSbCl_4$, however, were problematic and eventually deemed unsuccessful. Efforts made to circumvent this issue will be discussed in Chapter 5.

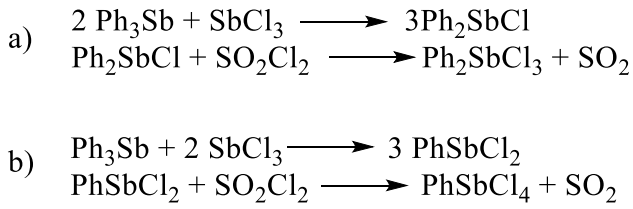

Scheme 2.1: Synthetic pathway to a) Ph_2SbCl_3 and b) $PhSbCl_4$.

2.1. Complexes Featuring Oxygen Donors

As previously mentioned, choice of ligand is important for the successful isolation of antimony(V) coordination complexes. Hard donors (O, N) were shown to be effective at forming stable complexes, while soft donors (As, Sb, Se, S) elicited no reaction. Oxygen

donors were first investigated as they are unable to be further oxidized by antimony, and are less basic and therefore less prone to unwanted protonation compared to nitrogen-based donors.

A systematic approach was taken and reactions of Ph_2SbCl_3 with AgOTf in the presence of OPyrMe or $OPEt_3$ were carried out per **Scheme 2.1.1**. All reactions are facile and rapid in either DCM or CH_3CN at room temperature. Upon removal of AgCl, the samples were crystallized in order to afford complexes of the general formula $[Ph_2Sb(L)_mCl_{3-n}][OTf]_n$. Additionally, the lower charged species can be converted to more highly charged species with appropriate stoichiometric addition of AgOTf and ligand. Attempts to form the five coordinate species have resulted only in the isolation of the six coordinate species. This observed preference for an octahedral configuration contrasts the speculated trigonal bipyramidal structures of $R_2SbL_3^{3+}$, that were previously proposed on the basis of elemental analysis and ^1H NMR.[40] Indeed, NMR data of both the reaction mixture and the isolated solid are inconsistent with a trigonal bipyramidal assignment. $[Ph_2SbL_4][OTf]_3$ represent the first structurally characterized examples of a pnictogen(V) tricationic complex.

$$Ph_2SbCl_3 + mL + nAgOTf \longrightarrow [Ph_2Sb(L)_mCl_{3-n}][OTf]_n + nAgCl \qquad L = OPyrMe \text{ or } OPEt_3$$

Scheme 2.1.1: Generic equation for the formation of monodentate oxygen donor Sb(V) complexes (m = 1, n = 0), (m = 2, n = 1), (m = 3, n = 2), or (m = 4, n = 3).

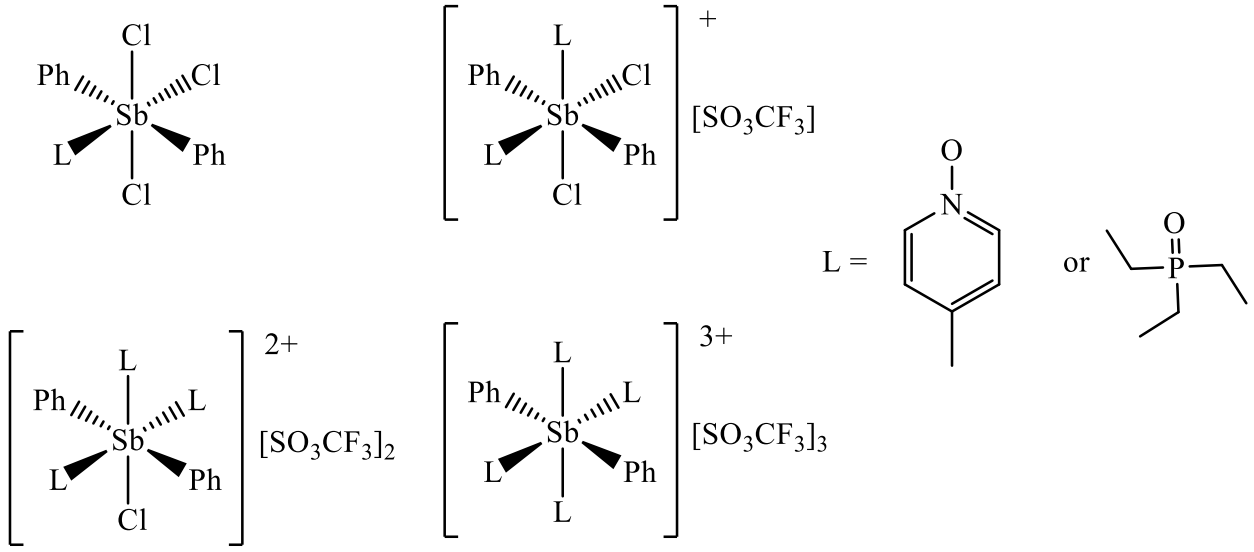

Figure 2.1.1: General structure of synthesised Sb(V) complexes featuring oxygen-donors.

The solid-state structures of compounds $Ph_2SbCl_3(OPyrMe)$, $[Ph_2SbCl_2(OPyrMe)][OTf]$ and $[Ph_2Sb(OPyrMe)_4][OTf]_3$ are shown in **Figure 2.1.2** with selected structural parameters listed in **Table 2.1.1**. It has not been possible to determine the solid-state structure of $[Ph_2SbCl(OPyrMe)_3][OTf]_2$. In each of the compounds the antimony center adopts a distorted octahedral geometry with the two phenyl substituents in a *trans* configuration (C-Sb-C = 168.62 - 177.45°), imposing a planar arrangement for the OPyrMe ligands and chloride substituents. Attempts to form the five-coordinate species have resulted only in the isolation of the six-coordinate species. This observed preference for an octahedral configuration contrasts the speculated trigonal bipyramidal structures of $R_2SbL_3^{3+}$, that were previously proposed on the basis of elemental analysis and ^1H NMR spectroscopy.[40]

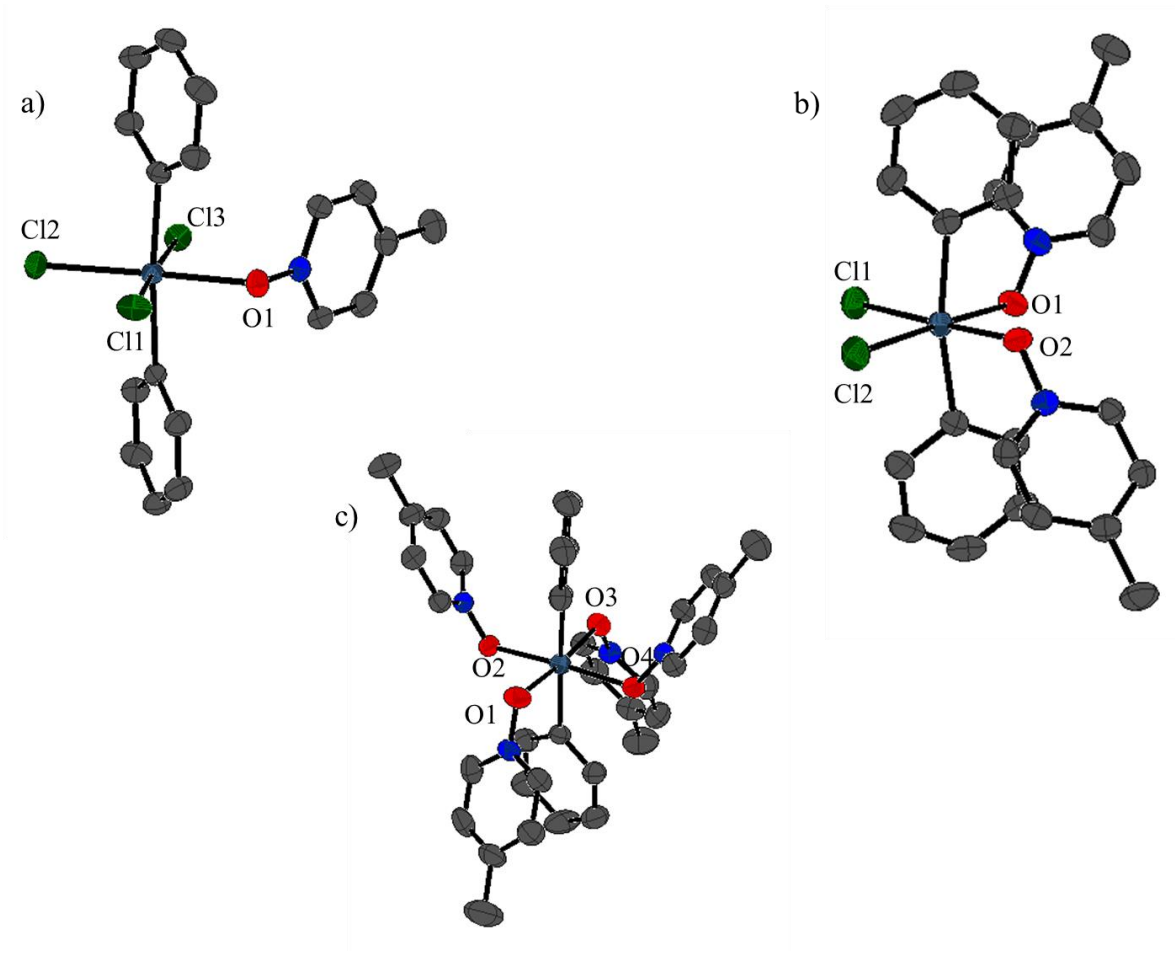

Figure 2.1.2: Solid state structures of a) $Ph_2SbCl_3(OPyrMe)$, b) The cation in $[Ph_2SbCl_2(OPyrMe)_2][OTf]$, and c) The cation in $[Ph_2Sb(OPyrMe)_4][OTf]_3$. All hydrogen atoms and counter-anions omitted for clarity. Thermal ellipsoids are shown at 50% probability.

The Sb-O(PyrMe) bonds in all three compounds are slightly longer than the sum of the covalent radii of Sb and O ($\Sigma_{CRSb\text{---}O}$ = 2.03Å), and the Sb---O(Tf) contacts are outside the sum of the van der Waals radii ($\Sigma_{vdWSb\text{---}O}$ = 3.58Å), indicating that all compounds are ionic in nature. The Sb-O(PyrMe) bond in each compound are all shorter than that in $[Ph_4Sb(OPyrMe)][OTf]$, while the Sb-O bond in $Ph_2SbCl_3OPyrMe$ and in

$[Ph_2SbCl_2(OPyrMe)_2][OTf]$ are longer than that in $[Ph_3Sb(OPyrMe)_2][OTf]_2$,[36] and the shortest Sb-O bond is observed in $[Ph_2Sb(OPyrMe)_4][OTf]_3$: this trend is consistent with the magnitude of the cationic charge. The Sb-Cl bonds in the neutral $Ph_2SbCl_3OPyrMe$ are similar to those in Ph_3SbCl_2 (average Sb-Cl = 2.463(2) Å),[41] and the Sb-Cl bond *trans* to OPyrMe is the shortest, indicating that the *trans* influence of Cl^- is greater than that of OPyrMe. This observation is consistent with the bond distances observed for the monohydrate, $Ph_2SbCl_3(OH_2)$: [Sb-Cl(t*rans* to OH_2) = 2.331(4)Å, Sb-Cl(t*rans* to Cl) = 2.490(4)Å].[42] The *cis* configuration and bond lengths of the Sb-Cl bonds in $[Ph_2SbCl_2(OPyrMe)_2][OTf]$ are similar to those in $Ph_2SbCl_2(acac)$: [Sb-Cl = 2.418(3)Å].[43] The degree of twisting of the phenyl rings increases across the series, likely due to π interactions between the phenyl and pyridine rings.

Table 2.1.1: Selected bond lengths (Å) and angles (°) in the solid-state structures of $Ph_2SbCl_2(OPyrMe)$, $[Ph_2SbCl_2(OPyrMe)_2][OTf]$, and $[Ph_2Sb(OPyrMe)_4][OTf]_3$, with comparison to $[Ph_4Sb(OPyrMe)][OTf]$ and $[Ph_3Sb(OPyrMe)_2][OTf]_2$.[39]

	$Ph_2SbCl_3(OPyrMe)$	$[Ph_2SbCl_2(OPyrMe)_2][OTf]$	$[Ph_2Sb(OPyrMe)_4][OTf]_3$	$[Ph_4Sb(OPyrMe)][OTf]$	$[Ph_3Sb(OPyrMe)_2][OTf]_2$
Sb-O1	2.1779(12)	2.164(2)	2.117(4)	2.4486(12)	2.1381(15)
Sb-O2	-	2.160(2)	2.098(3)	-	2.1392(15)
Sb-O3	-	-	2.135(4)	-	-
Sb-O4	-	-	2.123(4)	-	-
Average Sb-O	2.1779(12)	2.162(2)	2.1183(4)	2.4486(12)	2.1387(15)
Sb-Cl1	2.4561(5)	2.4086(10)	-	-	-
Sb-Cl2	2.4380(5)	2.4187(10)	-	-	-
Sb-Cl3	2.4449(5)	-	-	-	-
Ph-Ph Twist angle	12.4	32.7	51.8	-	-

The solid-state structures of compounds $[Ph_2SbCl_2(OPEt_3)][OTf]$, $[Ph_2Sb(OPEt_3)_3][OTf]_2$, and $[Ph_2Sb(OPEt_3)_4][OTf]_3$ are shown in **Figure 2.1.3**, with selected structural parameters listed in **Table 2.1.2**. Attempts to obtain a crystal adequate for X-ray diffraction of the neutral $Ph_2SbCl_3(OPEt)$ were hampered by its low solubility in most solvents. Weakly diffracting crystals were obtained, suitable only for determination of atomic connectivity that revealed an equivalent structure to that of $Ph_2SbCl_3(OPyrMe)$.

^{31}P NMR spectroscopy can help estimate Lewis acidity for these compounds *via* the Gutmann-Beckett method.[44] The Gutmann-Becket method is a NMR technique in which the difference in ^{31}P NMR chemical shift of free $OPEt_3$ (41.0 ppm) and that of its adduct with a Lewis acid is assessed: the greater the difference, the more potent the Lewis acid. From the difference in chemical shift, an "acceptor number" (AN) can be calculated to act as a simple numerical representation of Lewis acidity, and allow facile comparisons between Lewis acids. The scale for acceptor numbers have been arbitrarily assigned such that the AN of free $OPEt_3$ in hexane is 0, and that of Et_3PO-$SbCl_5$ is 100.[45]. In the compounds studied herein, there is a clear trend in ^{31}P chemical shift shifting to higher frequencies as the cationic charge increases. The ^{31}P chemical shifts for $Ph_2SbCl_3(OPEt_3)$, $[Ph_2SbCl_2(OPEt_3)][OTf]$, $[Ph_2SbCl(OPEt_3)_3][OTf]_2$, and $[Ph_2Sb(OPEt_3)_4][OTf]_3$ are 76.3, 81.2, 85.2, 89.3 ppm, giving AN values of 78.1, 81.8, 97.8, and 106.7, respectively. This shows that these compounds are indeed potent Lewis acids; for context, the AN of the well-known Lewis acid $B(C_6F_5)_3$ is 82.[46]

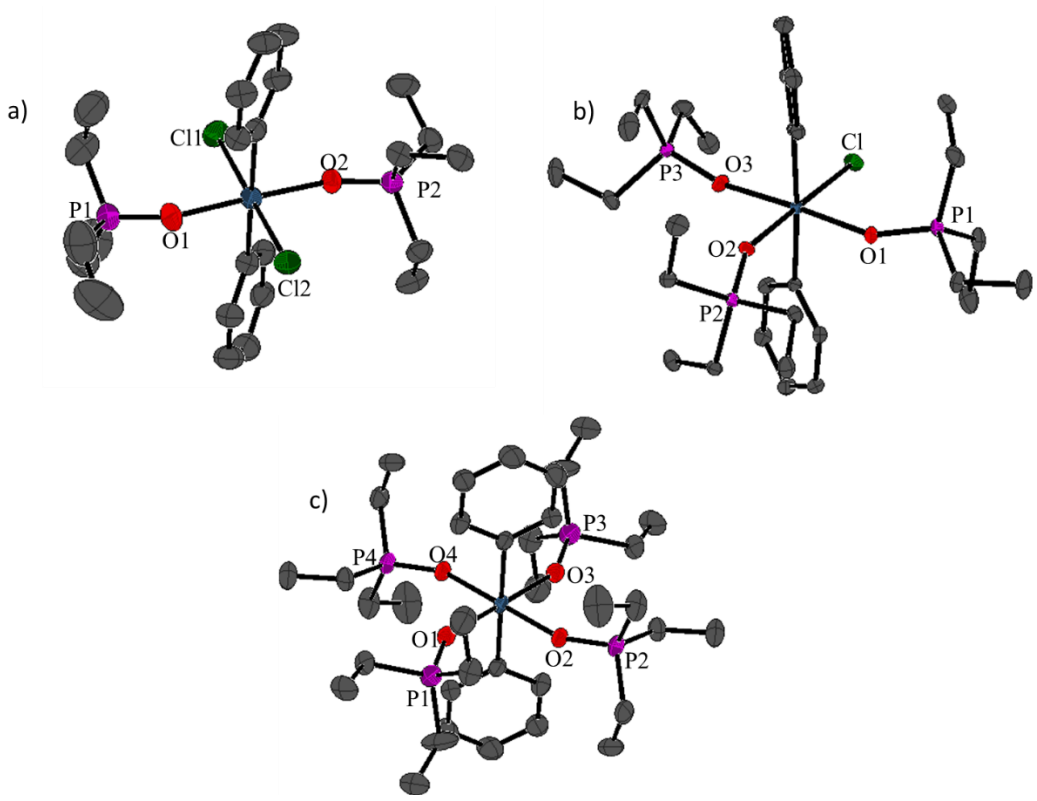

Figure 2.1.3: Solid state structures of the cation in a) $[Ph_2SbCl_3(OPEt_3)_2][OTf]$, b) $[Ph_2SbCl_2(OPEt)_3][OTf]_2$, and c) $[Ph_2Sb(OPEt_3)_4][OTf]_3$. All hydrogen atoms and counter-anions omitted for clarity. Thermal ellipsoids are shown at 50% probability.

Similar to the OPyrMe derivatives, the antimony center of each cation adopts a distorted octahedral geometry with the two phenyl substituents in a *trans* configuration (C-Sb-C = 176.25-180°). Again, preference for adoption of an octahedral geometry is displayed as, regardless of the stoichiometry of ligand employed, only octahedral complexes are isolated. As all three cations are octahedral there are no Sb---O(Tf) contacts in the solid-state. Interestingly, unlike the monocationic OPyrMe derivative, $[Ph_2SbCl_2(OPEt_3)_2][OTf]_2$ adopts a configuration in which the ligands are *trans* to each other.

In general, the Sb-O bonds in each species are very similar in length with no significant change as the cationic charge varies, however, the Sb-O in $[Ph_4Sb(OPMe_3)][OTf]$ is significantly longer than the rest of the series. This is likely due to steric congestion imposed by the four phenyl substituents rather than any electronic effect. Similarly, there is no change in Sb-Cl bond length when the cationic charge is increased from $[Ph_2SbCl_2(OPEt_3)_2]^+$ to $[Ph_2SbCl(OPEt_3)_3]^{2+}$. There is a slight increase in P-O bond length as the cationic charge increases which would be consistent with binding to a more Lewis acidic center.

Table 2.1.2: Selected bond lengths (Å) and angles (°) in the solid-state structures $[Ph_2SbCl_2(OPEt_3)_2][OTf]$, $[Ph_2SbCl(OPEt_3)_3][OTf]_2$, and $[Ph_2Sb(OPEt_3)_4][OTf]_3$ with comparison to $[Ph_4Sb(OPMe_3)][OTf]$ and $Ph_3Sb(OPMe_3)_2][OTf]_2$.[39]

	$[Ph_2SbCl_2(OPEt_3)_2][OTf]$	$[Ph_2SbCl(OPEt_3)_3][OTf]_2$	$[Ph_2Sb(OPEt_3)_4][OTf]_3$	$[Ph_4Sb(OPMe_3)][OTf]$	$Ph_3Sb(OPMe_3)_2][OTf]_2$
Sb-O1	2.096(4)	2.0885(19)	2.092(6)	2.406(2)	2.104(3)
Sb-O2	2.087(4)	2.0731(19)	2.084(6)	-	2.074(3)
Sb-O3	-	2.0790(18)	2.092(6)	-	-
Sb-O4	-	-	2.084(6)	-	-
Average Sb-O	2.092(4)	2.0802(19)	2.088(6)	2.406(2)	2.089(3)
Sb-Cl1	2.4485(14)	2.4442(6)	-	-	-
Sb-Cl2	2.4487(14)	-	-	-	-
P1-O1	1.532(4)	1.5382(19)	1.539(6)	1.499(2)	1.526(3)
P2-O2	1.520(5)	1.5415(19)	1.552(6)	-	1.530(3)
P3-O3	-	1.528(2)	1.539(6)	-	-
P4-O4	-	-	1.552(6)	-	-
Average P-O	1.526(5)	1.536(2)	1.546(6)	1.499(2)	1.528(3)

2.2. Redox Chemistry

Reaction of Ph_2SbCl_3 with two equivalents of 2,2'-bipyridine (bipy) followed by three equivalents of trimethylsilyltrifluoromethanesulfonate (TMSOTf) results in formation of $[Ph_2SbCl_2(bipy)][OTf]$ as the major product and $[PhSb(bipy)][OTf]_2$ as the minor product, both of which were isolated by fractional crystallization and have been comprehensively characterized (**Figure 2.2.1**). Under different conditions, $[Ph_2SbCl_2(bipy)][OTf]$ can also be synthesised as the sole product and will be discussed in the following section. Regarding the reduced Sb(III) species, $[PhSb(bipy)][OTf]_2$, it can be seen that two chloride substituents have been abstracted from Ph_2SbCl_3 yielding a 2+ charge and an effective loss of a phenyl and chloride substituent. Signals corresponding to chlorobenzene were observed in the ^{13}C NMR spectrum of the crude reaction mixture, indicating that reduction of Sb(V) to Sb(III) is associated with the oxidative coupling of phenyl and chloride. Similarly, reaction of $PhSbCl_4$ under similar conditions yielded the reduced $[Sb(bipy)_2][OTf]_3$ from a mixture of products (**Scheme 2.2.1**).

a) $Ph_2SbCl_3 + 2\ bipy + 3\ TMSOTf \longrightarrow [Ph_2SbCl_2(bipy)[OTf]_2$ (71%) $+ [PhSb(bipy)][OTf]_2$ (16%)

b) $PhSbCl_4 + 2\ bipy + 4\ TMSOTf \longrightarrow [Sb(bipy)_2][OTf]_3 +$ other compounds (13%)

Scheme 2.2.1: Observed reduction of Sb(V) to Sb(III). Percent yields are crystalline isolated yields.

These observations are consistent with the previously reported decomposition of R_3SbI_2 to give RI and R_2SbI (R = Me_3SiCH_2 and Me_3CCH_2) through thermal decomposition. [42],[47] Moreover, cationic phosphine complexes of Sb(III) and Sb(V) centers are known to oxidatively couple R_3P to form diphosphonium cations (R =Me, Et, Pr).[35],[48],[49] The redox behavior of Ph_2SbCl_3 in the presence of bipy and TMSOTf contrasts the apparent redox stability of the previously reported $[Ph_3Sb(bipy)][OTf]_2$,[35],[36] which contains a formal dication. I speculate that the bipy ligand is unable to sufficiently stabilize the cationic charge on $[Ph_2Sb(bipy)Cl][OTf]_2$ or $[PhSbCl(bipy)_2][OTf]_3$ which results in the reductive elimination of PhCl in order to decrease the charge density.

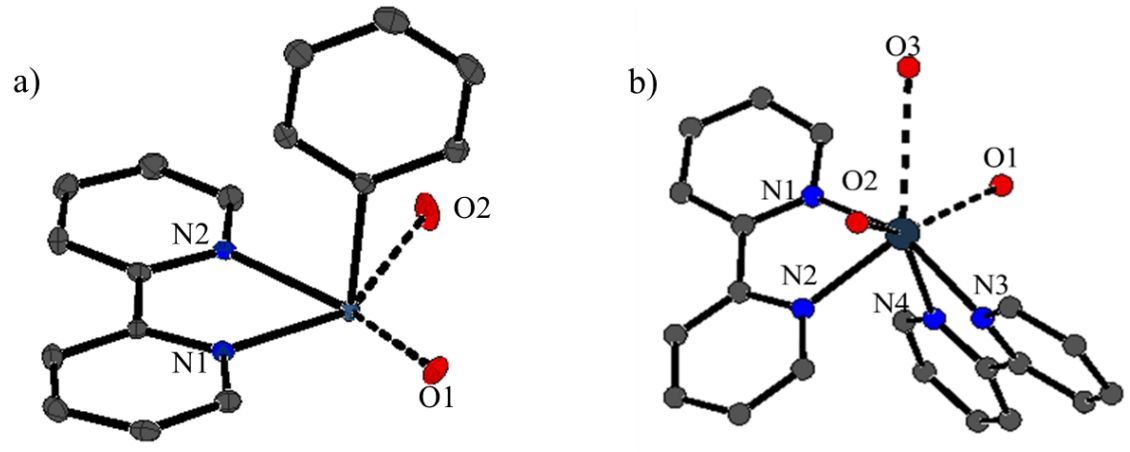

Figure 2.2.1: Solid-state structure of $[PhSb(bipy)][OTf]_2$ and $[Sb(bipy)_2][OTf]_3$. All hydrogen atoms omitted for clarity. Thermal ellipsoids are shown at 50% probability.

2.3. Complexes Featuring Nitrogen Donors

In an attempt to rationally assess the redox reactivity observed, a systematic series of cationic $[Ph_2SbX_{3-n}L_m][OTf]_n$ complexes were synthesised as per **Scheme 2.3.1** using the monodentate nitrogen based donor 4-dimethylaminopyridine (dmap). All reactions were performed in DCM and produced high yields of the neutral, monocationic and dicationic species $Ph_2SbCl_3(dmap)$, $[Ph_2SbCl_2(dmap)_2][OTf]$, and $[Ph_2SbCl(dmap)_2][OTf]_2$ (**Figure 2.3.1**). Unlike the reactions with bipy, no redox reactivity was observed. Reactions performed in CH_3CN result in formation of a significant quantities of protonated dmap, likely due to the activation of CH_3CN by the Lewis acidic antimony center. Similar activation and deprotonation of CH_3CN has been reported in reactions of the electrophilic $(C_2F_5)_3PF_2$ with amines.[50]

$$Ph_2SbCl_3 + n\ dmap + m\ AgOTf \xrightarrow[-m\ AgCl]{} [Ph_2SbCl_{(3-m)}(dmap)_n][OTf]_m$$

Scheme 2.3.1: Synthesis of $Ph_2SbCl_3(dmap)$ (n=1,m=0), $[Ph_2SbCl_2(dmap)_2][OTf]$ (n=2,m=1), $[Ph_2SbCl(dmap)_2][OTf]_2$ (n=2,m=2).

All attempts to synthesise the tricationic $[Ph_2Sb(dmap)_4][OTf]_3$, resulted in the formation of a pale blue solution from which the known $[Ag(dmap)_2][OTf]$[51],[52] crystallizes. This reaction, occurs over the course of an hour, indicated by the colour change; if halted early, $[Ph_2SbCl(dmap)_2][OTf]_2$ is isolated. Alternative halide abstractors such as TMSOTf, $NaPF_6$, $NaBF_4$, $AlCl_3$, and $GaCl_3$ in the presence of dmap have been attempted to remove the last chloride from $[Ph_2SbCl(dmap)_2][OTf]_2$ to no avail.

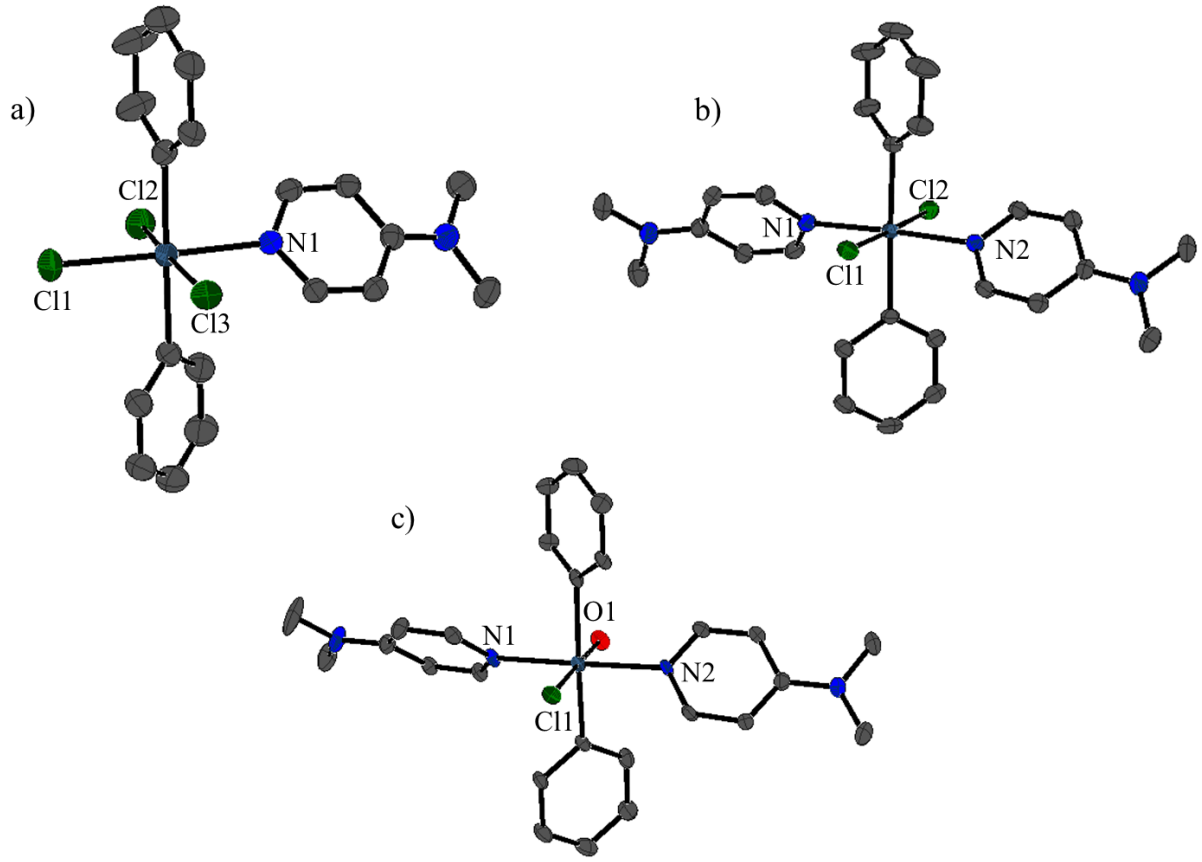

Figure 2.3.1: Solid state structure of a) $Ph_2SbCl_3(dmap)$, b) $[Ph_2SbCl_2(dmap)_2][OTf]$, and c) $[Ph_2SbCl(dmap)_2][OTf]$. All hydrogens and counter-anions omitted for clarity. Thermal ellipsoids are shown at 50% probability.

All three complexes possess an octahedral environment around the antimony center with the phenyl substituents in a *trans* configuration (C-Sb-C=170-178°). The neutral $Ph_2SbCl_3(dmap)$ and monocationic $[Ph_2SbCl_2(dmap)_2][OTf]$ are structurally analogous to the oxygen donors described above. $[Ph_2SbCl(dmap)_2][OTf]_2$, however, displays a short Sb---OTf contact: this inter-ion contact is within the sum of the van der Waals radii but slightly longer than the Sb-O interactions considered "fully coordinated."[53],[54] The second triflate is non-interacting and $[Ph_2SbCl(dmap)_2][OTf]_2$ is thus ionic, but contains a

monocation more accurately depicted as $[Ph_2SbCl(dmap)_2(OTf)][OTf]$. Attempts to substitute the coordinated triflate with an additional equivalent dmap were unsuccessful. Perhaps the steric pressure at antimony is too great to allow for binding of a third dmap ligand. This would also explain the prevalence of the formation of $Ag(dmap)_2^+$ and the difficult synthesis of $[Ph_2Sb(dmap)_4][OTf]_3$. There is a slight decrease in Sb-N and Sb-Cl bond lengths across the series, consistent with the increasing molecular charge. The Sb-N bonds are relatively short (Σ_{CR} = 2.11 Å),[55] but are consistent with $[Ph_3Sb(dmap)_2][OTf]_2$ and other reported Sb(V)-N bonds (range 2.27-2.81 Å).[56]

Table 2.3.1: Selected bond lengths (Å) and angles (°) in the solid-state structures of $Ph_2SbCl_3(dmap)$, $[Ph_2SbCl_2(dmap)_2][OTf]$, and $[Ph_2SbCl(dmap)_2][OTf]_2$ and sums of covalent ($\Sigma_{r,cov}$)[57] and van der Waals ($\Sigma_{r,vdW}$)[58] radii for selected atom pairs.

	$Ph_2SbCl_3(dmap)$	$[Ph_2SbCl_2(dmap)_2][OTf]$	$[Ph_2SbCl(dmap)_2][OTf]_2$	$[Ph_3Sb(dmap)_2][OTf]_2$
Sb-N_1	2.2334(13)	2.225(3)	2.182(8)	2.2219(17)
Sb-N_2	-	2.216(3)	2.201(8)	2.2210(17)
Average Sb-N	2.2334(13)	2.221(3)	2.192(8)	2.2215(17)
Sb-Cl_1	2.4374(5)	2.4515(9)	2.387(4)	-
Sb-Cl_2	2.4643(5)	2.4493(9)	-	-
Sb-Cl_3	2.4636(5)	-	-	-
Average Sb-Cl	2.4551(5)	2.4504(9)	2.387(4)	-
Sb---O_{OTf}	-	-	2.202(13)	2.7143(17)
$\Sigma_{r,cov}$(Sb,O)	2.03			
$\Sigma_{r,vdW}$(Sb,O)	3.58			
N1-Sb-N2	-	177.15(11)	174.4(4)	170.69(6)
N1-Sb-Cl1	86.65(4)	89.19(8)	93.6(3)	-
N1-Sb-Cl2	178.47(3)	91.75(8)	-	-
N1-Sb-Cl3	87.17(4)	-	-	-
N2-Sb-Cl1	-	89.52(8)	91.9(2)	
N2-Sb-Cl2	-	89.56(8)	-	

It is worth noting that the dmap ligands are consistently oriented in a *trans* fashion, which is counter to what is observed for phosphine and phosphine chalcogenide complexes of Sb(III): here, with the exception of PPh_3, the donor is bound in a strictly *cis* manner.[59],[60] This observation is consistent with the *trans* configuration of $[Ph_2SbCl_2(OPEt_3)_2][OTf]$ and distinct from the *cis* configuration of ligands in $[Ph_2SbCl_2(OPyrMe)][OTf]$. One explanation for this is that the neutral adduct is formed first with the dmap donating into an Sb-Cl σ^* orbital *trans* to it, thus weakening the bond and allowing easier abstraction by the Ag^+. From this intermediate the ligand can bind to form an exclusively *trans* product (**Scheme 2.3.2** pathway **a**). Alternatively, the intermediate may relax to a trigonal bipyramidal geometry prior to attack of the second equivalent of ligand which would allow the two ligands to either be *cis* or *trans* to each other (**Scheme 2.3.2** pathway **b**).

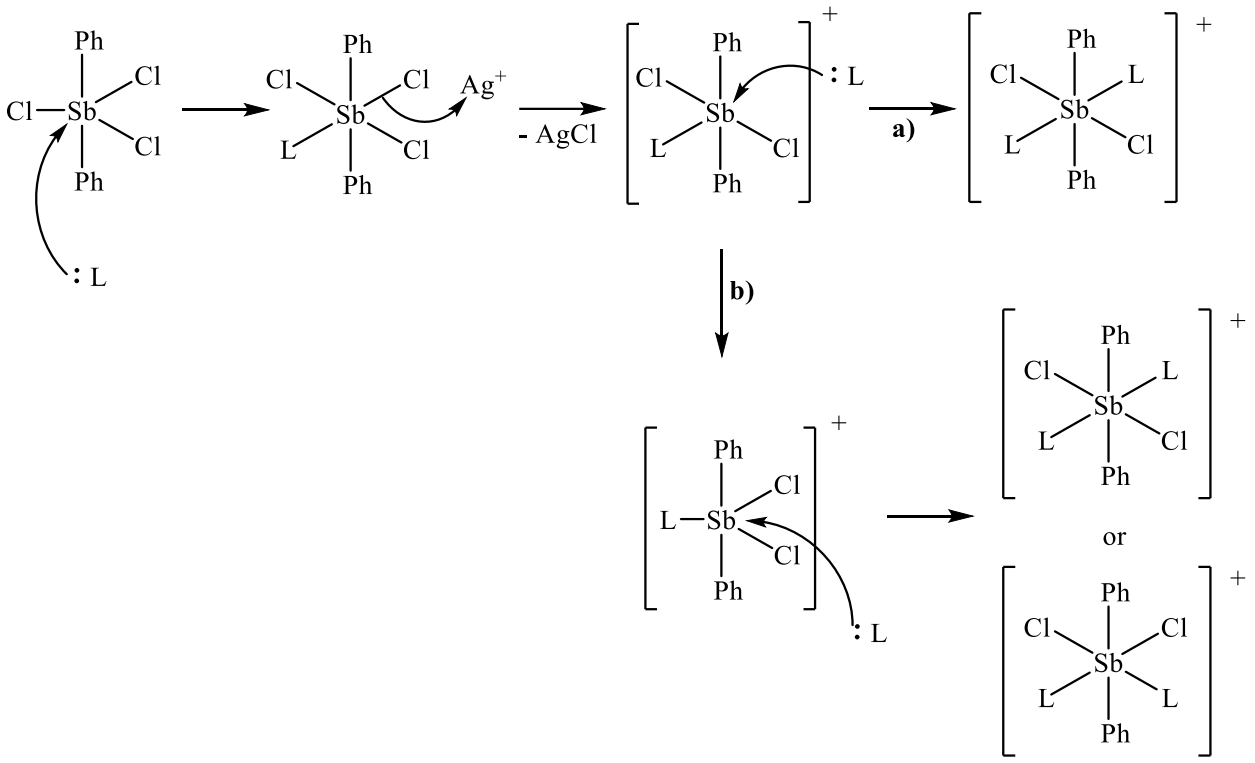

Scheme 2.3.2: Proposed mechanism for the synthesis of **a)** exclusive synthesis of *trans,trans,trans*-$[Ph_2SbCl_2L_2]^+$ and **b)** synthesis of both *trans,trans,trans*-$[Ph_2SbCl_2L_2]^+$ and *trans,trans,cis*-$[Ph_2SbCl_2L_2]^+$.

As reactions with dmap offered no insight on the redox reactivity previously observed with bipy, further investigation with bidentate nitrogen donors was continued. In an attempt to elucidate the conditions that favor redox chemistry, a series of reactions varying either the ligand (bipy or 4,4'-di-*tert*-butyl-2,2'-dipyridyl (*t*Bubipy)), halide abstractor (AgOTf or TMSOTf), or solvent (DMC or CH_3CN) was performed (**Scheme 2.3.2**). The choice of halide abstractor was varied as AgOTf is a more potent chloride abstractor due to the high lattice energy of AgCl; conversely, TMSOTf is a less potent chloride abstractor and, in solution, exists in equilibrium with TMSCl reducing the driving force for complete chloride abstraction. The coordinating solvent CH_3CN was tested

against weakly coordinating DCM to determine whether solvent plays a role in the stabilization of any potential intermediates prior to reductive elimination of PhCl.

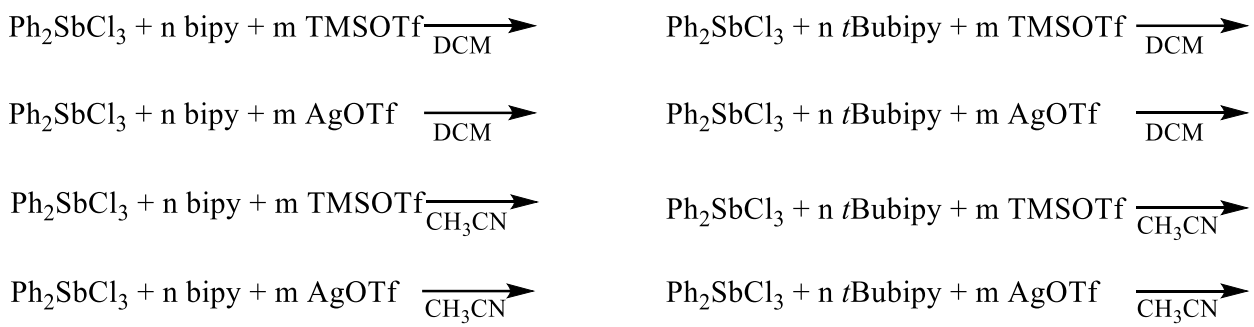

Scheme 2.3.3: Reactions performed in order to rationalize conditions required for redox chemistry and complex formation (n = 1, m = 0), (n = 1, m = 1), (n = 2, m = 2), (n = 2, m = 3).

It was determined that solvent did not play a role, as identical reactivity was observed regardless of solvent in all cases. Choice of halide abstractor and ligand, however, were significant. Reaction of Ph_2SbCl_3 with bipy in the absence of halide abstractor led to the formation of $[Ph_2SbCl_2(bipy)][Ph_2SbCl_4]$. The addition of one equivalent of either TMSOTf or AgOTf results in the formation of $[Ph_2SbCl_2(bipy)][OTf]$. The cation $[Ph_2SbCl_2(bipy)]^+$ exists as two isomers in a 60:40 ratio according to ^1H NMR. Attempts to selectively crystallize one isomer, using a variety of solvent systems, temperatures, and sublimation, failed and resulted in a mixture of both visually indistinct isomers. Nevertheless, single crystal X-ray data was obtained for both isomers and verified their identities, revealing bipy to be in a *trans* configuration to either the chloride or phenyl substituents (**Figure 2.3.3**).

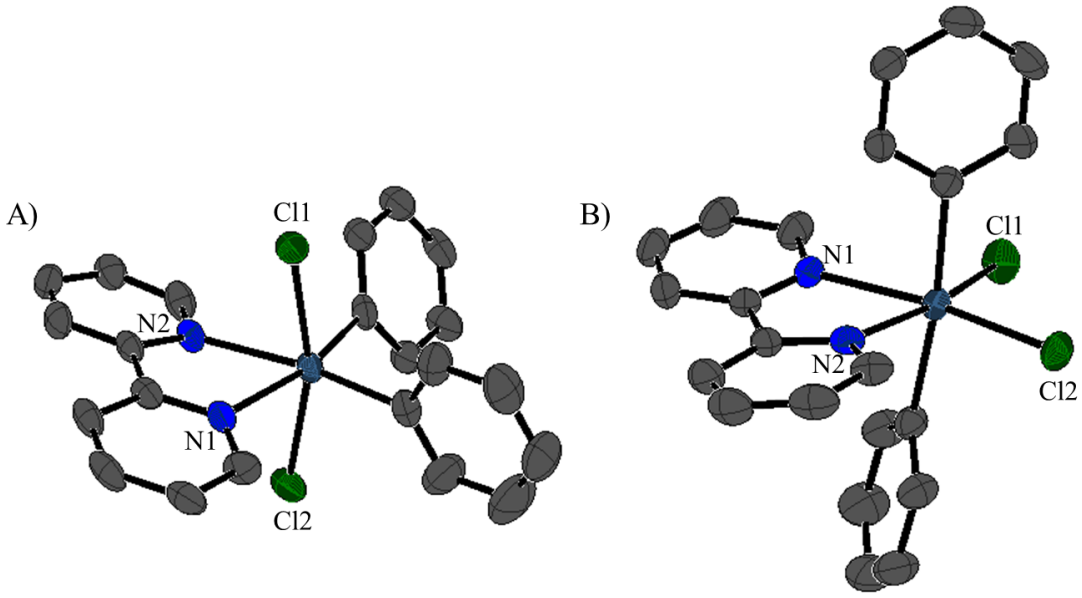

Figure 2.3.2: Solid state structure of the two isomers of the cation in $[Ph_2SbCl_2(bipy)][OTf]$. Isomer A) *cis,trans, cis*-$[Ph_2SbCl_2(bipy)][OTf]$, isomer B) *trans, cis, cis*-$[Ph_2SbCl_2(bipy)][OTf]$. All hydrogens and counter-anions omitted for clarity. Thermal ellipsoids are shown at 50% probability.

In the solid-state, the cation $[Ph_2SbCl_2(bipy)]^+$ adopts a distorted octahedral geometry about antimony. Isomer A displays greater distortion from ideal octahedral geometry (*trans*-Cl-Sb-Cl = 163.62°) than isomer B (*trans*-C-Sb-C = 173.44°) perhaps due to steric pressure of the *cis* oriented phenyl substituents. The Sb-N bond distances for both isomers are statistically indistinct and slightly longer than those present in the dmap derivative $[Ph_2SbCl_2(dmap)_2]^+$. The Sb-Cl bonds are also very similar in length between the two isomers (isomer A average Sb-Cl = 2.3997(17) Å, isomer B = 2.4136(12) Å), these are notably shorter than those in $[Ph_2SbCl_2(dmap)_2]^+$ (average Sb-Cl = 2.4504(9) Å).

Table 2.3.2: Selected bond lengths (Å) and angles (°) in the solid-state structures of the two isomers of the cation in $[Ph_2SbCl_2(bipy)][OTf]$. Isomer A) *cis,trans, cis*-$[Ph_2SbCl_2(bipy)]$, isomer B) *trans, cis, cis*-$[Ph_2SbCl_2(bipy)][OTf]$.

	Isomer A	Isomer B
Sb-N1	2.275(3)	2.261(5)
Sb-N2	2.260(3)	2.255(5)
Sb-Cl1	2.4071(12)	2.3924(17)
Sb-Cl2	2.4200(11)	2.4069(16)
C-Sb-C	173.44(14)	103.4(2)
Cl1-Sb-Cl2	98.91(4)	163.62(5)
N1-Sb-N2	72.70(12)	72.06(18)
N1-SbCl1	167.51(9)	84.46(13)
N1-Sb-Cl2	93.45(9)	81.50(13)
N2-Sb-Cl1	94.92(9)	84.04(12)
N2-Sb-Cl2	166.14(8)	83.65(13)

Reaction of Ph_2SbCl_3 with two equivalents of bipy in the presence of two equivalents of TMSOTf exhibited the same reactivity as when only one equivalent of the halide abstractor was used. Conversely, utilizing two equivalents of AgOTf or three equivalents of TMSOTf as chloride abstractor both resulted in formation of $[Ph_2SbCl_2(bipy)][OTf]$ and the reduced $[PhSb(bipy)][OTf]_2$ as described in the previous section. Using three equivalents of AgOTf resulted in isolation of the reduced $[Sb(bipy)_2][OTf]_3$, presumably along with the reductive elimination of biphenyl. Further investigation is required, however, if this is the case it is the first example of C-C bond formation from a Group 15 center.[61] These results suggest that, similar to $[Ph_2SbCl(bipy)]^{2+}$ and $[PhSbCl(bipy)_2]^{3+}$, $[Ph_2SbCl(bipy)]^{2+}$ is unstable with respect to

reductive elimination. I postulate this is due to the inability of bipy to stabilize the cationic charge and the fact that a second equivalent of bipy is unable to bind due to the bidentate nature of the ligand and steric pressure about antimony. $[Ph_2SbCl(bipy)]^{2+}$, however, is sufficiently long-lived for AgOTf to abstract the final chloride, allowing a second equivalent of bipy to bind and thus form $[Ph_2Sb(bipy)_2]^{3+}$. This, too, is unstable with respect to reduction, suggesting that two equivalents of bipy are insufficient to stabilize the cationic charge of $[Ph_2Sb]^{3+}$.

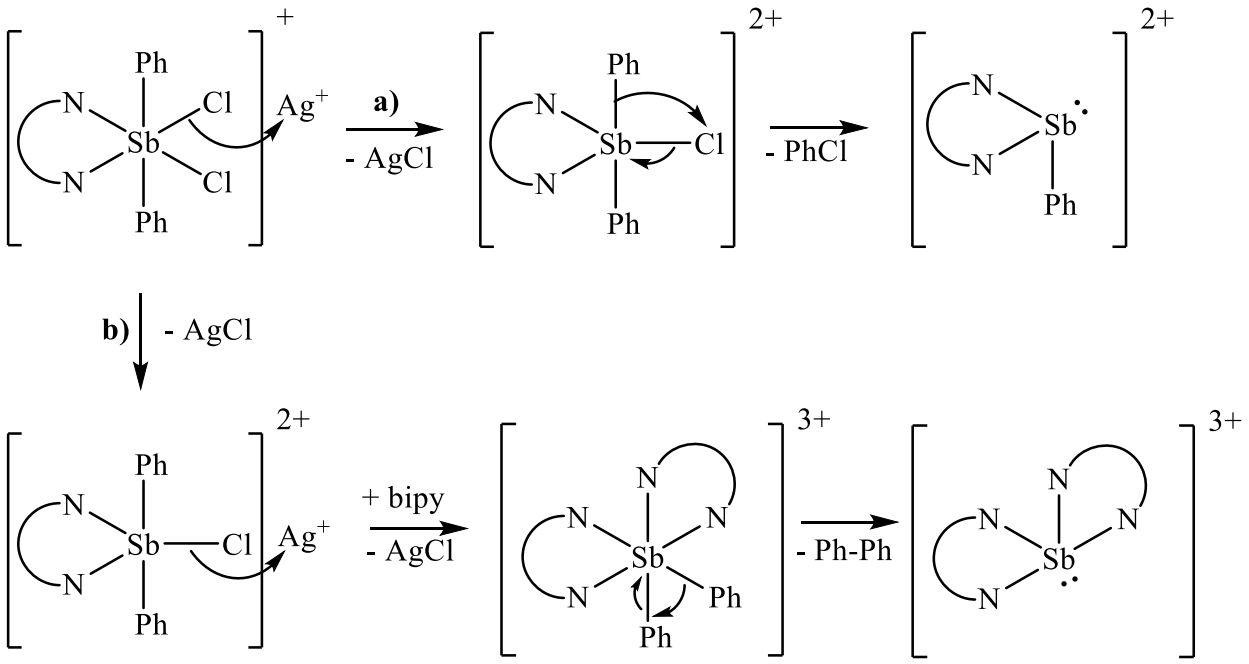

Scheme 2.3.4: Potential mechanism for the formation of **a)** $[PhSb(bipy)]^{2+}$ and **b)** $[Sb(bipy)_2]^{3+}$.

Reaction of Ph_2SbCl_3 with *t*Bubipy in the presence of one or two equivalents of TMSOTf or one equivalent of AgOTf results in the formation of two isomers in an 80:20 ratio by ^1H NMR. Only one isomer, in which the *t*Bubipy ligand is *trans* to the phenyl

substituents, was successfully crystallized (**Figure 2.3.4**). Extrapolating through comparison to the bipy derivative, the other isomer likely has *t*Bubipy *trans* to the chloride substituents. Reaction of Ph_2SbCl_3 with two equivalents of *t*Bubipy and three equivalents of TMSOTf or two equivalents of AgOTf resulted in a mixture of products from which only $[Ph_2SbCl_2(tBubipy)][OTf]$ has been isolated. Notably, no evidence of PhCl was observed, indicating that, if formed, $[Ph_2SbCl(tBubipy)]^{2+}$ may be more stable than the bipy derivative. In a similar vein, when three equivalents of AgOTf were used as halide abstractor, clean formation of $[Ph_2Sb(tBubipy)_2][OTf]_3$ occurs.

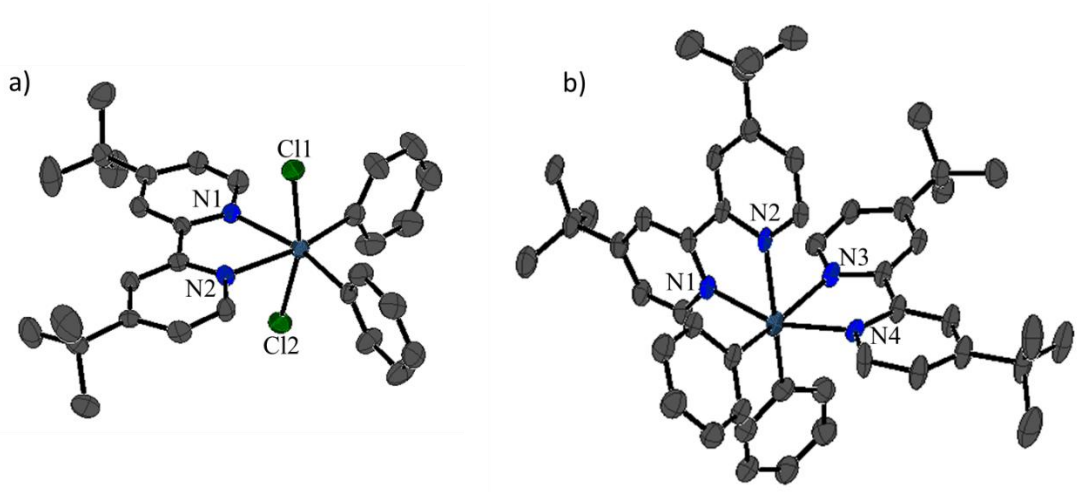

Figure 2.3.3: Solid state structure of the cation in a) $[Ph_2SbCl_2(tBubipy)][OTf]$ and b) $[Ph_2Sb(tBubipy)_2][OTf]_3$. All hydrogens and counter-anions omitted for clarity. Thermal ellipsoids are shown at 50% probability.

In the solid-state, both $[Ph_2Sb(tBubipy)_2][OTf]_3$ and the isomer of $[Ph_2SbCl_2(tBubipy)][OTf]$ that crystallized adopts a distorted octahedral geometry about antimony with the two phenyl substituents *cis* to each other. The Sb-N bonds in

$[Ph_2SbCl_2(t\text{Bubipy})][OTf]$ are slightly shorter than those in the unsubstituted bipy derivative and slightly longer than those in $[Ph_2Sb(t\text{Bubipy})_2][OTf]_3$. The C-Sb-C angle for all three species with *cis* configured phenyl substituents are identical. In $[Ph_2Sb(t\text{Bubipy})_2][OTf]_3$, the Sb-N bonds *trans* to phenyl are slightly longer than those *trans* to nitrogen indicating a larger trans influence of phenyl compared to *t*Bubipy.

Table 2.3.3: Selected bond lengths (Å) and angles (°) in the solid-state structures of the $[Ph_2SbCl_2(t\text{Bubipy})][OTf]$ and $[Ph_2Sb(t\text{Bubipy})_2][OTf]_3$.

	$[Ph_2SbCl_2(t\text{Bubipy}][OTf]$	$[Ph_2Sb(t\text{Bubipy})_2][OTf]_3$
Sb-N1	2.238(4)	2.204(9)
Sb-N2	2.236(4)	2.228(9)
Sb-N3	-	2.237(9)
Sb-N4	-	2.208(8)
Sb-Cl1	2.4083(15)	-
Sb-Cl2	2.3957(16)	-
C-Sb-C	104.14(18)	104.4(4)
Cl1-Sb-Cl2	163.84(4)	-
N1-Sb-N2	72.07(13)	72.5(3)
N1-Sb-N3	-	89.6(3)
N1-Sb-N4	-	158.9(3)
N2-Sb-N3	-	75.6(3)
N2-Sb-N4	-	90.2(3)
N3-Sb-N4	-	74.2(3)
N1-SbCl1	81.87(11)	-
N1-Sb-Cl2	85.37(11)	-
N2-Sb-Cl1	82.84(12)	-
N2-Sb-Cl2	83.82(11)	-

It is unexpected that redox chemistry is observed in the case of the bipy derivatives, while stable Sb(V) complexes are formed with *t*Bubipy as the ligand. I believe that these two pathways are very similar energetically, and that the slight increase in donor ability of *t*Bubipy compared to bipy allows for the formation of stable Sb(V) complexes rather than redox chemistry. I predict that the use of a weakly activated or deactivated bipy derivative (*e.g.* 4,4'-di-fluoro-2,2'-dipyridyl, 4,4'-di-nitro-2,2'-dipyridyl) would further facilitate redox chemistry.

2.4. Oxidation of $[Pn(III)]^{3+}$

An alternative synthetic route to access Pn(V) cations is through the oxidation of suitable Pn(III) cations. A series of tricationic Pn(III) compounds of the generic formulae $[Pn(L)_2][OTf]_3$ (L = bipy or *t*Bubipy) has previously been reported.[62] Reaction of $[Sb(tBubipy)_2][OTf]_3$ with one equivalent of the oxidant $SeCl_4$ or SO_2Cl_2 resulted in isolation of $[Sb(tBubipy)Cl_4][OTf]$ and protonated ligand instead of the expected $[SbCl_2(tBubipy)_2][OTf]_3$.

Reactions of $[P(tBubipy)_2][OTf]_3$ with the oxidants SO_2Cl_2, $SeCl_4$, and PCl_5 were also investigated. In all cases, complete consumption of $[P(tBubipy)_2]^{3+}$ and formation of a new species which resonates at -147 ppm on ^{31}P NMR—and at 219 ppm when PCl_5 was used as the oxidant, corresponding to PCl_3—was observed. Through independent reaction of PCl_5 with tBubipy and AgOTf, the species was verified to be $[P(tBubipy)Cl_4][OTf]$.

While oxidation of $[Pn(tBubipy)_2][OTf]_3$ did occur, the apparent lability of the *t*Bubipy ligand allowed for redistribution of substituents. This could potentially be prevented through the use of a less labile ligand. This has recently been shown to be successful in the

preparation of $[P(BIMEt_3)][OTf]_3$ ($BIMEt_3$ = *tris*((1-ethyl-benzoimidazol-2-yl)methyl)amine) and subsequent oxidation with XeF_2 to from $[PF_2(BIMEt_3)][OTf]_3$.[63] The tetradentate nature of $BIMEt_3$ allows for additional stabilization upon oxidation by reorganization of the ligand and shortening of the apical P-N bond (**Figure 2.4.1**).

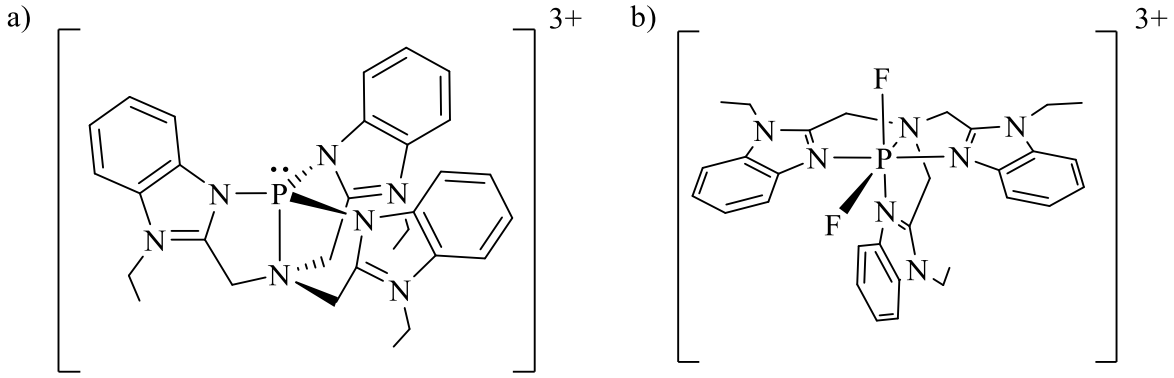

Figure 2.4.1: General structure of the cation a) $[P(BIMEt_3]^{3+}$ and b) $[PF_2(BIMEt)]^{3+}$.

2.5. Summary

A systematic approach was taken to synthesize several series of antimony(V) cations featuring nitrogen and oxygen donors, including the first examples of structurally characterised pnictogen(V) trications. Two different routes were explored: halide abstraction-ligand substitution from an Sb(V) precursor, and oxidation of a previously synthesized Sb(III) cation. It was found that an octahedral geometry is preferred in all cases. During preparation of these compounds, redox chemistry was observed, and determined to be the result of reductive elimination of chlorobenzene and biphenyl from an antimony center. This process was studied in depth, and leads us to believe the redox

chemistry is facilitated through a buildup of cationic charge which cannot be effectively stabilized by the ligands.

Chapter 3: Pyridine complexes of antimony(III)

While more established than the coordination chemistry of Pn(V), survey of the literature indicates few systematic assessments of structural trends within Pn(III) complexes, despite a diverse array of structures and bonding environments available. A feature of note when considering Sb(III) is that, unlike Sb(V) and most metals, Sb(III) possesses a localized and stereochemically active lone pair. The presence of a lone pair of electrons on the acceptor element, also referred to as electron rich acceptor, offers electronic and structural features unique from those of the transition metals and which offer potential applications in catalysis.[64],[65] While VSEPR theory is generally quite accurate in predicting the geometry of main group compounds; when multiple substituents, ligands, and a lone pair are present, it is often impossible to predict the structure of a compound facilitating the need for systematic investigations.

One diverse class of electron rich acceptors are antimony acceptors with phosphine ligands, with examples of neutral,[66],[67] anionic,[68] and cationic[69],[70],[71],[72] compounds known. In addition, a recent systematic investigation on the structural diversity of PR_3 complexes of chloro-antimony acceptors has been performed which highlights the structural diversity of the series.[59]

While pyridine-based ligands are a ubiquitous class in transition metal coordination chemistry, their chemistry with antimony(III) acceptors remains underdeveloped. There are several examples of neutral antimony(III) pyridine complexes—some of which have been utilized for their anti-parasitic activity[73]—but few cationic derivatives are reported. Our recent reports of a number of pyridine chelate complexes (**Figure 3.2**) revealed the importance of a cationic charge on the viability of the coordination chemistry of

antimony(III). In this context, we have performed a more systematic assessment of such complexes including $SbCl_3$, $SbCl_2^+$, $SbCl^{2+}$, $PhSbCl_2$, $PhSbCl^+$ and Ph_3Sb as acceptors and 2,2'bipyridine (bipy) or 4-dimethylaminopyridine (dmap) as ligands.

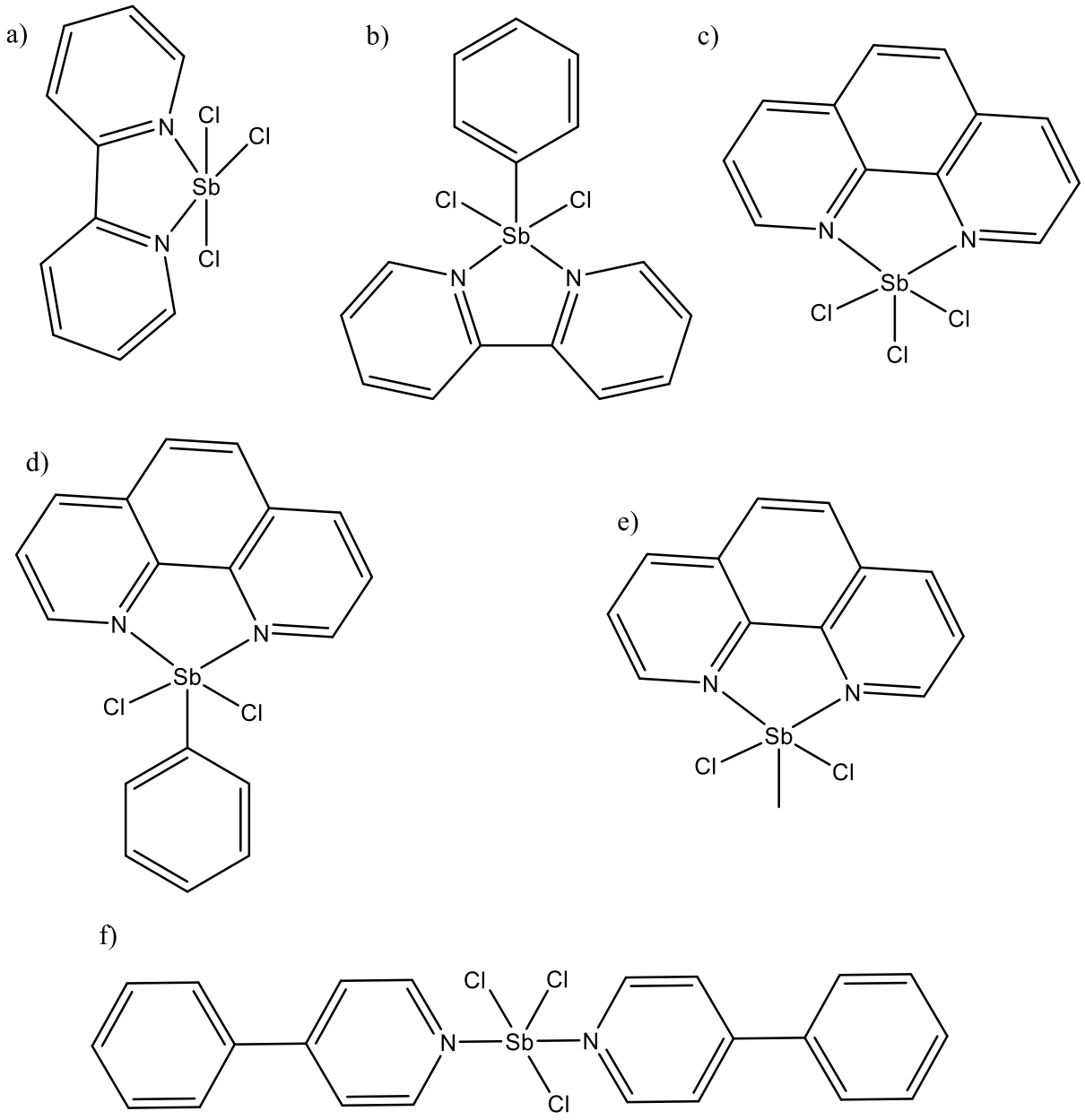

Figure 3.1: Examples of structurally characterized neutral Sb(III) complexes with pyridine donors: a) $SbCl_3$(bipy),[74] b) $PhSbCl_2$(bipy),[75] c) $SbCl_3$(phen),[73] d) $PhSbCl_2$(phen),[73] e) $MeSbCl_2$(phen),[76] f) $SbCl_3$(4-phenylpyridine)$_2$.[77]

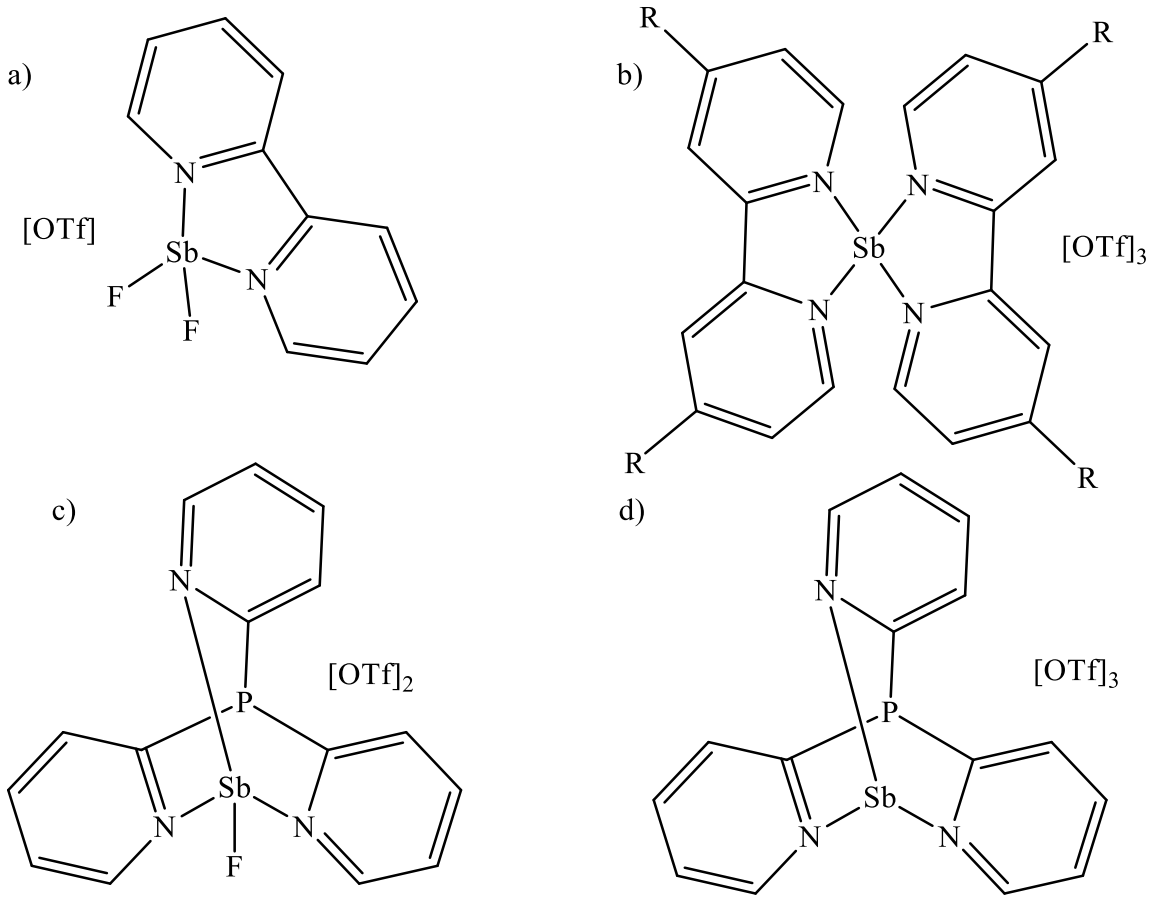

Figure 3.2 Examples of structurally characterized cationic Sb(III) complexes with pyridine donors: a) $[SbF_2(bipy)][OTf]$,[78] b) $[Sb(bipy)_2][OTf]_3$: R= H,[78] tBu,[79] c) [SbF(tris(2-pyridyl)phosphine)]$[OTf]_2$,[80] d) [Sb(tris(2-pyridyl)phosphine)]$[OTf]_3$[80].

3.1. Bipy Complexes of $SbCl_3$

Reactions of $SbCl_3$ with bipy in the presence of TMSOTf were carried out as per **Scheme 3.1.1** and occur rapidly at room temperature as observed by ^1H NMR spectroscopy. The formation of $SbCl_3(bipy)$, $[SbCl_2(bipy)][OTf]$, and $[SbCl(bipy)_2][OTf]_2$ proceed cleanly and are based on reagent stoichiometry (**Figure 3.1.1**). Reaction of $SbCl_3$

with two equivalents of bipy and three equivalents of TMSOTf results in incomplete abstraction of chloride and the formation of $[SbCl(bipy)_2][OTf]_2$, exclusively, indicating that TMSOTf is insufficient to abstract a chloride from the $[SbCl]^{2+}$ moiety. The fully dehalogenated derivative, $[Sb(bipy)_2][OTf]_3$, has been previously synthesised from $SbCl_3$ with the potent halide abstractor AgOTf, and from SbF_3 using TMSOTf.[78],[79]

a) $SbCl_3 + bipy \longrightarrow SbCl_3(bipy)$

b) $SbCl_3 + bipy + TMSOTf \xrightarrow[-\ TMSCl]{} [SbCl_2(bipy)][OTf]$

c) $SbCl_3 + 2\ bipy + ex\ TMSOTf \xrightarrow[-\ TMSCl]{} [SbCl(bipy)_2][OTf]_2$

d) $SbCl_3 + 2\ bipy + 3\ AgOTf \xrightarrow[-3\ AgCl]{} [Sb(bipy)][OTf]_3$

Scheme 3.1.1: Reactions of $SbCl_3$ with bipy and TMSOTf. For reaction c) excess TMSOTf (>2 equivalents) is required.

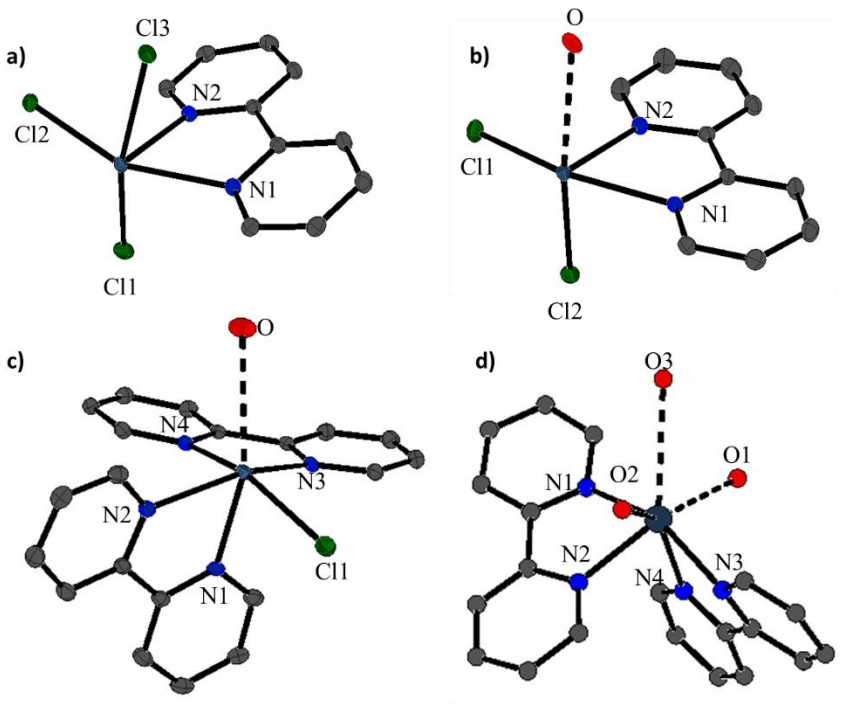

Figure 3.1.1: View of the antimony environment in the solid-state structures of a) $SbCl_3(bipy)$, the cation in b) $[SbCl_2(bipy)][OTf]$, c) $[SbCl(bipy)_2][OTf]_2$, and d) $[Sb(bipy)_2][OTf]_3$[78] showing interacting oxygen atoms of triflate anions. Hydrogen atoms are omitted for clarity. Thermal ellipsoids are shown at 50% probability.

The solid-state structure of the neutral $SbCl_3(bipy)$ is simply an adduct of $SbCl_3$ and bipy, with a distorted square pyramidal geometry at the antimony center. The solid-state structure of $[SbCl_2(bipy)][OTf]$ is best described as a triflate salt of a dichlorostibenium cation $[SbCl_2]^+$ which is chelated by bipy; the antimony center also engages in weak interactions with the neighboring oxygen center of the triflate anion, again, imposing a distorted square pyramidal geometry. This is in contrast to the related fluoride derivative which achieves an octahedral geometry through the interaction of a neighbouring fluorine atom.[78] The solid-state structure of $[SbCl(bipy)_2][OTf]_2$ is best described as a bis-triflate

salt of $[SbCl]^{2+}$ which is chelated by two bipy ligands; the antimony center engages in weak interactions with two neighbouring oxygen centers of the triflate anions, inducing a distorted pentagonal bipyramidal geometry. The cause of distortion in all cases is the stereochemically active lone pair and the rigid nature of the bipy ligand. With respect to bond lengths, both cationic complexes have Sb---O interactions which are significantly longer than the sum of the covalent radii implying a degree of ionic character. One would expect the bond lengths to decrease as the cationic charge of the molecule increases; however, it can be see that both the average Sb-N and Sb-Cl distances are longer in the dicationic $[SbCl(bipy)_2][OTf]_2$ than the mono- or tri-cationic derivatives. The increased Sb-Cl bond length is likely due to the chloride substituent *trans* to N4. Moreover, the second equivalent of bipy would quench some of the Lewis acidity thereby elongating the bonds relative to $[SbCl_2(bipy)][OTf]$.

Table 3.1.1: Selected bond lengths (Å) and angles (°) in the solid state structure of $SbCl_3$(bipy), [$SbCl_2$bipy][OTf], and [$SbCl(bipy)_2$][$OTf]_2$ compared to [$Sb(bipy)_2$][$OTf]_3$[78].

	$SbCl_3$(bipy)	[$SbCl_2$(bipy)] [OTf]	[$SbCl(bipy)_2$] [$OTf]_2$	[$Sb(bipy)_2$][$OTf]_3$
Sb-N1	2.3659(13)	2.3481(11)	2.2683(18)	2.2843(12)
Sb-N2	2.2358(13)	2.2512(11)	2.3438(18)	2.2333(12)
Sb-N3	-	-	2.3033(18)	2.3322(12)
Sb-N4	-	-	2.3339(18)	2.2434(12)
Average Sb-N	2.3009(13)	2.2997(11)	2.3123(18)	2.2733(12)
Sb-Cl1	2.6492(4)	2.4901(3)	2.5270(7)	-
Sb-Cl2	2.4963(4)	2.3970(4)	-	-
Sb-Cl3	2.6492(4)	-	-	
Sb-O	-	2.6515(11)	2.9782(12) 3.7097(5)	2.598(2) 2.650(2) 3.077(1) 3.247(1) 3.367(1)
$\Sigma_{r,cov}$(Sb,O)	2.03			
$\Sigma_{r,vdW}$(Sb,O)	3.58			
N1-Sb-N2	70.27(4)	70.48(4)	69.90(6)	72.09(4)
N1-Sb-N3	-	-	85.11(6)	156.02(4)
N1-Sb-N4	-	-	77.16(6)	87.87(4)
N2-Sb-N3	-	-	150.62(6)	91.42(4)
N2-Sb-N4	-	-	88.54(6)	78.66(4)
N3-Sb-N4	-	-	70.52(6)	71.53(4)

3.2. Dmap Complexes of $SbCl_3$

Reactions of $SbCl_3$ and dmap occur rapidly at room temperature. ^1H NMR spectra of the reaction mixtures show a downfield shift of the dmap resonances, indicative of coordination of dmap. The formation of $SbCl_3(dmap)_2$ occurs regardless of the stoichiometry employed: using less than two equivalents of dmap results in the precipitation of exclusively $SbCl_3(dmap)_2$ by ^1H NMR with presumably unreacted $SbCl_3$ remaining in solution, while the addition of more than two equivalents of dmap leads to the formation of the same compound with free dmap in solution by ^1H NMR. Abstraction of chloride occurs readily with AgOTf or similarly as above with TMSOTf. Attempts to form $[Sb(dmap)_3][OTf]_3$ by abstraction with AgOTf in DCM or CH_3CN continually led to the formation of a large amount of [H-dmap][OTf] that could not be separated from the desired product. Addition of dmap to $Sb(OTf)_3$ generated *in situ* by fluoride abstraction of SbF_3 with TMSOTf, however, afforded the desired $[Sb(dmap)_3][OTf]_3$.

a) $SbCl_3 + dmap \longrightarrow SbCl_3(dmap)_2$

b) $SbCl_3 + dmap + TMSOTf \xrightarrow[-\ TMSCl]{} [SbCl_2(dmap)_2][OTf]$

c) $SbCl_3 + dmap + AgOTf \xrightarrow[-\ AgCl]{} [SbCl_2(dmap)_2][OTf]$

d) $SbCl_3 + 2\ dmap + ex\ TMSOTf \xrightarrow[-\ TMSCl]{} [SbCl(dmap)_2][OTf]_2$

e) $SbCl_3 + 2\ dmap + 2\ AgOTf \xrightarrow[-2\ AgCl]{} [SbCl(dmap)_2][OTf]_2$

f) $SbF_3 + 3\ dmap + 3\ TMSOTf \xrightarrow[-3\ TMSCl]{} [Sb(dmap)_3][OTf]_3$

Scheme 3.2.1: Reactions of $SbCl_3$ with dmap and halide abstractor.

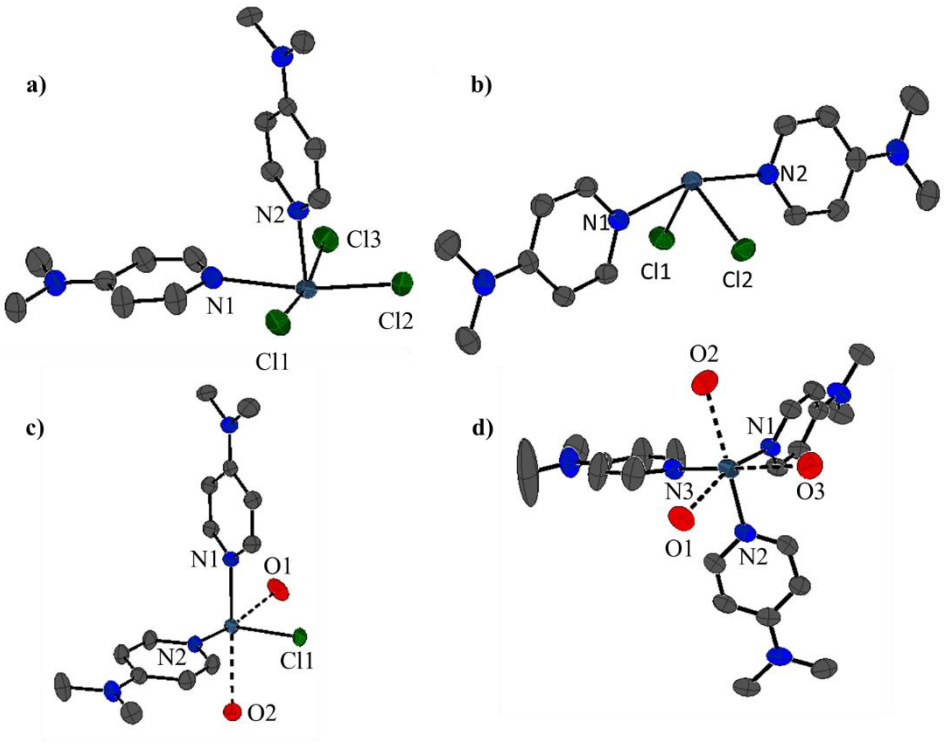

Figure 3.2.1: View of the antimony environment in the solid-state structures of a) $SbCl_3(dmap)_2$, the cation in b) $[SbCl_2(dmap)_2][OTf]$, c) $[SbCl(dmap)_2][OTf]_2$, and d) $[Sb(dmap)_3][OTf]_3$ showing interacting oxygen atoms of triflate anions. Hydrogen atoms are omitted for clarity. Thermal ellipsoids are shown at 50% probability.

In the solid-state, $SbCl_3(dmap)_2$ adopts a square pyramidal arrangement with meridionally configured chlorine substituents. The longer Sb-N1 interaction is presumably due to the *trans*-influence of Cl2. The monocationic $[SbCl_2(dmap)_2][OTf]$ adopts a see-saw configuration with the dmap ligands in the axial positions and chloride in the equatorial. This is in contrast to the PMe_3 analogue[59] in which the ligands adopt an exclusively *cis* configuration. The greater steric demands of the dmap ligand likely facilitates this configuration. The dicationic $[SbCl(dmap)_2][OTf]_2$ adopts a square pyramidal geometry with two long Sb-OTf contacts and a facial arrangement of dmap and

Cl. Unlike the previous example, this is in agreement with the PMe_3 analogue[59] which adopts a distorted octahedral arrangement with a third short triflate contact due to the less sterically demanding PMe_3 ligands. The tricationic $[Sb(dmap)_3][OTf]_3$ adopts a pyramidal geometry with one short and two longer Sb-OTf contacts for an overall distorted octahedral geometry. This configuration is equivalent to the phosphorus and arsenic derivatives previously reported.[62] The Sb-N bond distances decrease with increasing cationic charge as expected with only slight decrease from the dicationic to tricationic complexes, explained by the additional equivalents of dmap diminishing the Lewis acidity of the antimony center. Additionally, the Sb-N distances of $[Sb(dmap)_3][OTf]_3$ are shorter than the corresponding values of the bipy derivative $[Sb(bipy)_2][OTf]_3$, consistent with the greater donor strength of dmap over bipy.

Table 3.2.1: Selected bond lengths (Å) and angles (°) in the solid state structure of $SbCl_3(dmap)_2$, $[SbCl_2(dmap)_2][OTf]$, $[SbCl(dmap)_2][OTf]_2$, $[Sb(dmap)_3][OTf]_3$.

	$SbCl_3(dmap)_2$	$[SbCl_2(dmap)_2][OTf]$	$[SbCl(dmap)_2][OTf]_2$	$[Sb(dmap)_3][OTf]_3$
Sb-N1	2.4841(19)	2.344(2)	2.166(2)	2.187(3)
Sb-N2	2.1704(18)	2.344(2)	2.177(2)	2.156(3)
Sb-N3	-	-	-	2.161(33)
Sb-Cl1	2.5943(6)	2.3923(7)	2.3331(6)	-
Sb-Cl2	2.5145(7)	2.3923(7)	-	-
Sb-Cl3	2.5616(7)	-	-	-
Sb-O	-	-	2.567(2) 3.359(3)	2.501(3) 2.759(3) 2.769(4)
$\Sigma_{r,cov}$(Sb,O)	2.03			
$\Sigma_{r,vdW}$(Sb,O)	3.58			
N1-Sb-N2	83.61(7)	160.05(12)	86.63(9)	84.42(11)
N1-Sb-N3	-	-	-	91.26(11)
N2-Sb-N3	-	-	-	89.18(11)
N1-Sb-Cl1	88.19(5)	83.04(6)	89.09(6)	-
N1-Sb-Cl2	169.37(5)	83.44(6)	-	-
N1-Sb-Cl3	87.03(5)	-	-	-
N2-Sb-Cl1	83.90(5)	83.44(6)	92.22(6)	-
N2-Sb-Cl2	85.76(5)	83.04(6)	-	-
N2-Sb-Cl3	84.56(5)	-	-	-

3.3. Bipy Complexes of $PhSbCl_2$

Reaction of $PhSbCl_2$ with bipy in the presence of AgOTf in DCM occurs rapidly to afford [PhSbCl(bipy)][OTf] or $[PhSb(bipy)][OTf]_2$, depending on the stoichiometry (**Figure 3.3.1**). Interestingly, in contrast to the $SbCl_3$ reactions, no chloride abstraction from $PhSbCl_2$ occurs in the presence of TMSOTf, even with a 2.5-fold excess. Moreover, regardless of the stoichiometry employed or halide abstractor chosen, attempts to form $[PhSb(bipy)_2][OTf]_2$ were unsuccessful. $[PhSb(bipy)][OTf]_2$ has been previously synthesised through reduction of Ph_2SbCl_3 in the presence of bipy and TMSOTf in Chapter 2.

a) $PhSbCl_2 + bipy \longrightarrow PhSbCl_2(bipy)$

b) $PhSbCl_2 + bipy + TMSOTf \longrightarrow$ No Reaction

c) $PhSbCl_2 + bipy + AgOTf \xrightarrow[-\ AgCl]{} [PhSbCl(bipy)][OTf]$

d) $PhSbCl_2 + n\ bipy + 2\ AgOTf \xrightarrow[\substack{-2\ AgCl \\ n = 1,2}]{} [PhSb(bipy)][OTf]_2$

Scheme 3.3.1: Reactions of $PhSbCl_2$ with bipy and halide abstractor.

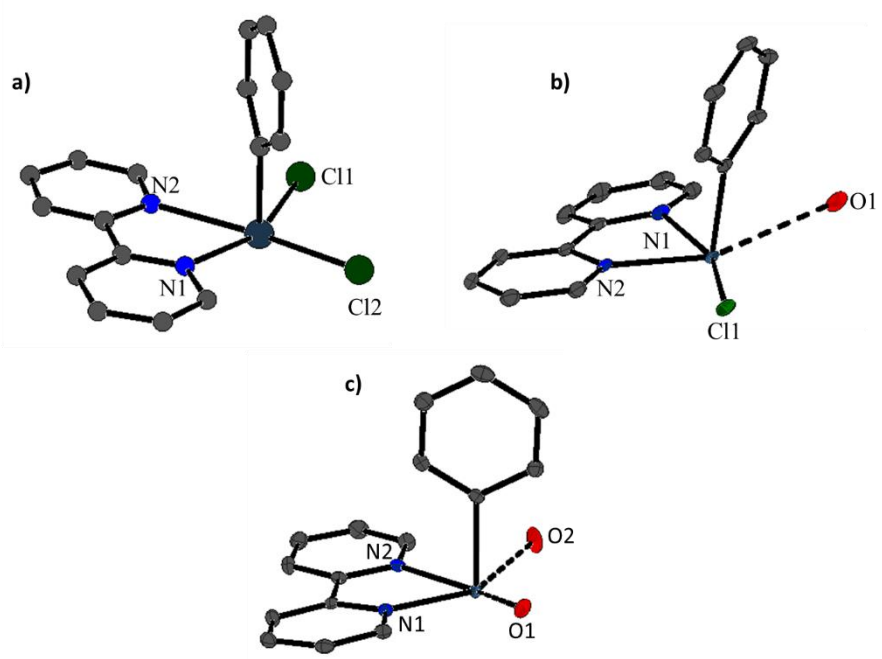

Figure 3.3.1: View of the antimony environment in the solid-state structures of a) $PhSbCl_2(bipy)$, the cation b) [PhSbCl(bipy)][OTf], and c) $[PhSb(bipy)][OTf]_2$ showing interacting oxygen atoms of triflate anions. Hydrogen atoms are omitted for clarity. Thermal ellipsoids are shown at 50% probability.

In the solid state, all three compounds adopt a distorted square pyramidal geometry at antimony with the phenyl substituent in the axial position. The mono- and di-cation possess one and two Sb---OTf contacts, respectively, to achieve a coordination number of 5. As expected, the Sb-N bond length deceases across the series, consistent with increasing cationic charge. In addition, the N-Sb-N angle widens much more drastically than the $SbCl_3$ derivatives.

Table 3.3.1: Selected bond lengths (Å) and angles (°) in the solid state structure of [PhSbCl(bipy)][OTf], [PhSb(bipy)][OTf]$_2$ compared to PhSbCl$_2$(bipy)[75].

	PhSbCl$_2$(bipy)	[PhSbCl(bipy)][OTf]	[PhSb(bipy)][OTf]$_2$
Sb-N1	2.43(1)	2.2327(17)	2.229(2)
Sb-N2	2.43(1)	2.3581(18)	2.2434(19)
Sb-Cl1	2.556(5)	2.3606(6)	-
Sb-Cl2	2.556(5)	-	-
Sb-O	-	2.9599(4)	2.4681(16) 2.4926(18)
$\Sigma_{r,cov}$(Sb,O)	2.03		
$\Sigma_{r,vdW}$(Sb,O)	3.58		
N1-Sb-N2	66.9(7)	71.73(6)	73.39(7)
N1-SbCl1	159.2(4)	156.59(5)	-
N1-Sb-Cl2	93.3(4)	-	-
N2-Sb-Cl1	93.3(4)	85.02(4)	-
N2-Sb-Cl2	159.2(4)	-	-

3.4. Dmap Complexes of PhSbCl$_2$

Reaction of PhSbCl$_2$ with dmap in the presence of AgOTf occurs rapidly to afford [PhSbCl(dmap)$_2$][OTf] or [PhSb(dmap)$_3$][OTf]$_2$, depending on the stoichiometry (**Figure 3.4.1**). Without AgOTf, the neutral complex PhSbCl$_2$(dmap)$_2$ forms regardless of the stoichiometry imposed, showing preference for a 5-coordinate antimony just as seen in SbCl$_3$(dmap)$_2$. As with the aforementioned PhSbCl$_2$ reactions with bipy (**Section 3.3**), no halide abstraction of PhSbCl$_2$ occurs when using TMSOTf. While X-ray quality crystals

have yet to be obtained for $[PhSb(dmap)_3][OTf]_2$, ^1H and $^{13}C\{^1H\}$ NMR spectroscopy and elemental analysis is consistent with this formulation.

a) $PhSbCl_2 + 2\ dmap \longrightarrow PhSbCl_2(dmap)_2$

b) $PhSbCl_2 + dmap + TMSOTf \longrightarrow$ No Reaction

c) $PhSbCl_2 + 2\ dmap + AgOTf \xrightarrow[-\ AgCl]{} [PhSbCl(dmap)_2][OTf]$

d) $PhSbCl_2 + 3\ dmap + 2\ AgOTf \xrightarrow[-2\ AgCl]{} [PhSb(dmap)_3][OTf]_2$

Scheme 3.4.1: Reactions of $PhSbCl_2$ with dmap and halide abstractor.

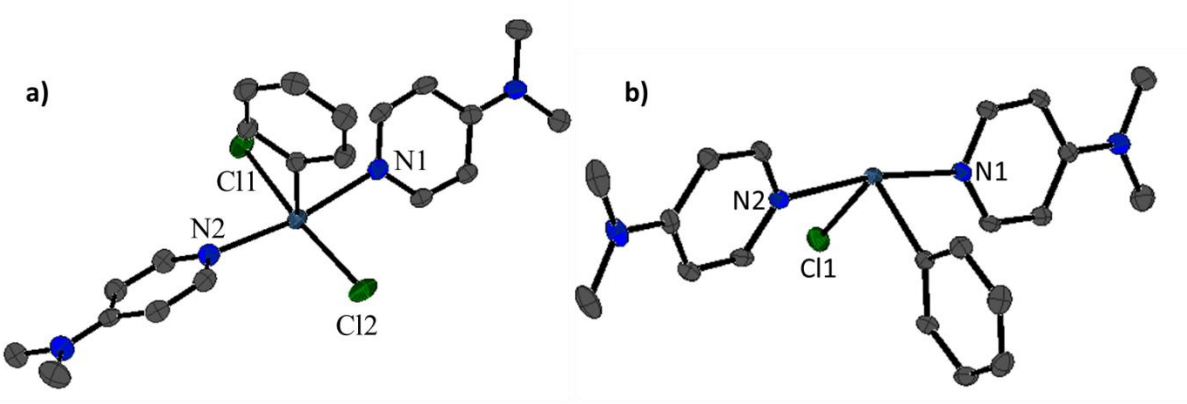

Figure 3.4.1: View of the antimony environment in the solid-state structures of a) $PhSbCl_2(dmap)_2$ and the cation in b) $[PhSbCl(dmap)_2][OTf]$. Hydrogen atoms are omitted for clarity. Thermal ellipsoids are shown at 50% probability.

In the solid state $PhSbCl_2(dmap)_2$ adopts a square pyramidal geometry at antimony, with the phenyl substituent in the axial position, two *trans* dmap ligands, and two *trans* chloride substituents. The cation $[PhSbCl(dmap)_2]^+$ adopts a see-saw geometry at antimony, with the dmap ligands occupying the axial positions. The closest Sb-OTf contact

is far outside the sum of the Van der Waals radii. In both cases, one Sb-N is slightly longer than the other.

Table 3.4.1: Selected bond lengths (Å) and angles (°) in the solid state structure of $[PhSbCl_2(dmap)_2]$ and $[PhSbCl(dmap)_2][OTf]$.

	$PhSbCl_2(dmap)_2$	$[PhSbCl(dmap)_2][OTf]$
Sb-N1	2.417(2)	2.3369(13)
Sb-N2	2.378(2)	2.3227(14)
Sb-Cl1	2.6702(9)	2.3737(4)
Sb-Cl2	2.5523(8)	-
Sb-O	-	3.99525(11)
$\Sigma_{r,cov}$(Sb,O)	2.03	
$\Sigma_{r,vdW}$(Sb,O)	3.58	
N1-Sb-N2	169.39(7)	169.32(5)
N1-Sb-Cl1	94.29(6)	84.82(3)
N1-Sb-Cl2	88.87(6)	-
N2-Sb-Cl1	90.11(6)	85.68(4)
N2-Sb-Cl2	85.87(6)	-

3.5. Dmap Complexes of Ph_2SbCl

Reaction of Ph_2SbCl with dmap in the presence of AgOTf or TMSOTf occurs rapidly to afford $[Ph_2Sb(dmap)_2][OTf]$. In the absence of a halide abstractor, the neutral complex $Ph_2SbCl(dmap)$ forms regardless of the stoichiometry imposed.

a) $Ph_2SbCl + dmap \longrightarrow Ph_2SbCl(dmap)$

b) $Ph_2SbCl + 2\ dmap + TMSOTf \xrightarrow[-TMSOTf]{} [Ph_2Sb(dmap)_2][OTf]$

c) $PhSbCl_2 + 2\ dmap + AgOTf \xrightarrow[-\ AgCl]{} [Ph_2Sb(dmap)_2][OTf]$

Scheme 3.5.1: Reaction of Ph_2SbCl with dmap and halide abstractor.

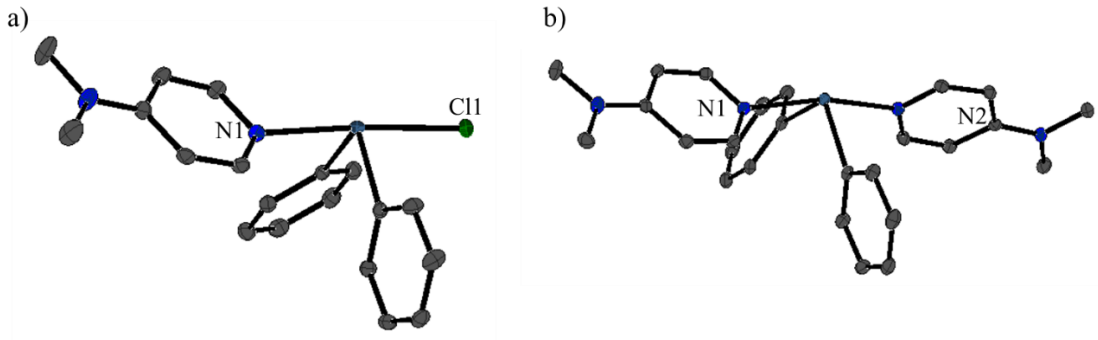

Figure 3.5.1: View of the antimony environment in the solid-state structures of a) $Ph_2SbCl(dmap)$, the cation in b) $[Ph_2Sb(dmap)_2][OTf]$. Hydrogen atoms and counter-ions are omitted for clarity. Thermal ellipsoids are shown at 50% probability.

In the solid state, both $Ph_2SbCl(dmap)$ and $[Ph_2Sb(dmap)_2][OTf]$ adopt a see-saw geometry about the antimony with the phenyl substituents occupying equatorial positions. The two Sb-N distances in $[Ph_2Sb(dmap)_2][OTf]$ are not equivalent, with one being extended compared to the other.

Table 3.5.1: Selected bond lengths (Å) and angles (°) in the solid state structure of $Ph_2SbCl(dmap)$ and $[Ph_2Sb(dmap)_2][OTf]$.

	$Ph_2SbCl(dmap)$	$[Ph_2Sb(dmap)_2][OTf]$
Sb-N1	2.392(2)	2.3819(12)
Sb-N2	-	2.3237(11)
Sb-Cl1	2.5881(6)	-
Sb-O	-	4.3648(9)
$\Sigma_{r,cov}$(Sb,O)	2.03	
$\Sigma_{r,vdW}$(Sb,O)	3.58	
N1-Sb-N2	-	167.77(4)
N1-Sb-Cl1	175.77(5)	-

3.6. Bipy Complexes of Ph_2SbCl

Isolating the product of the reaction of Ph_2SbCl with bipy reveals the formation of $PhSbCl_2$(bipy), rather than the expected Ph_2SbCl(bipy). Similarly, reaction of Ph_2SbCl with bipy in the presence of AgOTf or TMSOTf affords [PhSbCl(bipy)][OTf]. Performing the reaction in dilute solutions has no effect on the reactivity, suggesting redistribution may be occurring during crystallization. Comparison to the dmap derivatives show a preference for four-coordinate antimony: perhaps steric effects imposed by the phenyl substituents prevent the formation of five-coordinate Ph_2SbCl(bipy).

3.7. Bipy and dmap Complexes of Ph_3Sb

All attempts to form Ph_3Sb(bipy) or Ph_3Sb(dmap) have been unsuccessful. In the case of Ph_3Sb(dmap), ^1H NMR of the crude reaction mixture indicates an interaction

between the ligand and antimony center by a shift of the dmap resonances to higher frequencies, but all attempts at isolation result in free ligand and acceptor. This interaction in solution suggests that Ph_3Sb may be sufficiently Lewis acidic to form weak interactions with a donor, but the steric pressure imposed by the phenyl substituents is too great for complex formation.

3.8. Summary

Several series of Sb(III) pyridine complexes were synthesized and structurally characterized. The structural parameters were varied through the choice of ligand (either monodentate dmap or bidentate bipy), the substituents on antimony (either phenyl or chloride), and the cationic charge. It was found that TMSOTf is often insufficient for chloride abstraction. Unlike in the case of phosphine complexes of Sb(III), a *trans* configuration of monodentate ligands is often preferred. While the complexes $Ph_2SbCl(dmap)$ and $[Ph_2Sb(dmap)_2][OTf]$ are isolable, the equivalent bipy derivatives are not and result in substituent rearrangement to $PhSbCl_2(bipy)$ and [PhSbCl(bipy)][OTf], respectively.

Chapter 4: Reactivity of Complexes of $[Ph_2Sb]^{3+}$

The activation of small molecules by transition metal species has been studied extensively and these species are routinely used in catalytic transformations of substrates in both academia and industry. Conversely, the activation of small molecules by main group species has not received the same level of assessment. In recent years, however, this area of research has garnered a great deal of interest.[15],[61] One landmark example is the activation of dihydrogen with the aim to transfer the equivalent of H_2 to a substrate catalytically.

To perform these molecular transformations, transition metals engage in a variety of fundamental reactions that can be broadly categorized as oxidation, reduction, coordination, insertion, and reaction at the ligand. These reactivities are a consequence of the small energy gap between the d-orbital centered HOMO and LUMO of transition metal complexes. Main group complexes are able to simulate this electronic environment through multiple bonds between heavy main group elements,[81],[82] low-valent species with open coordination sites,[83],[84] and stable radical character.[85],[86] While the Pn(V) complexes synthesised in Chapter 2 do not possess these electronic characteristics, other transition metal chemistry should be accessible. The redox chemistry reported in Chapter 2 should be available in general for Sb(V) cations. Coordination reactions should be accessible with the use of a stronger donor. Finally, the electrophilic nature of complexes with large cationic charge may allow for ligand centered reactivity.

The new antimony(V) trications reported in Chapter 2 prompted an assessment of the reactivity of this class of compounds. The majority of these reactions were performed with $[Ph_2Sb(OPyrMe)_4][OTf]_3$, which is most readily synthesised and purified.

4.1. Ligand Substitution

Fundamental ligand substitution reactions could also offer a potential synthetic route to complexes that were inaccessible by direct synthesis from Ph_2SbCl_3, described in Chapter 2. To assess the lability of OPyrMe, synthesis of $[Ph_2Sb(OPEt_3)_4][OTf]_3$ was undertaken as ^{31}P NMR spectroscopy would easily confirm its formation. Treatment of $[Ph_2Sb(OPyrMe)_4][OTf]_3$ with four equivalents of $OPEt_3$ results in a species with a broad resonance at 87.1 ppm, assigned to incomplete substitution of OPyrMe for $OPEt_3$. If an excess, 4.5 equivalents, of $OPEt_3$ is used, complete substitution occurs and the desired $[Ph_2Sb(OPEt_3)_4][OTf]_3$ is formed as confirmed by $^{31}P\{^1H\}$ NMR spectroscopy. This demonstrates that OPyrMe is sufficiently labile to allow for ligand substitution and potential reactivity at the antimony center.

Synthesis of $[Ph_2Sb(dmap)_4][OTf]_3$ was targeted as its synthesis was previously hindered by the formation of $[Ag(dmap)_2][OTf]$, as described in Chapter 2. Reaction of $[Ph_2Sb(OPyrMe)_4][OTf]_3$ with 4.5 equivalents of dmap in a variety of solvents resulted in a pale yellow solution which turned dark red over 10 minutes of stirring. When the reaction was performed in CH_3CN, a substantial amount of protonated dmap is formed. In DCM, colourless crystals determined to be $[CH_2(dmap)_2][OTf]_2$ were isolated (**Figure 4.1.1**). This is surprising as $[Ph_2Sb(OPyrMe)_4][OTf]_3$ itself is formed and stable in DCM with no sign of decomposition over the course of weeks. Visually, the reaction proceeds analogously in DMF, DMSO, and CH_3NO_2, but the antimony species has yet to be identified.

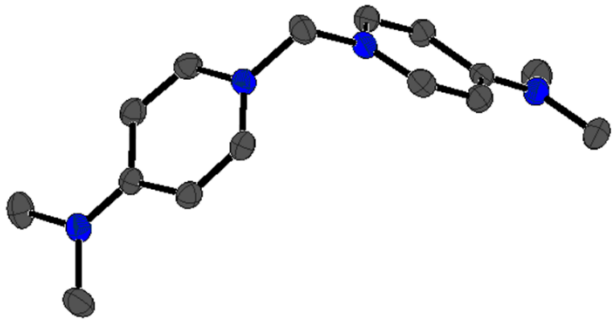

Figure 4.1.1: Solid-state state structure of the cation in $[CH_2(dmap)_2][OTf]_2$. All hydrogens and counter-anions omitted for clarity. Thermal ellipsoids are shown at 50% probability.

The ability of $[Ph_2Sb(OPyrMe)_4][OTf]_3$ to react with hydrogen was probed through the reaction of Me_2HNBH_3, which can be considered a source of pre-polarized H_2. Upon reaction, the solution turned pale yellow, consistent with the release of OPyrMe. The byproduct $[Me_2HNBH_2(OPyrMe)][OTf]$ was crystallized (**Figure 4.1.2**), indicating the transfer of a hydride to antimony with no reaction involving protic hydrogen. No evidence of an antimony hydride species was observed by ^1H NMR spectroscopy, but this is not unexpected as the large quadrupole moment of antimony often broadens out or masks atoms directly bound. This reactivity suggests that $[Ph_2Sb(OPyrMe)_4][OTf]_3$ may be able to act as the Lewis acid in a frustrated Lewis pair. On the other hand, addition of *t*Bu_3P, a common Lewis base for frustrated Lewis pair chemistry, results in separate reactivity that is discussed below.

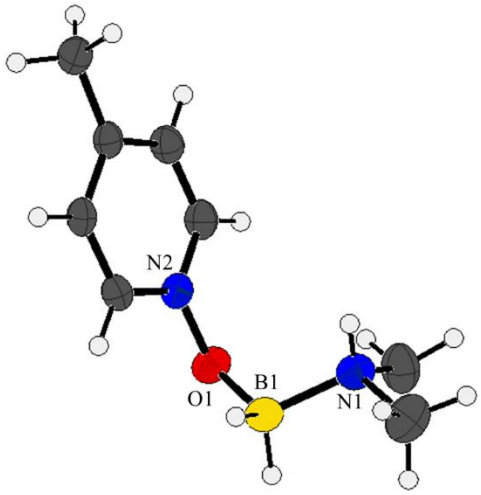

Figure 4.1.2: Solid-state state structure of the cation in $[Me_2HNBH_2OPyrMe][OTf]$. Counter-anion omitted for clarity. Thermal ellipsoids are shown at 50% probability.

4.2. Reactions with Phosphines

Prompted by the reductive elimination of chlorobenzene from the reaction of Ph_2SbCl_3 with bipy and TMSOTf as described in Chapter 2, the redox behaviour of $[Ph_2Sb(OPyrMe)_4][OTf]_3$ was investigated. No reaction occurred with a variety of metals (Mg, Zn, Cp_2Fe), with isolation of only starting material by ^1H NMR spectroscopy. Reaction with Na resulted in the immediate formation of an insoluble black precipitate, likely Sb metal.

While electron transfer has proven unsuccessful, another potential route for reduction is through the reaction of $[Ph_2Sb(OPyrMe)_4][OTf]_3$ with phosphines. Triphenylantimony bistriflate has been shown to oxidatively couple phosphines to diphosphonium dications along with reduction of antimony (**Scheme 4.2.1**).[39][48] The

mechanism of this reaction is unknown, but likely involves binding of the phosphine to antimony and the subsequent reductive elimination of a diphosphonium dication.[35]

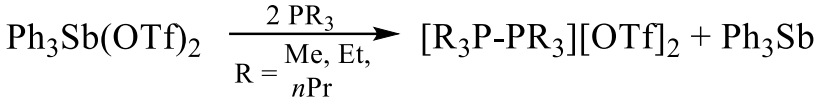

Scheme 4.2.1: Oxidative coupling of trialkylphosphines.

This chemistry has also been exploited to form novel cationic 4-membered antimony rings (**Scheme 4.2.2**).[49] The reaction of PMe_3 and $Sb(OTf)_3$, either prepared and isolated independently or generated *in situ* by reaction of SbF_3 and TMSOTf, results in the formation of $[Me_3P\text{-}PMe_3][OTf]_2$ and the cationic antimony ring $[(PMe_3)_4Sb_4][OTf]_4$. While the mechanism of this reaction is not known, it is believed that a highly electrophilic $[Sb(PMe_3)_3]^{3+}$ cation is formed and promptly undergoes reductive elimination to form $[Me_3P\text{-}PMe_3][OTf]_2$, as well as the intermediate $[Sb(PMe_3)]^+$ which then assembles into a tetraantimony ring.

Scheme 4.2.2: Reductive coupling to form a *catena* antimony complex.

While the reduction of antimony(IIII) resulted in *catena* antimony, reported reduction of antimony(V) resulted solely in the formation of the stable Ph_3Sb, and hence no *catenation*.[36] However, perhaps the reduced antimony species resulting from these antimony(V) trications would lead to interesting *catena* antimony(III) chains or rings. To

investigate this, reactions of $[Ph_2Sb(OPyrMe)_4][OTf]_3$ with various PR_3 phosphines were attempted.

Reactions of $[Ph_2Sb(OPyrMe)_4][OTf]_3$ with one to four equivalents of PMe_3 resulted in quantitative conversion to a single species by ^{31}P NMR spectroscopy with a resonance at 22.2 ppm, while reactions with more than four equivalents yielded the same species and unreacted PMe_3. This chemical shift does not correspond to the expected hexamethyldiphosphonium dication (^{31}P δ = 28.4 ppm) or another potential oxidation product, trimethylphosphine oxide (^{31}P δ = 36.2 ppm). Single crystals were grown and allowed for the identification of the phosphorus containing product as $[Me_3P$(2-4-methylpyridine)$][OTf]$, resulting from oxidation of phosphorus, and reduction of the nitrogen atom instead of the expected reduction of antimony.

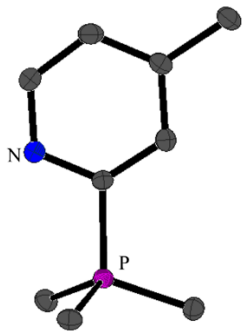

Figure 4.2.1: Solid-state structure of the cation in $[Me_3P$(2,4-methylpyridine)$][OTf]$. All hydrogen atoms and counter-anions omitted for clarity. Thermal ellipsoids are shown at 50% probability.

The generality of this reaction was investigated by performing the reaction with a variety of simple PR_3 phosphines and monitored with $^{31}P\{^1H\}$ NMR spectroscopy (**Figure 4.2.2**). Reactions with PEt_3 and P*n*Pr_3 proceeded analogously to PMe_3 with complete

consumption of phosphine and appearance of species with a resonance at 35.2 and 28.5 ppm, respectively. All three of these reaction mixtures possess a minor unidentified phosphorus-containing side product at slightly higher chemical shift than the major product. The similarity in chemical environment of this species leads us to believe this may be the *meta*-substituted product. When using PCy_3, the reaction proceeds similarly with a major product at 28.8 ppm, but the side product is much more prevalent in this reaction: if this side product is the *meta*-substituted pyridine, the high steric demand of PCy_3 would explain its prevalence. Reaction with PPh_3 results in a product at 15.2 ppm and a large amount of unreacted PPh_3. Finally, reactions with P*i*Pr$_3$ and P*t*Bu$_3$ proceed to very limited extent, consisting mostly of unreacted phosphine by $^{31}P\{^1H\}$ NMR. In the reaction with P*t*Bu$_3$, a pair of doublets at 83.4 ppm and 79.5 ppm, $J_{P\text{-}P}$ = 34Hz, may indicate the trace formation of a diphosphonium dication, albeit in very low yield. Crystals were isolated in the case of reaction with P*i*Pr$_3$ that verified that the species at 40 ppm was [*i*Pr$_3$P(2-4-methylpyridine)][OTf], indicating that phosphonium formation does occur but to a minute extent (**Figure 4.2.3**).

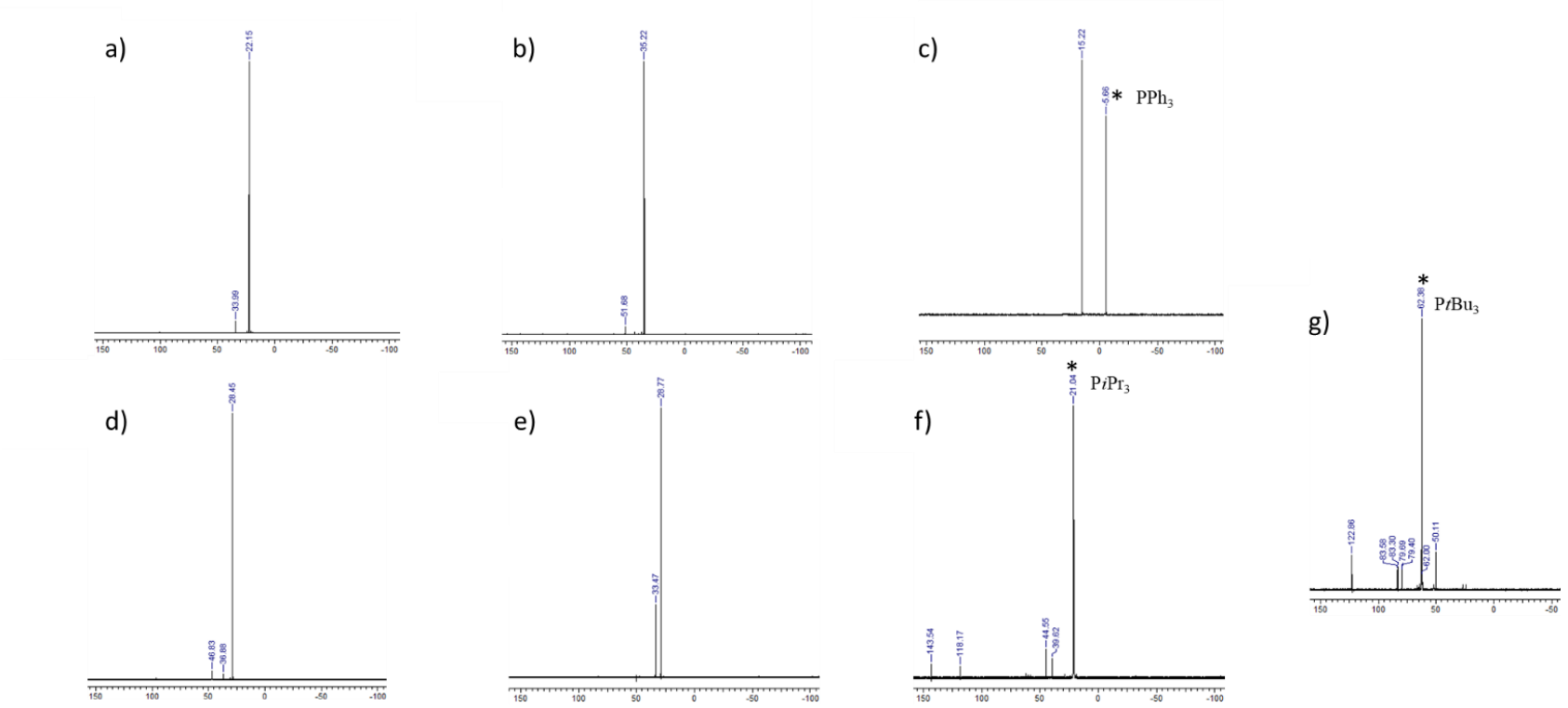

Figure 4.2.2: $^{31}P\{^{1}H\}$ NMR spectra of the reactions of $[Ph_2Sb(OPyrMe)_4][OTf]_3$ with four equivalents of a) PMe_3, b) PEt_3, c) PPh_3, d) P*n*Pr_3, e) PCy_3, f) P*i*Pr_3, or g) P*t*Bu_3.

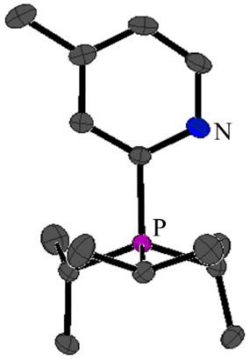

Figure 4.2.3: Solid-state structure of the cation in [*i*Pr$_3$P(2,4-methylpyridine)][OTf]. All hydrogen atoms and counter-anions omitted for clarity. Thermal ellipsoids are shown at 50% probability.

It is noteworthy that these reactions proceed analogously when [Ph$_2$Sb(OPyrMe)$_4$][OTf]$_3$ is generated *in situ* with no need to isolate or purify the antimony salt. In those reactions that resulted in complete conversion of phosphine (R = Me, Et, *n*Pr, Cy), the antimony byproduct is believed to be the anion [Ph$_2$Sb(OH)$_4$]$^-$ or its potential decomposition product [Ph$_2$Sb(O)(OH)$_2$]$^-$ (**Scheme 4.2.3**). This is supported by characterization of crystals isolated from the reaction with PPh$_3$ which structurally verified the antimony-containing product to be [Ph$_2$Sb(OPyrMe)$_3$(OH)][OTf]$_2$ (**Figure 4.2.4**).

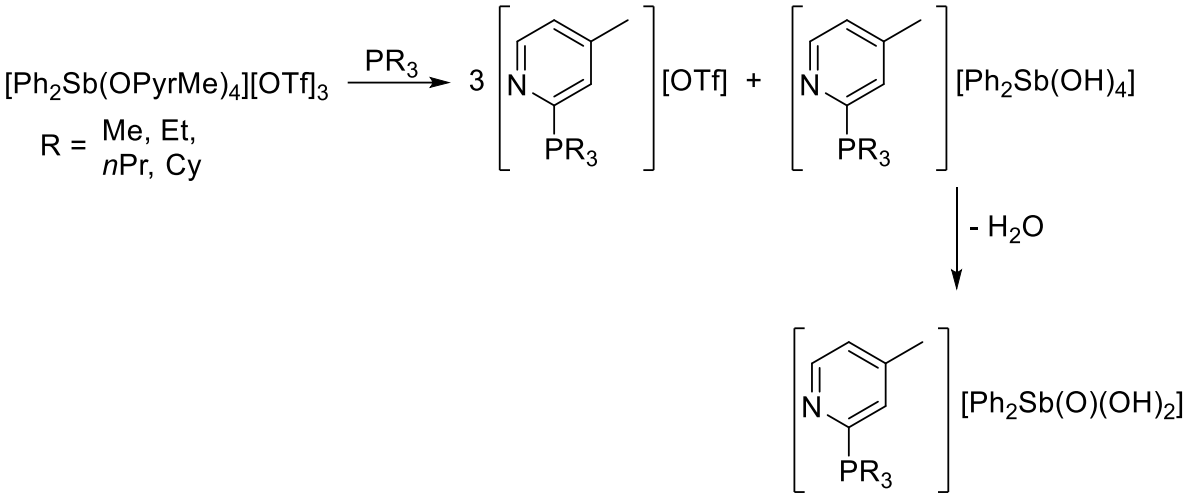

Scheme 4.2.3: Reaction of $[Ph_2Sb(OPyrMe)_4][OTf]_3$ with trialkylphosphines.

In the solid-state, the cation adopts a distorted octahedral environment at the antimony center with *trans* phenyl substituents (C-Sb-C = 172.9°). The Sb-O(H) bond length (1.974 Å) is similar to other terminal Sb(V)-O(H) distances,[87],[88],[89],[90] and significantly shorter than the Sb-O(PyrMe) bonds (2.121(4)-2.162(4) Å), consistent with the anionic OH substituent. One triflate is close to the hydroxy substituent (O-H---O(Tf) = 2.056), indicating a potential hydrogen bonding interaction. Additionally, there is an apparent loss of the π-interaction between the pyridine and phenyl ring in $[Ph_2Sb(OPyrMe)_3(OH)]^{2+}$ when compared to $[Ph_2Sb(OPyrMe)_4]^{3+}$.

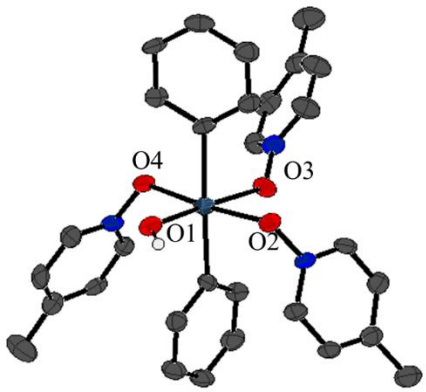

Figure 4.2.4: Solid-state structure of the cation in $[Ph_2Sb(OPyrMe)_3(OH)][OTf]_2$. Non-hydroxy hydrogen atoms and counter-anions omitted for clarity. Thermal ellipsoids are shown at 50% probability.

Among the scope of phosphines tested, there does not seem to be a clear trend of which reactions proceed to completion and which do not. Reactions involving PMe_3, PEt_3, P*n*Pr_3, and PCy_3 showed complete consumption of parent phosphine, while a significant amount of starting material remained for PPh_3, P*i*Pr_3, and P*t*Bu_3. Comparison of cone angles as a measure of steric bulk (**Table 4.2.1**) shows that PCy_3 lies between P*i*Pr_3, and P*t*Bu_3, meaning sterics cannot solely explain reactivity, nor can basicity since the donor ability of the alkyl phosphines is similar. That said, the incomplete reactivity of PPh_3 can be rationalized by its weak donor ability.

Table 4.2.1: Cone angle of phosphines employed.[91]

Phosphine	Cone Angle (°)
PMe_3	118
PEt_3	132
P*n*Pr_3	132
PPh_3	145
P*i*Pr_3	160
PCy_3	170
P*t*Bu_3	182

Mechanistically, the reaction is believed to follow a nucleophilic aromatic substitution (S_NAr) pathway in which the phosphine attacks the 2-position of the pyridine followed by deprotonation and subsequent rearomatization (**Scheme 4.2.4**). Nucleophilic attack of the pyridine is believed to be facilitated through coordination to antimony, which increases its electrophilicity. The antimony salt acts as the base to facilitate the rearomatization of the pyridine.

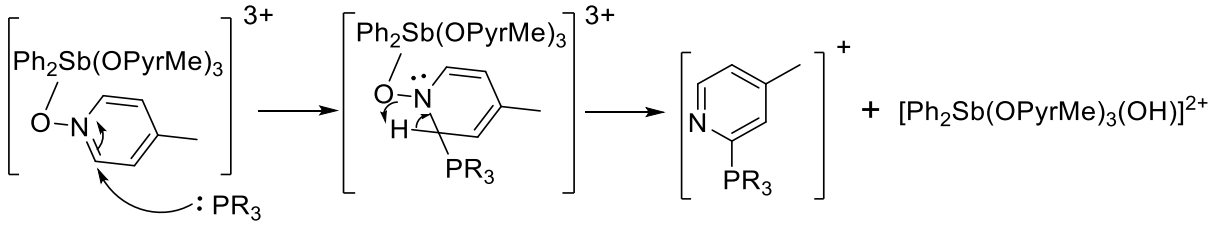

Scheme 4.2.4: Proposed pathway for the formation of phosphonium salt [R_3P(2-4-methylpyridine)]$^+$.

The oxidation state of antimony is significant for the reaction to occur. While reaction of $[Ph_2Sb(OPyrMe)_4][OTf]_3$ with PMe_3 occurs instantaneously, no evidence of reaction between *in situ* generated $[Sb(OPyrMe)_3][OTf]_3$ and PMe_3 was observed by ^{31}P NMR spectroscopy (**Scheme 4.2.5**).

$$SbF_3 + 3\ OPyrMe + 3\ TMSOTf \xrightarrow[-3\ TMSF]{} [Sb(OPyrMe)_3][OTf]_3 \xrightarrow{+\ PMe_3} \text{No Reaction}$$

Scheme 4.2.5: No reaction observed between *in situ* generated $[Sb(OPyrMe)_3][OTf]_3$ and PMe_3.

A similar mechanism has been proposed by the McNally group (**Scheme 4.2.6**) in which a pyridine is activated by reaction with triflic anhydride, followed by attack of PPh_3 and subsequently deprotonation and rearomatization by a base.[92] It is worth noting that this reaction is highly selective for installation of the phosphonium cation at the *para*-position. PPh_3 is the phosphine of choice due to its low cost and ease of use, although, for reasons not yet understood, the selectivity for the para-position is greater for PPh_3 than other phosphines.[93]

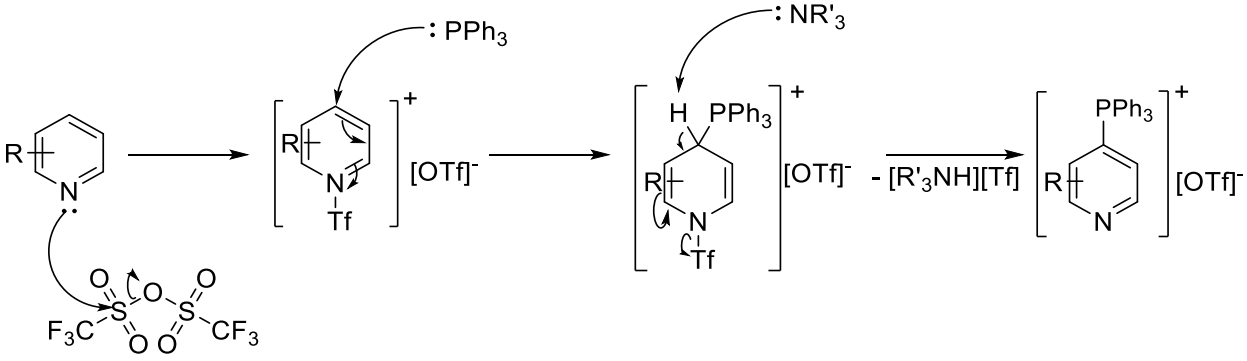

Scheme 4.2.6: Installation of phosphonium on a pyridine based substrates.

4.3. Applications of Phosphonium Salts

In 2016, Xiao *et al.* demonstrated that in the presence of caesium carbonate tetraarylphosphonium salts are able to perform, transition-metal free, nucleophilic arylation of carbonyls and imines.[94] These systems have the advantage over their transition metal counterparts of being relatively resilient to water and compatible with common functional groups such as cyano and ester moieties. It was found that the P-O affinity is a major driving force for the reaction.

More recently, the McNally group have used their triphenylphosphonium pyridine complexes to enact a variety of chemical transformations. It was found that phosphonium cations could act as pseudohalides in nickel catalyzed cross coupling reactions,[95] an effective leaving group for S_NAr reactions,[92],[96] enact amination of complex pro-drugs,[97],[98] and for the incorporation of deuterium and tritium into pyridines, diazines, and pharmaceuticals.[99]

In light of these findings, the activity of the synthesised phosphonium cations as aryl transfer reagents was investigated. [R_3P(2,4-methylpyridine)][OTf] (R = Me and Ph) were reacted with 4-chlorobenzaldehyde under the optimized reaction conditions reported by Xiao (**Scheme 4.3.1**).[94] ^{1}H NMR spectra show complete consumption of the starting benzaldehyde and formation of signals corresponding to the arylated product as well as the formation of phosphine oxide in the ^{31}P NMR. It is also worth noting that wet solvent was used with no apparent detriment to the reaction. In the case of R = Me, the reaction was repeated with an unpurified sample of [Me_3P(2-4-methylpyridine)][OTf] with no impact on product conversion.

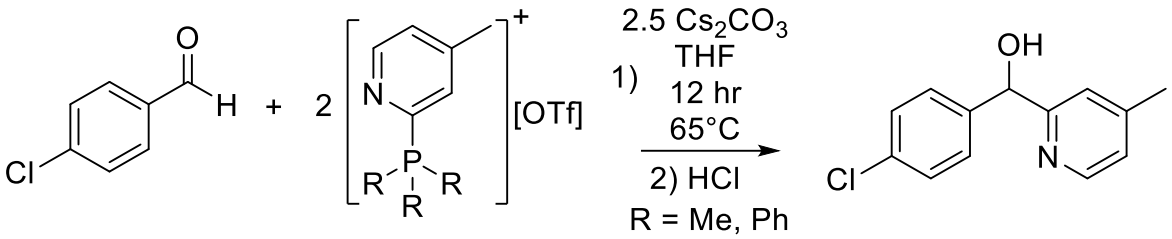

Scheme 4.3.1: Test reaction for arylation of 4-chlorobenzaldehyde.

Many drug fragments and therapeutic compounds contain pyridine moieties.[100] The facile synthesis of these phosphonium cations and their ability to transfer pyridine could offer a new, transition-metal free, synthetic route for medicinal chemists. Future investigation of addition of phosphine to the *meta*- and *para*-position of pyridine would be valuable and allow for greater flexibility in regiochemistry of drug fragments that could be produced by this method.

4.4. Summary

Investigation of the reactivity available to the novel $[Ph_2Sb(OPyrMe)_4][OTf]_3$ was initiated. It was found that the OPyrMe ligands are sufficiently labile to perform ligand substitution chemistry which may act as a route to complexes unobtainable from Ph_2SbCl_3 directly. However, simple ligand exchange does not occur when reacted with phosphines: instead, ligand-centered reactivity prevails. It was found that reactions of $[Ph_2Sb(OPyrMe)_4][OTf]_3$ and phosphines result in attack of the phosphine at the 2-position of the pyridine ring, along with reduction of nitrogen to yield the phosphonium salt [R_3P(2-4-methylpyridine)][OTf] and corresponding antimony hydroxide. Formation of phosphonium proceeds to completion by ^{31}P NMR spectroscopy for R = Me, Et, *n*Pr,

and Cy. These phosphoniums have the ability to transfer a pyridine to organic substrates which could offer a new, transition-metal free synthetic route for medicinal chemists.

Chapter 5: Attempted routes to tetra- and penta-cationic Pn(V)

As mentioned previously, there remains a vast amount of chemical space to explore in the area of Pn(V) cations, with no examples of Pn(V) tri-, tetra-, or penta-cations prior to this thesis. Synthesis and characterization of $Sb(V)^{3+}$ cations were reported in Chapter 2, but synthesis of higher charged analogues remains elusive. Much work remains in this area to develop methodologies necessary to realize these highly charged species. Hopefully, this chapter will assist future researchers in pursuing these compounds.

5.1. Attempted Synthesis of $RSbX_4$

While Ph_2SbCl_3 was a useful reagent in the preparation of tricationic antimony(V) species, finding a suitable precursor for tetra-cationic species has been more problematic. Analogous to Ph_2SbCl_3, literature states $PhSbCl_4$ can be synthesised through the mixture of $SbCl_3$ and Ph_3Sb in a 2:1 ratio followed by oxidation with a source of Cl_2.[38] Alternatively, the intermediate $PhSbCl_2$ can be isolated and oxidized (**Scheme 5.1.1**).

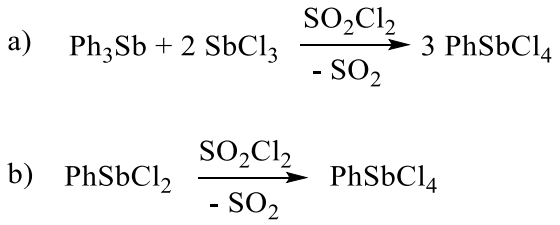

Scheme 5.1.1: Synthetic routes to $PhSbCl_4$.

Both synthetic routes proceed similarly, and while there is evidence for the formation of $PhSbCl_4$, it is not pure according to ^1H NMR spectroscopy and melting point. Attempts to purify the sample by crystallization in various solvent systems

yielded only Ph_2SbCl_3. This rearrangement likely involves the dimerization of $PhSbCl_4$ followed by a substituent rearrangement to yield Ph_2SbCl_3 and the colourless liquid $SbCl_5$ (**Scheme 5.1.2**), which is unobservable by standard NMR techniques.

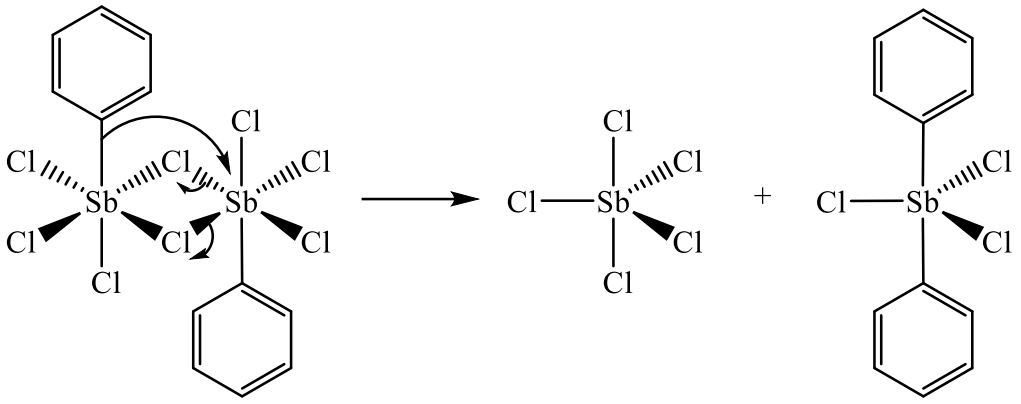

Scheme 5.1.2: Potential rearrangement pathway $PhSbCl_4$.

In efforts to prevent this rearrangement, a series of modifications were undertaken to attempt to isolate $PhSbX_4$ (**Scheme 5.1.3**). Firstly, the reaction mixture containing $PhSbCl_4$ was treated with either TMSOTf or AgOTf, working off the rationale that $PhSbCl_3(OTf)$ may be less prone to rearrangement; however, no pure material could be isolated from these reactions as demonstrated by broad melting point ranges. The rate of substituent rearrangement is reported to be slowest for fluoride,[101] so $PhSbF_2Cl_2$ and $PhSbF_4$ were targeted. Attempts to form $PhSbF_2Cl_2$ were carried out by oxidation of $PhSbCl_2$ with XeF_2. The attempted synthesis of $PhSbF_4$ involved first the formation of $PhSbF_2$, which was successfully performed through salt metathesis of $PhSbCl_2$ and CsF followed by oxidation of XeF_2. In the end, however, neither $PhSbCl_2F_2$ or $PhSbF_4$ could be isolated. Melting points of isolated solids displayed broad ranges and ^{19}F NMR showed

multiple fluorine containing species. These could be the result of substituent rearrangement or fluorination of the glass vials used.

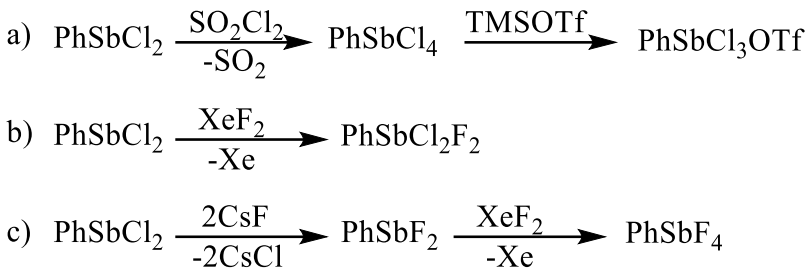

Scheme 5.1.3: Attempted synthetic routes to $PhSbX_4$, of which all failed.

5.2. Synthesis and Reactivity of $PhPX_4$

As the isolation of $PhSbX_4$ was problematic, other sources of $RPnX_4$ were investigated. Phosphorus was the pnictogen of choice, as attempts to synthesis Bi(V) cations was plagued with decomposition to bismuth metal and sources and As(V) are relatively uncommon. Additionally, phosphorus provides a useful NMR handle for monitoring reactions.

The synthesis of $PhPCl_4$ was attempted by the oxidation of the commercially available $PhPCl_2$ (**Scheme 5.2.1**). Attempts to chlorinate $PhPCl_2$ with SO_2Cl_2 led to the formation of a single product which resonates at 33.6 ppm in ^{31}P NMR, determined to be $PhP(O)Cl_2$. The reaction was repeated multiple times and with different samples of SO_2Cl_2 and freshly dried solvents to verify that the oxygen is originating from SO_2Cl_2. No reaction occurred between $PhPCl_2$ and C_2Cl_6 over the course of 24 hours. Reaction with $SeCl_4$ or PCl_5 were, however, more promising.

a) $PhPCl_2 \xrightarrow{SO_2Cl_2} PhP(O)Cl_2$

b) $PhPCl_2 \xrightarrow{C_2Cl_6}$ No Reaction

c) $PhPCl_2 \xrightarrow{SeCl_4} PhPCl_4 + [PhPCl_3][Cl]$

d) $PhPCl_2 \xrightarrow{PCl_5} PhPCl_4 + [PhPCl_3][Cl]$

Scheme 5.2.1: Attempted synthesis of $PhPCl_4$.

When $SeCl_4$ or PCl_5 was used as the oxidant in DCM two species were isolated, one which remained in solution while the other precipitated out. $^{31}P\{^1H\}$ NMR was acquired on both species and allowed for the assignment of the precipitate as the ionic formulation $[PhPCl_3][Cl]$ (δ = 98.9 ppm), and the filtrate as the molecular formulation $PhPCl_4$ (δ = -33.9 ppm).[102] Further support for these assignments is provided by the reaction of species with AgOTf resulting in the identical product. Unfortunately, the stability of both formulations is quite low in solution. A solution of $PhPCl_4$, in either molecular or ionic form, in CH_3CN changes from colourless to orange over 10 minutes, $^{31}P\{^1H\}$ spectroscopy showing loss of $PhPCl_4$ and the formation of several new species from 47-26 ppm, a range associated with P(III). This is also observed in solutions of DCM, but over the course of an hour rather than minutes. Addition of a ligand to try to stabilize $PhPCl_4$ only accelerates the decomposition.

As the use of $PhPCl_4$ as a reagent was problematic it was decided to target $PhPF_4$. The P-F bond is much stronger than P-Cl (405 kJ/mol *vs.* 376 kJ/mol)[103] which was expected to prevent the reductive decomposition that was observed for $PhPCl_4$. Additionally, the high Si-F affinity should allow for ease of fluoride abstraction by TMSOTf when

synthesizing cations. A survey of the literature resulted in one published synthesis of $PhPF_4$,[104] which was modified for this work (**Scheme 5.2.2**). Four equivalents of SbF_3 were added to neat $PhPCl_2$ and heated at 60 °C for one hour, after which $PhPF_4$ was isolated as a colourless liquid *via* distillation between 134-136 °C. $^{31}P\{^1H\}$ NMR spectroscopy shows a pentet centered at -50.3 ppm with $^1J_{P-F}$ = 963 Hz with a corresponding doublet center at -54.6 ppm in the ^{19}F NMR.

$$PhPCl_2 + 4\ SbF_3 \xrightarrow[-\ 2\ Sb]{-\ 2\ SbCl_3} PhPF_4$$

Scheme 5.2.2: Synthesis of $PhPF_4$.

The reactivity of $PhPF_4$ with a variety of donors was investigated. No reaction occurs when $PhPF_4$ is combined with TMSOTf. However, upon addition of dmap, $PhPF_4$ is consumed and a mixture of products forms, with the major product showing overlapping doublet of triplets (^{31}P δ = -141.9 ppm J_{P-F} = 882, 742 Hz) in the $^{31}P\{^1H\}$ NMR along with a set doublet of doublets (^{19}F δ = -67.2 ppm J_{P-F} = 882 Hz, J_{F-F} = 38 Hz) and triplet of doublets (^{19}F = -38.3 ppm, J_{P-F} = 742 Hz, J_{F-F} = 38 Hz) with a 2:1 integration in the ^{19}F NMR. This is consistent with an octahedral structure with two chemically inequivalent fluorine environments. Crystallization from a saturated DCM solution layered with Et_2O yielded X-ray quality crystals which have been characterized as $[PhPF_3(dmap)_2][OTf]$ (**Figure 5.2.1**).

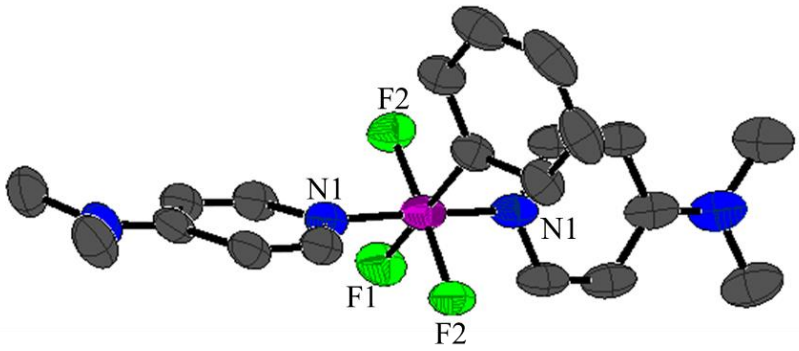

Figure 5.2.1: Solid-state structure of the cation in $[PhPF_3(dmap)_2]$. All hydrogen atoms and counter anions omitted for clarity. Thermal ellipsoids are shown at 50% probability.

In the solid-state, the cation in $[PhPF_3(dmap)_2][OTf]$ adopts an octahedral geometry about phosphorus with the two dmap ligands *trans* to each other. The two P-F bonds show no difference in length. This is in contrast to $K[PhPF_5]$ in which the fluorine *trans* to phenyl is significantly shorter (1.5857(19) Å) than those *trans* to other fluorines (average 1.6356(16) Å). This difference may be due to F---K interactions present in $K[PhPF_5]$. The P-N bond length is slightly shorter than that of PF_5(pyridine) (1.8849(2) Å).[105]

Table 5.2.1: Selected bond lengths (Å) and angles (°) in the solid-state structures of $[PhPF_3(dmap)_2][OTf]$.

	$[PhPF_3(dmap)_2][OTf]$
P-F1	1.6187(17)
P-F2	1.6162(11)
P-N1	1.849(2)
N1-P-N2	174.41(11)
N1-P-F1	87.21(5)
F2-P-N1	90.15(7)
F1-P-F2	87.90(5)
F2-P-F3	175.79(10)

While $PhPF_4$ is stable when stored in a glass vial at -35 °C for months, $[PhPF_3(dmap)_2][OTf]$ is much more reactive. A solution of $[PhPF_3(dmap)_2][OTf]$ was stored for a week in a glass vial at -35 °C after which crystals determined to be $PhP(O)_2(dmap)$ were isolated. $^{31}P\{^1H\}$ NMR of the solution shows the complete loss of $[PhPF_3(dmap)_2][OTf]$ and the formation of various phosphorus-containing species. This decomposition is likely occurring through fluorination of the glass vial as etching of the glass was observed.

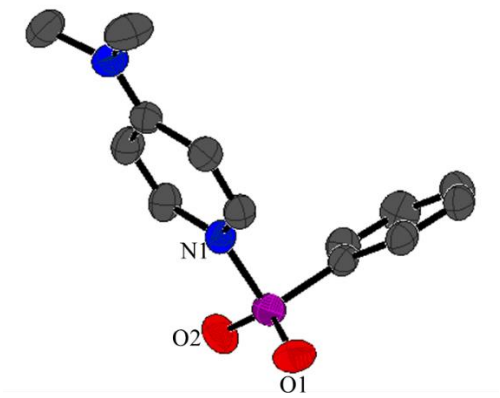

Figure 5.2.2: Solid-state structure of $PhP(O)_2(dmap)$. All hydrogens omitted for clarity. Thermal ellipsoids are shown at 50% probability.

Attempts to synthesise higher charged species by further abstraction of fluoride from $[PhPF_3(dmap)_2][OTf]$ were unsuccessful. No reaction occurs in a mixture of $[PhPF_3(dmap)_2][OTf]$ with varying equivalents of TMSOTf and dmap by $^{31}P\{^1H\}$ NMR spectroscopy. Boiling in neat TMSOTf also fails to abstract a second equivalent of fluoride, with only $[PhPF_3(dmap)_2][OTf]$ and the known [TMS-dmap][OTf][106] being isolated. Other donors (OPyrMe, bipy, pyridine, trialkylphosphines, and $OPEt_3$) and alternative fluoride abstractors (AgOTf, $Ph_3Sb(OTf)_2$, and $SbCl_5$) were attempted, resulting in either abstraction of only a single fluoride or decomposition. We believe the already strong P-F bond is being enhanced through the incorporation of a cationic charge, increasing the difficulty of subsequent fluoride abstraction.

5.3. Attempted Synthesis of tBuPF$_4$

Since the abstraction of multiple fluorides from $PhPF_4$ was not possible, further modification was attemped. Specifically, *t*$BuPF_4$ was targeted, with the hope that the bulky *t*Bu substituent would encourage the dissociation of fluoride and allow for the formation of highly charged species. First, in an analogous procedure to the synthesis of $PhPF_4$, *t*$BuPCl_2$ was reacted with four equivalents of SbF_3, but resulted only in trace amounts of *t*$BuPF_4$, with *t*$BuPF_2$ being the major product as determined by $^{31}P\{^1H\}$ spectroscopy. Survey of the literature reveals a one-pot synthesis in which SbF_3 is added to neat *t*$BuPCl_2$ followed by the addition of Cl_2 resulting in the formation of *t*$BuPF_4$.[107] Presumably, *t*$BuPCl_2$ reacts with SbF_3 to form *t*$BuPF_2$ which is then oxidized by Cl_2 and exchanged for fluoride from another equivalent of SbF_3 (**Figure 5.3.1**).

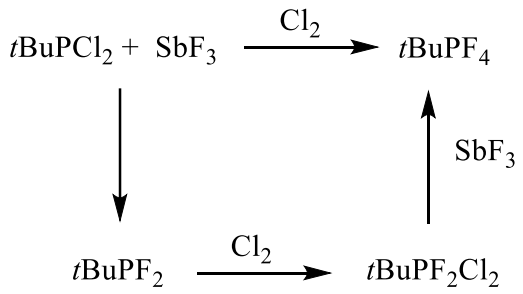

Figure 5.3.1: Pathway for the reported synthesis of *t*$BuPF_4$.

To emulate this reaction, SbF_3 was added to *t*$BuPCl_2$, and SO_2Cl_2 or $SeCl_4$ were subsequently added as sources of chlorine; this was done either at room temperature, -78 °C, or -96 °C. In all cases, a black precipitate formed and no distillate could be collected.

Filtration of this black precipitate produced only a few drops of liquid which contained many phosphorus species as determined by $^{31}P\{^{1}H\}$ spectroscopy.

To simplify the synthetic procedure, the direct fluorination of *t*BuPF$_2$ by XeF$_2$ was attempted. Addition of XeF$_2$ to neat *t*BuPF$_2$ inside a glovebox resulted in a small fire immediately upon addition of reagents. Attempts to control the exothermic nature of this reaction by dropwise addition of a solution of XeF$_2$ to a solution of *t*BuPF$_2$ also yielded the same result. This route was then abandoned without further exploration.

5.4. Reactions of PCl_5 and $SbCl_5$

While the synthesis of a RPnX$_4$ was problematic, PCl$_5$ and SbCl$_5$ are commercially available and could act as precursors to $[PnCl]^{4+}$ and $[Pn]^{5+}$ species. Choice of ligand and reaction conditions are of paramount importance due to the high electrophilicity imposed by the high cationic charge. This is demonstrated by reactions of PCl$_5$ or SbCl$_5$ with nitrogen-based donors (dmap, bipy, BIMEt$_3$, and tris(2-pyridylmethyl)amine)) in the presence of AgOTf in CH$_3$CN or DCM, all resulting in the isolation of protonated ligand. Without the halide abstractor, however, reaction of SbCl$_5$ and dmap results in the precipitation of SbCl$_5$(dmap) which has been crystallographically characterized (**Figure 5.4.1**).

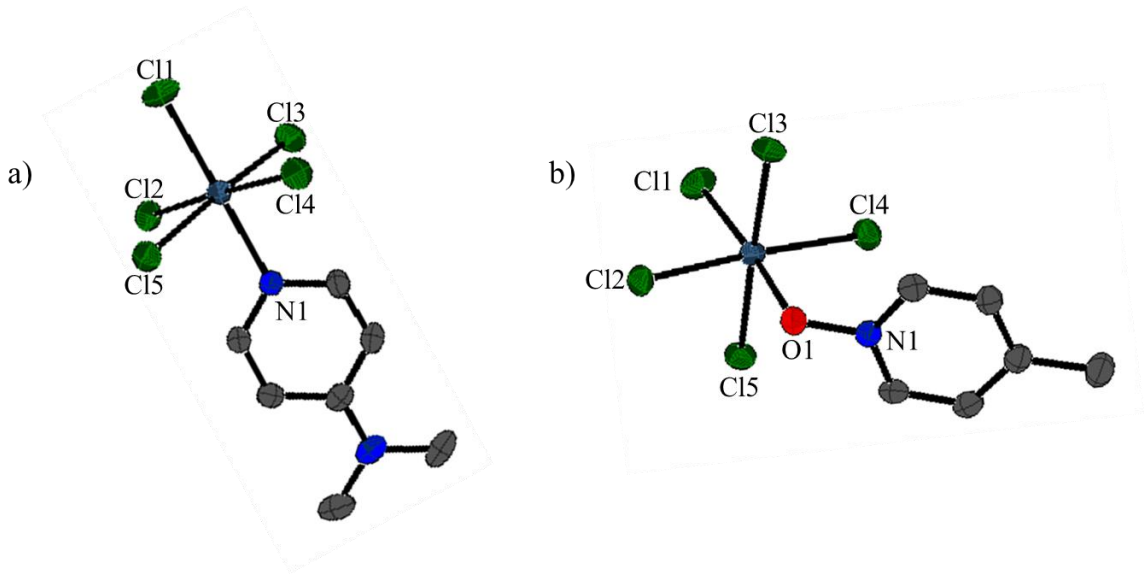

Figure 5.4.1: Solid-state structure of the cation in a) $SbCl_5$(dmap) and b) $SbCl_5$(OPyrMe). All hydrogen atoms omitted for clarity. Thermal ellipsoids are shown at 50% probability.

In the solid-state, both $SbCl_5$(dmap) and $SbCl_5$(OPyrMe) adopt an octahedral geometry about antimony. The Sb-N bond length in $SbCl_5$(dmap) is comparable to that of $SbCl_5${(N(*i*Pr)CN(*i*Pr)}[108] (2.153(4) Å) and shorter than that of Ph_2SbCl_3(dmap) (2.2334(13) Å), consistent with the potent Lewis acidity of $SbCl_5$. Similarly, the Sb-O bond length in $SbCl_5$(OPyrMe) is shorter than that of Ph_2SbCl_3(OPyrMe) (2.1779(12) Å). Sb-Cl1 is slightly shorter in both compounds than the remaining Sb-Cl bonds. This is also seen in $SbCl_5${(N(*i*Pr)CN(*i*Pr)} and $SbCl_5(NCCH_3)$.[108]

Table 5.4.1: Selected bond lengths (Å) and angles (°) in the solid-state structures of $SbCl_5$(dmap) and $SbCl_5$(OPyrMe).

	$SbCl_5$(dmap)	$SbCl_5$(OPyrMe)
Sb-N1	2.1497(3)	-
Sb-O1	-	2.072(2)
Sb-Cl1	2.3354(3)	2.3470(10)
Sb-Cl2	2.3566(5)	2.3568(9)
Sb-Cl3	2.3543(5)	2.3670(9)
Sb-Cl4	2.3638(5)	2.3521(9)
Sb-Cl5	2.3820(5)	2.3727(8)
Average Sb-Cl	2.3648(3)	2.3591(9)

Due to the success of oxygen-based donors in stabilizing complexes of $[Ph_2Sb]^{3+}$, we believed that they could be applied to the analogous higher charged species. Therefore, we investigated the reaction of $PnCl_5$ with OPyrMe and 2,2′-dipyridyl *N,N*′-dioxide (bipy-O_2) (**Scheme 5.4.1**). Unfortunately, obtaining X-ray quality crystals of these reactions has so far been unsuccessful, and analysis is currently dependent on NMR. This complicates analysis of reactions involving $SbCl_5$ as the only nuclei available for NMR analysis are those of the ligand which do not provide any insight on the species formed. Additionally, attempts to crystallize the products of these reactions results in a colourless solid slowly precipitating from solution, and which cannot be redissolved: this may be indicative of decomposition.

$$PnCl_5 + n\ OPyrMe + m\ AgOTf \xrightarrow[n = 1 - 6,\ m = 0 - 5]{Pn = P,\ Sb}$$

$$PnCl_5 + n\ bipy\text{-}O_2 + m\ AgOTf \xrightarrow[n = 2,3,\ m = 3 - 5]{Pn = P,\ Sb}$$

Scheme 5.4.1: Reactions of $PnCl_5$ with oxygen donors.

Reactions involving PCl_5 lend more insight into the formation of these highly charged complexes due to the availability of ^{31}P NMR. Reactions of PCl_5 with 2, 3, 4, 5, 6, and equivalents of OPyrMe and 1, 2, 3, 4, 5 equivalents of AgOTf results in the formation of increasingly dark red solutions and the precipitation of AgCl. After filtration, $^{31}P\{^1H\}$ NMR spectra of all five samples showed a mixture of products (**Figure 5.4.2**). As the ratio of OPyrMe and AgOTf is increased the relative integration of resonances at -4.2 ppm and -120 ppm increases compared to the species at -130 and -157 ppm. Further addition of OPyrMe and AgOTf to reactions a) to c) results in a spectrum identical to b) to d). This leads us to believe that the resonance -157.6 ppm, -145.4 ppm, -130.6 ppm, -119.2 ppm, and -4.2 ppm correspond to $[PCl_2(OPyrMe)_4]^+$, $[PCl_2(OPyrMe)_4]^{2+}$, $[PCl_2(OPyrMe)_4]^{3+}$, $[PCl(OPyrMe)_5]^{4+}$, and $[P(OPyrMe)_6]^{5+}$, respectively. It is expected that an excess of OPyrMe would result in the formation of only the species at -4.2 ppm.

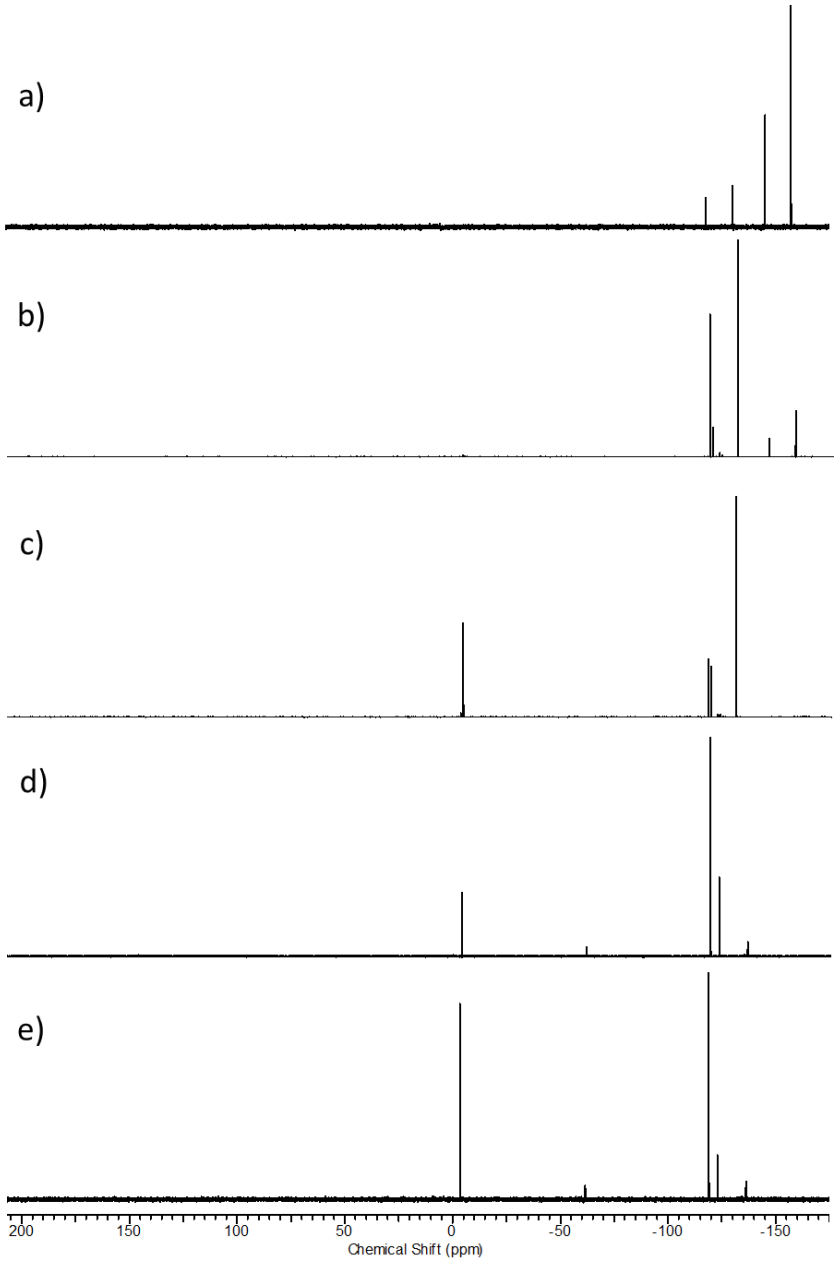

Figure 5.4.2: $^{31}P\{^{1}H\}$ NMR spectra of the reaction of PCl_5 with a) 2 equivalents of OPyrMe and 1 equivalents of AgOTf b) 3 equivalents of OPyrMe and 2 equivalents of AgOTf, c) 4 equivalents of OPyrMe and 4 equivalents of AgOTf, d) 5 equivalents of OPyrMe and 4 equivalents of AgOTf and, e) 6 equivalents of OPyrMe, and 5 equivalents of AgOTf.

Reaction of PCl_5 with the chelating ligand bipy-O_2 in the presence of AgOTf proceeds similarly. Due to the bidentate nature of bipy-O_2 and the apparent preference of phosphorus to adopt an octahedral geometry, sequential abstraction of halide is unfeasible, such that only $[PCl_4(O_2\text{-bipy})]^+$, $[PCl_2(O_2\text{-bipy})_2]^{3+}$, and $[P(O_2\text{-bipy})_3]^{5+}$ are likely to be attainable. Reactions of PCl_5 with 1, 2, and 3 equivalents of bipy-O_2 to a mixture of PCl_5 and AgOTf results in the precipitation of a large amount of colourless solid, more than can be accounted for by AgCl alone. The phosphorus-containing products can be extracted from AgCl after several washes with CH_3CN. $^{31}P\{^1H\}$ NMR spectrum of the reaction of PCl_5 with one equivalent of bipy-O_2 and AgOTf shows conversion to a single product with resonance a resonance at -147.2 ppm. Conversely, reaction of PCl_5 with 2 or 3 equivalents of bipy-O_2 and 3 or 5 equivalents of AgOTf results in a mixture of products, with a species at -0.2 ppm as the major product (**Figure 5.4.3**). Again, with further addition of bipy-O_2 and AgOTf reactions a) and b) can be converted to b) and c), respectively, leading us to believe that the resonance at -101.4 ppm, and -0.2 ppm correspond to $[PCl_2(O_2\text{-bipy})_2]^{3+}$ and $[P(O_2\text{-bipy})_3]^{5+}$.

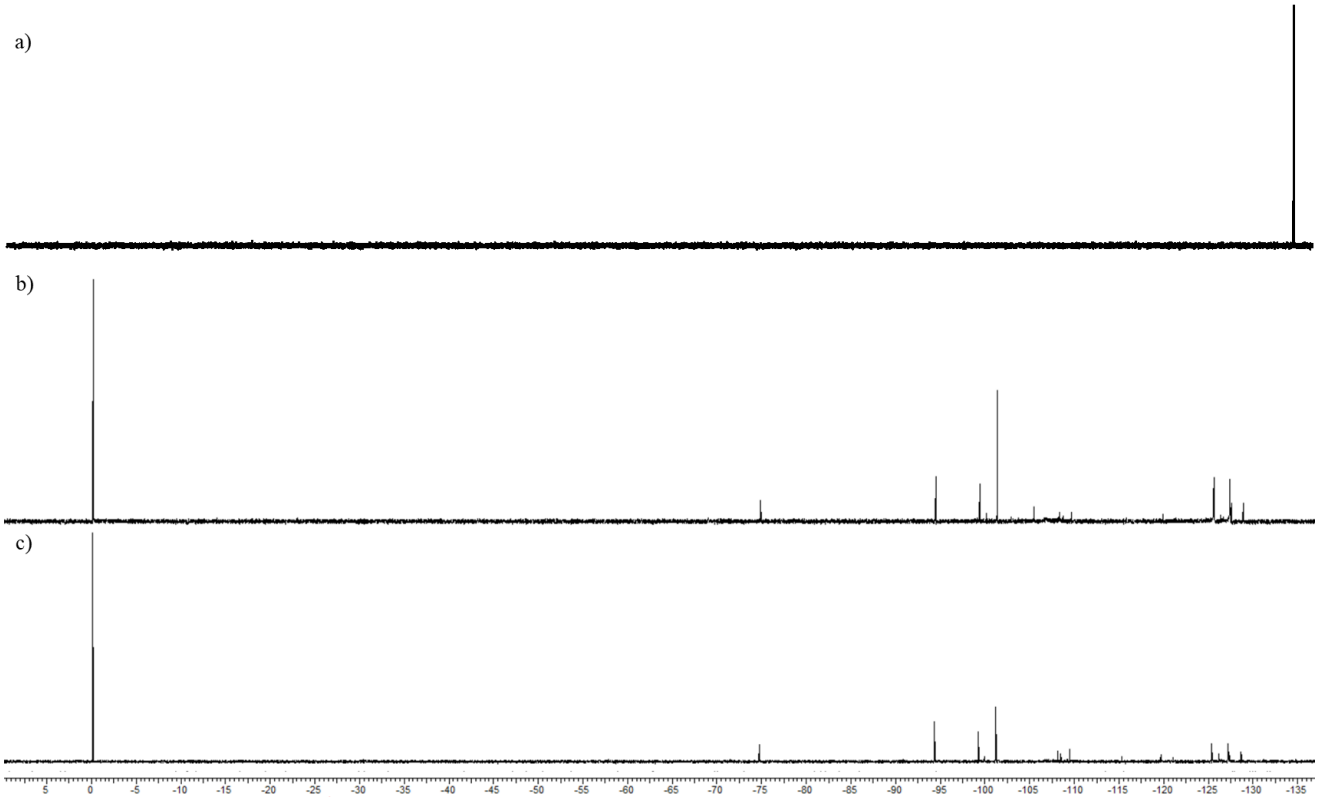

Figure 5.4.3: $^{31}P\{^{1}H\}$ NMR spectra of the reaction of PCl_5 with a) 1 equivalents of bipy-O_2 and 1 equivalents of AgOTf, b) 2 equivalents of bipy-O_2 and 3 equivalents of AgOTf, and c) 3 equivalents of bipy-O_2 and 5 equivalents of AgOTf.

5.5. Summary

Attempts to form unprecedented Pn(V) tetra- and penta-cations have, as of yet, been unsuccessful. Unfortunately, a suitable precursor to systematically approach the synthesis of these complexes has yet to be identified. Efforts to synthesise compounds of generic formula $PhSbX_4$ (X = Cl, F) were hampered by substituent rearrangement. $PhPF_4$ was successfully synthesized, but the strong P-F bond impedes fluoride abstraction. Conversely, $PhPCl_4$ is exceptionally reactive and reductively decomposes in a matter of minutes in CH_3CN or an hour in DCM. Reactivity of $SbCl_5$ was investigated, resulting in

the formation of $SbCl_5$(dmap) and $SbCl_5$(OPyrMe), however, attempts to abstract the halides have resulted in decomposition. Reactions of PCl_5 with mono- and bi-dentate oxygen donors seem promising based on observed ^{31}P NMR spectra, but isolation of these highly charged species remains problematic.

Chapter 6: Summary and Future Directions

The field of main group chemistry has experienced a renewed interest over the last couple decades, fuelled by the discovery of exotic structural and bonding motifs. Much academic research has been devoted towards the development of transition metal-like reactivity; although, before we are able to intelligently approach the reactivity of these species, there must be a fundamental understanding of their structure and bonding. The work presented in this dissertation focuses primarily on the structural characterization of a series of pnictogen complexes with an emphasis on species that possess a large cationic charge, in addition to some preliminary reactivity of these new compounds.

The objective of Chapter 2 was to expand the scope of known coordination chemistry of pnictogen(V) compounds. In service to this, several series of antimony(V) cations featuring nitrogen and oxygen donors were synthesized and structurally characterized, including the first examples of pnictogen(V) trications. Two different routes were explored: halide abstraction-ligand substitution from an Sb(V) precursor, and oxidation of a previously synthesized Sb(III) cation. The structural trends upon increasing cationic charge and the effects of steric bulk were discussed. During preparation of these compounds, redox chemistry was observed, and determined to be the result of reductive elimination of chlorobenzene and biphenyl from an antimony center. This process was studied in depth, and leads us to believe the redox chemistry is facilitated through a buildup of cationic charge which cannot be effectively stabilized by the ligands. Further investigation into the conditions required to selectively achieve redox chemistry is required. We believe that the use of a weakly activated or deactivated bipy derivatives (*e.g.*

4,4’-di-fluoro-2,2’-dipyridyl, 4,4’-di-nitro-2,2’-dipyridyl) would further facilitate redox chemistry given their weaker donor strength when compared to bipy.

In Chapter 3, a series of Sb(III) pyridine complexes were synthesized and structurally characterized. The structural parameters were varied through the choice of ligand (either monodentate dmap or bidentate bipy), the substituents on antimony (either phenyl or chloride), and the cationic charge. It was found that, unlike in the case of phosphine complexes of Sb(III), a *trans* configuration of ligands is preferred.

Chapter 4 begins to explore the reactivity of $[Ph_2Sb(OPyrMe)_4][OTf]_3$. It was found that the OPyrMe ligands are sufficiently labile to perform ligand substitution chemistry. However, simple ligand exchange does not occur when reacted with phosphines: instead, ligand-centered reactivity prevails. It was found that reactions of $[Ph_2Sb(OPyrMe)_4][OTf]_3$ and phosphines result in attack of the phosphine at the 2-position of the pyridine ring, along with reduction of nitrogen to yield the phosphonium salt $[R_3P(2\text{-}4\text{-methylpyridine})][OTf]$ and corresponding antimony hydroxide. Formation of phosphonium proceeds to completion by ^{31}P NMR spectroscopy for R = Me, Et, *n*Pr, and Cy. These phosphoniums have the ability to transfer a pyridine to organic substrates which could offer a new, transition-metal free synthetic route for medicinal chemists. The potential to add phosphine to the meta- and para-position of pyridine would be valuable in its provision of greater flexibility in regiochemistry of drug fragments, but must be further studied.

The work in Chapter 5 attempts to form unprecedented Pn(V) tetra- and penta-cations. Unfortunately, a suitable precursor to systematically approach the synthesis of these complexes has yet to be identified. Attempts to synthesise compounds of generic formula $PhSbX_4$ (X = Cl, F) were hampered by substituent rearrangement. $PhPF_4$ was

successfully synthesized, but the strong P-F bond impedes fluoride abstraction. Survey of the literature indicates that one example of $RSbX_4$, $Mes_2C_6H_3SbCl_4$ (Mes = 2,4,6-$Me_3C_6H_2$), has been isolated. The bulky terphenyl substituent likely prevents bridging interactions that are required for substituent rearrangements. For this reason, this compound may be a suitable precursor for the synthesis of complexes of the form $[RSb]^{4+}$. Reactivity of PCl_5 with mono- and bi-dentate oxygen donors seem promising based on observed ^{31}P NMR spectra, but isolation of these highly charged species remains problematic.

A systematic study of the synthesis of antimony(V) and antimony(III) has been described here, which led to the unprecedented identification of the first pnictogen(V) trication and novel redox chemistry. Much work remains to be done to achieve isolable pnictogen tera- and pentacations, however, it is expected the work here will aid in future endeavors. It is expected that the design of multidentate, hard donor ligands with low basicity will be required in order to isolate these highly charged species.

Chapter 7: Experimental Procedures

7.1. General Considerations

As the majority of compounds prepared in this dissertation are oxygen and water sensitive, stated all experiments were carried out under an atmosphere of nitrogen. Unless otherwise stated, all preparative work was carried out either using standard Schlenk techniques or within one of the following gloveboxes: Innovative Technologies, MBraun Labmaster 130, MBraun Labmaster 110. Reactions performed in a glovebox were carried out in 4- or 8-dram screw cap vials which were previously dried at 200 °C for at least 2 hours before being placed under dynamic vacuum (glovebox antechamber) while still hot. The atmosphere of the glovebox was maintained through daily 15 minute purges with nitrogen gas at the end of the working day and circulation over a bed of catalyst, consisting of copper and activated sieves, overnight. Additionally, a 10 minute purge with nitrogen gas was carried out after the use of particularly volatile reagents such as PMe_3 or $SbCl_5$.

NMR spectra were recorded using either Bruker Avance 360, or 300 MHz spectrometers. Chemical shifts are reported relative to residual protonated solvent peaks. Elemental analyses were carried out by Canadian Microanalytical Ltd. in Delta, British Columbia.

X-ray crystallographic data was collected at either a) University of British Columbia, b) University of Alberta, or c) University of New Brunswick.

a) Data was collected on a Bruker APEX DUO diffractometer with graphite monochromated Mo-Kα radiation in a series of φ and ω scans in 0.5° oscillations.

Data were collected and integrated using the Bruker SAINT[109] software package, corrected for absorption effects using the multi-scan technique (SADABS)[110] and solved using SHELXT[111] and refined against all Fo2 data using SHELXL-2013.[112]

b) Crystallographic analysis was carried at on aBruker D8/APEX II CCD by using graphite-monochromated MoKa radiation. Structures were solved by using SHELXT[112] and refined against all Fo2 data with using SHELXL-97.[112]

c) Single crystals were coated with Paratone-N oil, mounted using a polyimide MicroMount and frozen in the cold nitrogen stream of the goniometer. A hemisphere of data was collected on a Bruker AXS P4/SMART 1000 diffractometer using ω and ϕ scans with a scan width of 0.3 ° and 10 s exposure times. The detector distance was 5 cm. The data were reduced (SAINT)[109] and corrected for absorption (SADABS).[110] The structure was solved by direct methods and refined by full-matrix least squares on F^2(SHELXTL).[112] All non-hydrogen atoms were refined using anisotropic displacement parameters. Hydrogen atoms were included in calculated positions and refined using a riding model.

All solvents were distilled under nitrogen from their appropriate drying agent directly into Teflon-valved Strauss flask. Prior to use, all solvents were stored for at least 48 hours over 4 Å or 3 Å molecular sieves for CH_3CN that had been freshly activated at 300℃ under dynamic vacuum for 72 hours. Deuterated solvents were dried over activated molecular sieves for 48 hours prior to use.

7.2. Compounds in Chapter 2

7.2.1. Ph_2SbCl_3

Reaction was carried out *via* a modified literature procedure.[38] Ph_3Sb and $SbCl_3$ were combined in a 1:2 ratio to form a viscous, golden yellow melt which was left to stir at ambient temperature for three days after which DCM was added. 1 molar equivalent of 1M SO_2Cl_2 in DCM was added dropwise to the stirred solution and left to stir for 24 hours resulting in a mixture of golden yellow liquid and a colourless powder. A minimum amount of DCM was added to dissolve the powder and this was stored in a freezer at -30 °C to yield colourless crystals. The filtrate was concentrated and returned to the freezer to yield a second, smaller batch of crystals. Attempts to isolate a third batch of crystals resulted in an impure sample. Reaction was typically carried out on a 20 g scale, attempts to scale the reaction to 50 g resulted in a severe decrease in yield (15%). Yield: 33-38%. M.P. = 170-172 °C. ^{1}H NMR (300 MHz, CD_2Cl_2): δ_H = 8.29-8.35 (m, 2H, Ph), 7.62-7.70 (m, 3H, Ph). $^{13}C\{^1H\}$ (76 MHz, CD_2Cl_2): δ_C = 144.94, 133.94, 133.81, 130.64.

7.2.2. $[PhSb(bipy)][OTf]_2$

Ph_2SbCl_3 (0.189 g, 0.494 mmol) was dissolved in CH_3CN (3mL) and solid 2,2'-bipy (0.158 g, 1.01 mmol) was added to form a yellow mixture, addition of TMSOTf (272 μL, 1.50 mmol) resulted in a clear and colourless solution which was left to stir for 2 hours before removing all volatiles under high vacuum to leave

a colourless powder. This powder was redissolved in CH_3CN to which Et_2O diffused into to yield crystals suitable for X-Ray crystallography. Yield: 16% (crystalline). M.P. = 146-150 °C. ^{1}H NMR (300 MHz, CD_3CN): δ_H = 9.27-9.29 (d, J(H,H) = 6.4 Hz, 2H, Ar-H, [bipy]), 8.79-8.82 (d, J(H,H) = 8.2 Hz, 2H, Ar-H, [bipy]), 8.58-8.64 (dt, J(H,H) = 7.6 Hz, J(H,H) = 1.5 Hz, 2H, Ar-H, [bipy]), 8.06-8.11 (dt, J(H,H) = 6.0 Hz, J(H,H) = 1.2 Hz, 2H, Ar-H, [bipy]) 7.50-7.54 (m, 2H, Ph), 7.36-7.41 (m, 3H, Ph). $^{13}C\{^1H\}$ (76 MHz, CD_3CN): δ_C = 153.15, 150.60, 149.46, 146.65, 135.27, 132.47, 131.15, 130.93, 127.49.

7.2.3. $[Sb(bipy)_2][OTf]_3$

Ph_3Sb and $SbCl_3$ were combined in a 2:1 ratio to form a viscous, golden yellow melt which was left to stir at ambient temperature for three days after which DCM was added. 1 molar equivalent of 1M SO_2Cl_2 in DCM was added dropwise to the stirred solution and left to stir for 24 hours resulting in a mixture of golden yellow liquid. To this solution of *in situ* generated $PhSbCl_4$, two equivalents of solid bipy and four equivalents of TMSOTf was added. All volatiles were removed under vacuum and the resulting colourless solid redissolved in a minimum amount of CH_3CN and place in a freezer at -25 °C to afford a small amount of colourless crystals. Yield: 11% (crystalline). M.P. = 110-113 °C. ^{1}H NMR (300 MHz, CD_3CN): δ_H = 8.89 (d, 5.4 Hz, 4H, bipy), 8.81 (d, 8.3 Hz, 4H, bipy), 8.63 (dt, 8.2 Hz, 1.4 Hz, 4H, bipy), 8.07 (m, 4H, bipy).

7.2.4. $Ph_2SbCl_3(OPyMe)$

Ph_2SbCl_3 (0.379 g, 0.991 mmol) was dissolved in DCM (3mL) and solid OPyrMe (0.102 g, 0.934 mmol) was added to form a colourless mixture which was left to stir or 1 hr before removing all volatiles under high vacuum. The resulting colourless powder was redissolved in a minimal amount of DCM, forming crystals suitable for X-Ray crystallography. A melting point of both a single crystal and the powder was taken. Yield: 92% (powder). M.P. = 146-150 °C. ^{1}H NMR (300 MHz, CD_3CN): δ_H = 8.29-8.26 (m 4H, Ar-H, [Ph]), 8.01 (d, J(H,H) = 6.7 Hz, 2H, Ar-H, [OPyrMe]), 7.42-7.37 (m, 6H, Ar-H, [Ph]), 7.11 (d, J(H,H) = 6.7 Hz, 2H, Ar-H, [OPyrMe]), 2.35(s, 3H, Me), $^{13}C\{^1H\}$ (76 MHz, CD_3CN): δ_C = 140.61, 132.10, 130.53, 128.81, 127.63, 21.45 . Elemental Analysis: Calc: C: 43.99, H: 3.49, N: 2.85, Found: C: 43.99, H: 3.63, N: 2.82.

7.2.5. $[Ph_2SbCl_2(OPyMe)_2][OTf]$

Ph_2SbCl_3 (0.381 g, 0.997 mmol) was dissolved in DCM (3mL) and solid OPyrMe (0.220 g, 2.02 mmol) was added to form colourless solution, addition of AgOTf (0.256 g, 1.00 mmol) resulted in a colourless mixture which was left to stir for 1 hr in the dark. The mixture was then filtered and the pale yellow filtrate was concentrated and placed in a freezer at -30 °C. The resulting colourless powder was recrystalized by dissolving it in the minimum amount of DCM and placing in a freezer at -30 °C yielding X-ray quality crystals. A melting point of both a single crystal and the powder was taken. Yield: 73% (powder). M.P. = 132-136°C. ^{1}H

NMR (300 MHz, CD_3CN): δ_H = 8.37 (d, J(H,H) = 6.7 Hz, 4H, OPyrMe), 8.18-8.02 (m, 4H, Ph), 7.57 (d, J(H,H) = 6.7 Hz, 4H, OPyrMe) 7.65-7.62 (m, 6H, Ph), 2.51 (s, 6H, CH_3). $^{13}C\{^1H\}$ (76 MHz, CD_3CN): δ_C =141.40, 135.03, 133.47, 132.16, 131.24, 129.28, 21.61. Elemental Analysis: Calc: C: 42.04, H: 3.39, N: 3.92, Found: C:41.92, H:3.74, N:3.88.

7.2.6. $[Ph_2SbCl(OPyMe)_3][OTf]_2$

Ph_2SbCl_3 (0.381 g, 0.997 mmol) was dissolved in DCM (3mL) and solid OPyrMe (0.3271 g, 3.00 mmol) was added to form colourless solution, addition of AgOTf (0.520 g, 2.02 mmol) resulted in a colourless mixture which was left to stir for 1 hr in the dark. The mixture was then filtered and the pale yellow filtrate was concentrated and placed in a freezer at -30 °C. The resulting colourless powder was recrystallized once again to yield analytically pure powder. All attempts to grow X-ray quality crystals failed. Yield: 77% (powder). M.P. = 148-150°C. ^1H NMR (300 MHz, CD_2Cl_2): δ_H = 8.36 (d, J(H,H) = 6.4 Hz, 6H, OPyrMe), 8.05-8.02 (m, 4H, Ph), 7.76-7.65 (m, 6H, Ph) 7.57 (d, J(H,H) = 6.4 Hz 6H, OPyrMe), 2.49 (s, 9H, CH_3). $^{13}C\{^1H\}$ (76 MHz, CD_2Cl_2): δ_C = 152.91, 141.14, 135.33, 134.64, 131.15, 129.56, 21.61. Elemental Analysis: Calc(%): C: 40.89, H: 3.65, N:4.47 Found(%): C:40.61, H:3.18, N:4.41

7.2.7. $[Ph_2Sb(OPyrMe)_4][OTf]_3$

Ph_2SbCl_3 (0.383 g, 1.00 mmol) was dissolved in CH_2Cl_2 (4mL) and solid OPyrMe (0.436 g, 3.99 mmol) was added to form a clear and yellow solution, addition of AgOTf (0.779 g, 3.02 mmol) which was left to stir for 2 hours in the dark. The mixture was then filtered and the pale yellow filtrate was concentrated and placed in the freezer at -30 °C. The resulting colourless powder was recrystalized by dissolving it in the minimum amount of DCM at -30 °C. From the resulting analytically pure powder X-ray quality crystals were grown by vapour diffusion of Et_2O into DCM. Yield: 65% (powder). M.P. = 193-197°C. ^{1}H NMR (300 MHz, CD_2Cl_2): δ_H = 8.81 (d, J(H,H) = 7.0 Hz, 8H, OPyrMe), 7.84-7.81 (m, 4H, Ph), 7.43 (d, J(H,H) = 6.9 Hz, 8H, OPyrMe) 7.37-7.23 (m, 6H, Ph), 2.42 (s, 12H, CH_3). $^{13}C\{^1H\}$ (76 MHz, CD_2Cl_2): δ_C = 155.49, 142.02 135.45, 133.84, 131.5, 129.14, 21.93. EA: Calc (%): C: 40.39, H: 3.30, N: 4.83 Found (%): C: 40.50, H: 3.39, N: 4.69.

7.2.8. $Ph_2SbCl_3(OPEt_3)$

Ph_2SbCl_3 (0.199 g, 0.521 mmol) was dissolved in DCM (3mL) and solid $OPEt_3$ (0.071 g, 0.52 mmol) was added to form a clear, colourless solution which was left to stir or 1 hour before removing all volatiles under high vacuum. The resulting colourless powder was redissolved in a minimal amount of CH_3CN, forming crystals suitable for X-Ray crystallography. Yield: 87% (powder). M.P. = 153-155 °C. $^{31}P\{1H\}$ NMR: (122 MHz, CD_3CN): 76.33 ^{1}H NMR (300 MHz, CD_3CN): 8.29-8.26 (m, 4H, Ph), 7.63-7.46 (m, 6H, Ph), 1.73-1.62 (m, 6H, $P(C\mathbf{H}_2CH_3)_3$), 0.94-

0.83(m, 9H, P($CH_2C\mathbf{H}_3)_3$). $^{13}C\{^1H\}$ (76 MHz, CD_3CN): δ_C = 160.11, 131.58, 129.16, 19.01 (d, J(P,C) = 65.9 Hz), 5.39 (d, J(P,C) = 15.5 Hz).

7.2.9. $[Ph_2SbCl_2(OPEt_3)_2][OTf]$

Ph_2SbCl_3 (0.193 g, 0.505 mmol) was dissolved in DCM (3mL) and solid $OPEt_3$ (0.131 g, 0.976 mmol) was added to form a clear, colourless solution to which AgOTf (0.129 g, 0.502 mmol) was added and left to stir for 1 hour in the dark. The mixture was filtered and the colourless solution place in the freezer at -25 °C to afford colourless crystals. Yield: 78% (powder).$^{31}P\{^1H\}$ NMR: (122 MHz, CD_2Cl_2): 78.76 ^1H NMR (300 MHz, CD_2Cl_2): 8.26-8.06 (m, 4H, Ph), 7.60-7.52 (m, 6H, Ph), 1.88-1.73 (m, 12H, P($C\mathbf{H}_2CH_3)_3$)), 0.96-0.82 (m, 18H, P($CH_2C\mathbf{H}_3)_3$). $^{13}C\{^1H\}$ (76 MHz, CD_2Cl_2): δ_C = 159.85, 131.53, 129.51, 18.82 (d, J(P,C) = 65.2 Hz), 5.41 (d, J(P,C) = 15.5 Hz).

7.2.10. $[Ph_2SbCl(OPEt_3)_3][OTf]_2$

Ph_2SbCl_3 (0.191 g, 0.500 mmol) was dissolved in DCM (3mL) and solid $OPEt_3$ (0.201 g, 1.50 mmol) was added to form a clear, colourless solution to which AgOTf (0.257 g, 1.00 mmol) was added and left to stir for 1 hour in the dark. The mixture was filtered and the colourless solution place in the freezer at -25 °C to afford colourless crystals. Yield: 78% (powder). $^{31}P\{^1H\}$ NMR: (122 MHz, CD_2Cl_2): 85.24. ^1H NMR (300 MHz, CD_2Cl_2): 8.19-8.05 (m, 4H, Ph), 7.78-7.64 (m, 6H, Ph), 2.15-1.73 (m, 18H, P($C\mathbf{H}_2CH_3)_3$), 1.17-0.85 (m, 27H, P($CH_2C\mathbf{H}_3)_3$).

$^{13}C\{^{1}H\}$ (76 MHz, CD_2Cl_2): δ_C = 154.61, 131.18, 130.71, 18.54(d, J(P,C) = 63.0 Hz), 5.50 (d, J(P,C) = 4.4 Hz).

7.2.11. $[Ph_2Sb(OPEt_3)_4][OTf]_3$

Ph_2SbCl_3 (0.191 g, 0.500 mmol) was dissolved in DCM (3mL) and solid $OPEt_3$ (0.269 g, 2.00 mmol) was added to form a clear, colourless solution to which AgOTf (0.387 g, 1.43 mmol) was added and left to stir for 1 hour in the dark. The mixture was filtered and the colourless solution place in the freezer at -25 °C to afford colourless crystals. Yield: 88% (powder).$^{31}P\{^{1}H\}$ NMR: (122 MHz, CD_2Cl_2): 89.28. ^{1}H NMR (300 MHz, CD_2Cl_2): 7.91-7.72 (m, 10H, Ph), 2.05-1.78 (m, 24H, $P(C\mathbf{H}_2CH_3)_3$), 1.04-0.76 (m, 36H, $P(CH_2C\mathbf{H}_3)_3$). $^{13}C\{^{1}H\}$ (76 MHz, CD_2Cl_2): δ_C = 160.19, 131.62, 131.03, 19.12(d, J(P,C) = 62.1 Hz), 5.63 (d, J(P,C) = 3.7 Hz).

7.2.12. Ph_2SbCl_3(dmap)

Ph_2SbCl_3 (0.099 g, 0.26 mmol) was dissolved in MeCN (3mL) and solid dmap (0.030 g, 0.25 mmol) was added to form an opaque, colourless mixture which was left to stir for 2 hours before removing all volatiles under high vacuum to leave a colourless powder. The low solubility of the compound prevented the acquisition of $^{13}C\{^{1}H\}$ NMR. Yield: 76%. M.P. = 238-240 °C (dec). ^{1}H NMR (300 MHz, CD_2Cl_2): δ_H = 8.03-8.06 (d, J(H,H) = 7.6 Hz, 2H, Ar-H, [dmap]), 7.94-7.97 (m, 4H, Ph), 7.37-7.42 (m, 6H, Ph), 6.44-6.47 (d, J(H,H) = 7.6 Hz, 2H, Ar-H, [dmap]),

3.09 (s, 6H, NMe_2). Calc (%): C: 45.24, H: 4.00, N: 5.55. Found (%): C: 44.76, H: 4.36, N: 5.34

7.2.13. $[Ph_2SbCl_2(dmap)_2][OTf]$

Ph_2SbCl_3 (0.101 g, 0.264 mmol) was dissolved in DCM (4mL) and solid dmap (0.031 g, 0.25 mmol) was added to form an opaque, colourless mixture to which AgOTf (0.031 g, 0.25 mmol) was added and left to stir for 2 hours in the dark. The mixture was then filtered and all volatiles were removed under high vacuum to leave a colourless powder which was recrystallized from a mixture of DCM and Et_2O. Yield: 53%. M.P. = 158°C. ^1H NMR (300 MHz, CD_2Cl_2): 8.02 (d, J(H,H) = 7.61 Hz, 4H, dmap), 7.97-7.93 (m, 4H, Ph), 7.42-7.36 (m, 6H, Ph), 6.66 (d, J(H,H) = 7.4 Hz, 4H, dmap), 3.14 (s, 12H, NMe_2). $^{13}C\{^1H\}$ (76 MHz, CD_2Cl_2): δ_C = 145.6, 133.5, 132.5, 129.7, 128.8, 107.2, 40.3. EA: Calc (%): C: 43.81, H: 4.08, N: 7.57. Found (%): C: 42.55, H: 4.25, N: 7.31

7.2.14. $[Ph_2SbCl(dmap)_2][OTf]_2$

Ph_2SbCl_3 (0.100 g, 0.262 mmol) was dissolved in DCM (4mL) and solid dmap (0.061 g, 0.50 mmol) was added to form an opaque, colourless mixture to which AgOTf (0.134 g, 0.522 mmol) was added and left to stir for 2 hours in the dark. The mixture was then filtered and all volatiles were removed under high vacuum to leave a colourless powder which was recrystallized from a mixture of DCM and Et_2O. Yield: 47% (crystalline). M.P. = 184-186°C. ^1H NMR (300 MHz, CD_2Cl_2): δ_H = 7.77-7.81 (d, J(H,H) = 7.6 Hz, 4H, dmap), 7.50-7.67 (m, 10H, Ph), 6.60-6.65

(d, J(H,H) = 7.6 Hz, 4H, dmap), 3.18 (s, 12H, NMe_2). $^{13}C\{^1H\}$ (76 MHz, CD_2Cl_2): δ_C = 157.07, 147.40, 144.99, 133.59, 133.18, 130.47, 107.58, 40.32 (s, NMe_2). EA with one molecule of DCM: Calc (%): C: 36.98, H: 3.75, N: 5.95. Found (%): C: 37.81, H: 3.87, N: 5.87.

7.2.15. $[Ph_2SbCl_2(bipy)][OTf]$

Ph_2SbCl_3 (0.210 g, 0.550 mmol) was dissolved in DCM (4mL) and solid bipy (0.078 g, 0.50 mmol) was added to form an opaque, yellow mixture to which AgOTf (0.128 g, 0.498 mmol) was added and left to stir for 1 hours in the dark. The resulting colourless mixture was then filtered and all volatiles were removed under high vacuum to leave a colourless powder which was recrystallized from a mixture of DCM and Et_2O. The solid contains two isomers in a 2.6:1 ratio, attempts to separate the isomers have failed. Yield: 76% (mixture of two isomers). ^1H NMR (300 MHz, CD_3CN): δ_H = 9.58 (ddd, J(H,H) = 5.6 Hz, 1.5 Hz, 0.6 Hz, 2H, bipy A), 9.20 (d, J(H,H) = 8.2 Hz, 0.75H, bipy B), 9.00 (d, J(H,H) = 8.20 Hz, 2H, bipy A), 8.63 (td, J(H,H) = 7.61 Hz, 1.5 Hz, 0.75H, bipy B), 8.58 (td, J(H,H) = 8.2 Hz, 1.5 Hz, 2H, bipy A), 8.40 (ddd, J(H,H) = 5.9 Hz, 1.5 Hz, 0.6 Hz, 0.75H, bipy B), 8.37-8.31 (m, 1.7H, Ph B), 8.14 (td, J(H,H) = 5.6 Hz, 1.2 Hz, 2H, bipy A), 7.89 (dt, J(H,H) = 5.9 Hz, 1.2 Hz, 0.75H, bipy B), 7.12-7.67 (m, 2.2H, Ph B), 7.58-7.51 (m, 4H, Ph A), 7.35-7.28 (m, 6H, Ph A)

7.2.16. [Ph_2SbCl_2(*t*Bubipy)][OTf]

Ph_2SbCl_3 (0.210g, 0.550 mmol) was dissolved in DCM (4mL) and solid *t*Bubipy (0.134g, 0.499 mmol) was added to form an opaque, colourless mixture to which AgOTf (0.128 g, 0.498 mmol) was added and left to stir for 1 hours in the dark. The mixture was then filtered and all volatiles were removed under high vacuum to leave a colourless powder which was recrystallized from a mixture of DCM and Et_2O. The solid contains two isomers in a 1:1 ratio, attempts to separate the isomers have failed. Yield: 83% (crystalline mixture of both isomers). ^{1}H NMR (300 MHz, CD_3CN): δ_H = 9.44 (d, J(H,H) = 6.2 Hz, 1H, *t*Bubipy), 8.91 (d, J(H,H) = 2.1 Hz, 1H, *t*Bubipy), 8.70 (d, J(H,H) = 1.8 Hz, 1H, *t*Bubipy), 8.35-8.32 (m, 2H, Ph), 8.31 (d, J(H,H) = 6.4 Hz, 1H, *t*Bubipy), 8.07 (dd, J(H,H) = 5.8 Hz, 1.8 Hz, 1H, *t*Bubipy), 7.83 (dd, J(H,H) = 6.4 Hz, 2.1 Hz, 1H, *t*Bubipy), 7.68-7.65 (m, 3H, Ph), 7.57-7.54 (m, 2H, Ph), 7.33-7.29 (m, 3H, Ph), 1.51 (s, 9H, *t*Bu), 1.47 (m, 9H, *t*Bu).

7.2.17. [Ph_2Sb(*t*Bubipy)$_2$][OTf]$_3$

Ph_2SbCl_3 (0.210g, 0.549 mmol) was dissolved in DCM (4mL) and solid *t*Bubipy (0.268g, 1.00 mmol) was added to form an opaque, colourless mixture to which AgOTf (0.385g, 1.50 mmol) was added and left to stir for 2 hours in the dark. The mixture was then filtered and all volatiles were removed under high vacuum to leave a colourless powder which was recrystallized from a mixture of DCM and Et_2O. Yield: 19% (crystalline). ^{1}H NMR (300 MHz, CD_3CN): δ_H = 8.98 (d, J(H,H) = 6.2 Hz, 2H, *t*Bubipy), 8.82 (d, J(H,H) = 1.8 Hz, 2H, *t*Bubipy), 8.29 (d, J(H,H) =

2.3 Hz, 2H, *t*Bubipy), 8.06 (d, J(H,H) = 6.2 Hz, 2H, *t*Bubipy), 7.96 (dd, J(H,H) = 6.2 Hz, 1.7 Hz 2H, *t*Bubipy), 7.91 (d, J(H,H) = 6.2 Hz, 1.7 Hz, 2H, *t*Bubipy), 7.66-7.61 (m, 5H, Ph), 7.55-7.52 (m, 5H, Ph), 1.55 (s, 18H, *t*Bu), 1.41 (m, 18H, *t*Bu). $^{13}C\{^{1}H\}$ (76 MHz, CD_2Cl_2): δ_C = 176.3, 173.7, 147.4, 147.2, 146.4, 144.5, 143.3, 141.0, 135.7, 135.5, 132.9, 132.8, 130.0, 129.7, 126.7, 125.9, 125.6, 124.1, 122.2, 119.9, 38.5, 38.0, 30.4, 30.1.

7.2.18. [$SbCl_4$(*t*Bubipy)][OTf]

[Sb(*t*Bubipy)$_2$][OTf]$_3$ (0.552 g, 0.499 mmol) was dissolved in 8 mL of CH_3CN to which $SeCl_4$ (0.110g, 0.50 mmol) was added to yield a yellow-brown solution. All volatiles were removed under vacuum to furnish a yellow solid which was washed with 3x0.5 mL of DCM. The solid was redissolved in a minimum amount of CH_3CN to which Et_2O diffused into to yield X-ray quality crystals. Yield: 24% (crystalline). ^{1}H NMR (300 MHz, CD_3CN): δ_H = 9.60 (d, J(H,H) = 6.4 Hz, 2H, *t*Bubipy), 8.92 (d, J(H,H) = 2.1 Hz, 2H, *t*Bubipy), 8.32 (dd, J(H,H) = 6.4 Hz, 2.1 Hz, 2H, *t*Bubipy), 1.55 (s, 18H, *t*Bu).

7.2.19. [PCl_4(*t*Bubipy)][OTf]

[P(*t*Bubipy)$_2$][OTf]$_3$ (0.507 g, 0.50 mmol) was dissolved in 8 mL of CH_3CN to which PCl_5 (0.104 g, 0.498 mmol) was added to yield a yellow solution. All volatiles were removed under vacuum to furnish a yellow solid which was washed with 3x0.5 mL of DCM. Yield: 90%. $^{31}P\{^{1}H\}$ NMR: (122 MHz, CD_3CN): -146.9 ppm.

7.2.20. Crystallographic Information

Table 7.2.1: Crystallographic details for compounds in Chapter 2

	$Ph_2SbCl_3OPyrMe$	$[Ph_2SbCl_2(OPyrMe)_2][OTf]$	$[Ph_2Sb(OPyrMe)_4][OTf]_3$
Empirical formula	$C_{18}H_{17}NOCl_3Sb$	$C_{25}H_{24}Cl_2F_3N_2O_5SSb$	$C_{41}H_{42}Cl_4F_9N_4O_{13}S_3Sb$
Formula weight	491.42	714.17	1329.51
Temperature/K	188.15	188.15	173.15
Crystal system	Monoclinic	Triclinic	monoclinic
Space group	$P2_1/c$	P-1	$P2_1/n$
a/Å	18.457(2)	10.709(3)	11.7250(7)
b/Å	13.6093(18)	11.460(3)	22.5677(14)
c/Å	15.582(2)	12.859(3)	21.3088(13)
α/°	90	67.107(3)	90
β/°	106.525(2)	79.458(3)	104.407(4)
γ/°	90	85.651(3)	90
Volume/$Å^3$	3752.2(8)	1429.3(6)	5461.1(6)
Z	8	2	4
$\rho_{calc}g/cm^3$	1.740	1.659	1.617
Radiation	MoKα (λ = 0.71073)	MoKα (λ = 0.71073)	CuKα (λ = 1.54184)
Goodness-of-fit on F^2	1.064	1.025	1.056
Final R indexes [I>=2σ (I)]	R_1 = 0.0195, wR_2 = 0.0482	R_1 = 0.0364, wR_2 = 0.0964	R_1 = 0.0667, wR_2 = 0.1870
Final R indexes [all data]	R_1 = 0.0250, wR_2 = 0.0517	R_1 = 0.0404, wR_2 = 0.1012	R_1 = 0.0824, wR_2 = 0.2016

Table 7.2.2: Crystallographic details for compounds in Chapter 2 (cont.)

	$[Ph_2SbCl_2(bipy)][OTf] \bullet ½ CH_2Cl_2$	$[Ph_2SbCl_2(bipy)][Ph_2SbCl_4]$	$[Ph_2SbCl_2(t\text{Bubipy})][OTf]$
Empirical formula	$C_{23.50}H_{19}Cl_3F_3N_2O_3SSb$	$C_{38}H_{38}Cl_6N_2OSb_2$	$C_{32}H_{36}Cl_4F_3N_2O_3SSb$
Formula weight	694.57	994.90	849.24
Temperature/K	173(1)	188(1)	173(1)
Crystal system	Monoclinic	Triclinic	Triclinic
Space group	C2/c	P-1	P-1
a/Å	36.524(12)	9.289(5)	11.913(6)
b/Å	8.190(3)	13.887(7)	12.000(6)
c/Å	19.323(6)	16.384(8)	13.413(7)
α/°	90	77.671(6)	90.386(7)
β/°	107.666(6)	76.327(7)	104.529(6)
γ/°	90	83.923(6)	97.989(7)
Volume/$Å^3$	5508(3)	2002.8(17)	1836.4(16)
Z	8	2	2
$\rho_{calc}g/cm^3$	1.675	1.650	1.536
Radiation	MoKα (λ = 0.71073)	MoKα (λ = 0.71073)	MoKα (λ = 0.71073)
Goodness-of-fit on F^2	1.048	1.108	1.047
Final R indexes [I>=2σ (I)]	R1 = 0.0378, wR2 = 0.1068	R1 = 0.0538, wR2 = 0.1614	R1 = 0.0462, wR2 = 0.1257
Final R indexes [all data]	R1 = 0.0440, wR2 = 0.1130	R1 = 0.0731, wR2 = 0.1801	R1 = 0.0491, wR2 = 0.1294

Table 7.2.3: Crystallographic details for compounds in Chapter 2 (cont.)

	$[Ph_2Sb(t\text{Bubipy})_2][OTf]_3 \bullet CH_3CN \bullet Et_2O$	$Ph_2SbCl_3(dmap)$	$[Ph_2SbCl_2(dmap)_2][OTf]$
Empirical formula	$C_{51}H_{58}F_9N_4O_9S_3Sb$	$C_{19}H_{20}N_2Cl_3Sb$	$C_{20}H_{20}N_2O_3SF_3SbCl_2$
Formula weight	1259.94	504.47	618.09
Temperature/K	273.15	173.15	273.15
Crystal system	monoclinic	monoclinic	triclinic
Space group	$P2_1/n$	$P2_1/n$	$P2_1/n$
a/Å	16.4518(16)	11.0351(13)	8.6326(10)
b/Å	23.615(3)	15.0771(17)	21.343(3)
c/Å	16.7450(16)	12.3570(14)	16.1809(19)
α/°	90	90	90
β/°	98.064(5)	97.171(2)	90.786(3)
γ/°	90	90	90
Volume/$Å^3$	6441.2(11)	2039.8(4)	2980.9(6)
Z	4	4	1
$\rho_{calc}g/cm^3$	1.299	1.643	0.344
Radiation	MoKα (λ = 0.71073)	MoKα (λ = 0.71073)	MoKα (λ = 0.71073)
Goodness-of-fit on F^2	1.071	1.106	1.047
Final R indexes [I>=2σ (I)]	R_1 = 0.1166, wR_2 = 0.2833	R_1 = 0.0200, wR_2 = 0.0516	R_1 = 0.0485, wR_2 = 0.1111
Final R indexes [all data]	R_1 = 0.1559, wR_2 = 0.3004	R_1 = 0.0213, wR_2 = 0.0524	R_1 = 0.0652, wR_2 = 0.1191

Table 7.2.4: Crystallographic details for compounds in Chapter 2 (cont.)

	$[Ph_2SbCl(dmap)_2][OTf]_2 \bullet CH_2Cl_2$	$[Ph_2SbCl_3(OPEt_3)_2][OTf]$	$[Ph_2SbCl(OPEt_3)_3][OTf]_2$
Empirical formula	$C_{22}H_{25}S_2O_6F_6N_4SbCl$	$C_{26}H_{42}O_5F_3P_2SCl_4Sb$	$C_{32}H_{55}SbP_3S_2O_9F_6Cl$
Formula weight	776.78	849.14	1011.99
Temperature/K	273.15	173.25	296.15
Crystal system	orthorhombic	monoclinic	orthorhombic
Space group	$Pna2_1$	$P2_1$	$P2_12_12_1$
a/Å	27.612(2)	8.2417(2)	14.9656(7)
b/Å	12.5435(10)	14.9189(3)	15.4478(7)
c/Å	11.3274(9)	14.9172(3)	19.0979(9)
α/°	90	90	90
β/°	90	97.9486(10)	90
γ/°	90	90	90
Volume/$Å^3$	3923.2(5)	1816.55(7)	4415.2(4)
Z	1	2	1
$\rho_{calc}g/cm^3$	0.329	1.552	0.381
Radiation	MoKα (λ = 0.71073)	CuKα (λ = 1.54178)	MoKα (λ = 0.71073)
Goodness-of-fit on F^2	1.069	1.054	1.022
Final R indexes [I>=2σ (I)]	R_1 = 0.0827, wR_2 = 0.2473	R_1 = 0.0387, wR_2 = 0.1008	R_1 = 0.0255, wR_2 = 0.0510
Final R indexes [all data]	R_1 = 0.0909, wR_2 = 0.2542	R_1 = 0.0389, wR_2 = 0.1011	R_1 = 0.0301, wR_2 = 0.0528

Table 7.2.5: Crystallographic details for compounds in Chapter 2 (cont.)

	$[Ph_2SbCl(OPEt_3)_4][OTf]_3$	$[SbCl_4(t\text{Bubipy})][OTf]$
Empirical formula	$C_{39}H_{20}O_{13}F_9P_4S_3ClSb$	$C_{19}H_{22}N_2O_3F_3SCl_4Sb$
Formula weight	1244.81	678.99
Temperature/K	173.15	173.15
Crystal system	monoclinic	orthorhombic
Space group	$P2_1/c$	$P2_12_12_1$
a/Å	19.777(11)	10.0612(3)
b/Å	13.132(8)	11.8365(3)
c/Å	21.910(13)	22.1437(5)
α/°	90	90
β/°	94.835(8)	90
γ/°	90	90
Volume/Å^3	5670(6)	2637.08(12)
Z	4	4
ρ_{calc}g/cm^3	1.458	1.710
Radiation	MoKα (λ = 0.71073)	CuKα (λ = 1.54178)
Goodness-of-fit on F^2	1.188	1.070
Final R indexes [I>=2σ (I)]	R_1 = 0.1207, wR_2 = 0.2479	R_1 = 0.0332, wR_2 = 0.0850
Final R indexes [all data]	R_1 = 0.1462, wR_2 = 0.2585	R_1 = 0.0334, wR_2 = 0.0852

7.3. Compounds in Chapter 3

7.3.1. $PhSbCl_2$

Reaction was carried out *via* a modified literature procedure.[38] Ph_3Sb and $SbCl_3$ were combined in a 1:2 ratio to form a viscous, golden yellow melt which was left to stir at ambient temperature for three days. The melt was placed in a freezer at -25 °C and left to freeze (*ca.*3 hours) after which was left to thaw at room temperature to yield colourless crystals which was filtered from the remaining liquid and washed with cold DCM. Yield: 85%. M.P. = 68-70 °C.

7.3.2. Ph_2SbCl

Reaction was carried out *via* a modified literature procedure.[38] Ph_3Sb and $SbCl_3$ were combined in a 2:1 ratio to form a viscous, golden yellow melt which was left to stir at ambient temperature for three days. The melt was placed in a freezer at -25 °C and left to freeze (*ca.*3 hours) after which was left to thaw at room temperature to yield colourless crystals which was filtered from the remaining liquid and washed with cold DCM. Yield: 73%. M.P. = 64-67 °C.

7.3.3. $SbCl_3$(bipy)

$SbCl_3$ (0.225 g, 0.990 mmol) was dissolved in 5mL of DCM to which solid bipy (0.157 g, 1.01 mmol) was added to immediately form a yellow mixture which was stirred for 30 minutes. The mixture was filtered and the yellow powder washed with 3mL of Et_2O. The powder is only sparingly soluble in DCM and CH_3CN, however X-ray quality crystals were obtained from a concentrated solution in CH_3CN which was placed in a freezer at -30°C. Yield: 92% (powder). M.P. = 185-187 °C. ^1H NMR (300 MHz, CD_3CN): δ_H = 9.10 (d, J(H,H) = 4.9 Hz, 2H, bipy), 8.50 (dt, J(H,H) = 8.2 Hz, 1.1 Hz, 2H, bipy), 8.30 (td, J(H,H) = 8.2 Hz, 1.4 Hz, 2H, bipy), 7.80 (ddd, J(H,H) = 7.6 Hz, 5.2 Hz, 1.1 Hz, 2H, bipy) $^{13}C\{^1H\}$ (76 MHz, CD_3CN): 147.60, 143.57, 128.56, 124.68.

7.3.4. [$SbCl_2$(bipy)][OTf]

$SbCl_3$ (0.227 g, 1.00 mmol) was dissolved in 5mL of DCM to which solid bipy (0.161 g, 1.03 mmol) was added to immediately form a yellow mixture, followed by TMSOTf (181 µL, 1.00 mmol) resulting in a colourless solution which was stirred for 1hr. The solution was concentrated under vacuum and placed in a freezer at -30°C resulting in colourless crystals. Yield: 68% (powder). ^{1}H NMR (300 MHz, CD_3CN): δ_H = 9.04 (d, J(H,H) = 5.2 Hz, 2H, bipy), 8.41 (dd, J(H,H) = 8.1 Hz, 0.7 Hz, 2H, bipy), 8.33 (tt, J(H,H) = 7.9 Hz, 1.5 Hz, 2H, bipy), 7.83 (td, J(H,H) = 5.4 Hz, 1.65 Hz, 2H, bipy) $^{13}C\{^1H\}$ (76 MHz, CD_3CN): 147.40, 143.39, 127.78, 123.62. Elemental Analysis: Calculated (%): C: 26.48, H: 1.82, N: 5.61 Found (%): 26.72, 1.68, 5.57.

7.3.5. [$SbCl(bipy)_2$][$OTf]_2$

$SbCl_3$ (0.228 g, 1.00 mmol) was dissolved in 5mL of DCM to which solid bipy (0.321 g, 2.05 mmol) was added to immediately form a yellow mixture, followed by TMSOTf (543 µL, 3.00 mmol) resulting in a colourless solution which was stirred for 1hr. The solution was concentrated under vacuum and placed in a freezer at -30°C resulting in colourless crystals. Yield: 74% (powder). M.P. = 195-198 °C. ^{1}H NMR (360 MHz, CD_3CN): δ_H = 8.82 (dd, J(H,H) = 4.8 Hz, 0.6 Hz, 2H, bipy), 8.68 (d, J(H,H) = 8.2 Hz, 2H, bipy), 8.49 (td, J(H,H) = 8.2 Hz, 1.5 Hz, 2H, bipy), 7.91 (td, J(H,H)= 5.8 Hz, 1.2 Hz, 2H, bipy). $^{13}C\{^1H\}$ (90.59 MHz, CD_3CN): 148.78,

148.48, 145.90, 130.45, 126.44. Elemental Analysis: Calculated (%): C:34.28, H: 2.48, N: 7.27, Found (%): C: 34.45, H:2.07, N: 7.29.

7.3.6. $SbCl_3(dmap)_2$

$SbCl_3$ (0.115 g, 0.504 mmol) was dissolved in 5mL of DCM to which solid dmap (0.127 g, 1.05 mmol) was added to immediately form a colourless mixture which was stirred for 30 minutes. The mixture was filtered and the colourless powder washed with 3mL of Et_2O. The powder is only sparingly soluble in DCM and CH_3CN, however X-ray quality crystals were obtained from a concentrated solution in CH_3CN which was placed in a freezer at -30°C. Yield: 94% (powder). M.P. = 205 °C (dec) ^{1}H NMR (300 MHz, CD_3CN): δ_H = 8.45 (d, J(H,H) = 7.6 Hz, 4H, dmap), 6.67 (d, J(H,H) = 7.3 Hz, 4H, dmap), 3.07 (s, 12H, dmap). $^{13}C\{^1H\}$ (76 MHz, CD_3CN): 157.29, 152.28, 147.44, 40.24. Elemental Analysis: Calculated (%): C: 35.59, H: 4.27, N: 11.86 Found (%): C: 34.23, H: 4.27, N: 11.35.

7.3.7. $[SbCl_2(dmap)_2][OTf]$

$SbCl_3$ (0.227 g, 0.995 mmol) was dissolved in 5mL of DCM to which solid dmap (0.244 g, 2.00 mmol) was added to immediately form a colourless mixture, followed by TMSOTf (181 µL, 1.00 mmol) resulting in a colourless solution which was stirred for 1hr. The solution was concentrated under vacuum and placed in a freezer at -30°C resulting in colourless crystals. Yield: 75% (powder). M.P. = 137-142 °C. ^{1}H NMR (300 MHz, CD_3CN): δ_H = 8.03 (d, J(H,H) = 7.9 Hz, 4H, dmap),

6.86 (d, J(H,H) = 7.9 Hz, 4H, dmap), 3.16 (s, 12H, dmap) $^{13}C\{^{1}H\}$ (76 MHz, CD_3CN): 157.75, 143.74, 108.59, 40.27.

7.3.8. $[SbCl(dmap)_2][OTf]_2$

$SbCl_3$ (0.227 g, 0.995 mmol) was dissolved in 5mL of DCM to which solid dmap (0.254 g, 2.08 mmol) was added to immediately form a colourless mixture, followed by TMSOTf (543 µL, 3.00 mmol) resulting in a colourless solution which was stirred for 1hr. The solution was concentrated under vacuum and placed in a freezer at -30°C resulting in colourless crystals. Yield: 63% (powder). M.P. = 133-135 °C. ^{1}H NMR (300 MHz, CD_3CN): δ_H = 8.05 (d, J(H,H) = 7.9 Hz, 4H, dmap), 6.92 (d, J(H,H) = 7.9 Hz, 4H, dmap), 3.19 (s, 12H, dmap) $^{13}C\{^{1}H\}$ (76 MHz, CD_3CN): 158.01, 143.88, 108.98, 40.59.

7.3.9. $[Sb(dmap)_3][OTf]_3$

SbF_3 (0.180 g, 1.00 mmol) was dissolved in 3 mL of DCM to which TMSOTf (543 µL, 3.00 mmol) was added followed by the dropwise addition of dmap (0.367 g, 3.01 mmol) dissolved in 3 mL of DCM. The solution was stirred for 30 minutes then concentrated under vacuum and placed in a freezer at -30 °C to afford large colourless crystals. Yield: 43% (crystalline). M.P. = 140 °C. ^{1}H NMR (300 MHz, CD_2Cl_2): δ_H = 8.07 (d, J(H,H) = 7.4 Hz, 6H, dmap), 6.76 (d, J(H,H) = 7.6 Hz, 6H, dmap), 3.22 (s, 18 H, NMe_2). $^{13}C\{^{1}H\}$ (76 MHz, CD_2Cl_2): 158.08, 139.63, 107.44, 40.66.

7.3.10. [PhSbCl(bipy)][OTf]

$PhSbCl_2$ (0.133 g, 0.493 mmol) was dissolved in 3mL of DCM to which solid bipy (0.078 g, 0.50 mmol) to form a bright yellow precipitate, followed by TMSOTf (90.6 µL, 0.500 mmol) to afford a pale yellow solution which was stirred for 1hr. After ~10min a white precipitate formed. All volatiles were removed under vacuum, the powder washed with ether and a small portion redissolved in DCM and placed in a freezer at -30°C resulting in colourless crystals. Yield: 73% (crystalline). M.P. = 127-130 °C ^{1}H NMR (300 MHz, CD_3CN): δ_H = 9.26 (d, J(H,H) = 5.2 Hz, 2H, bipy), 8.60 (d, J(H,H) = 8.2 Hz, 2H, bipy), 8.45 (td, J(H,H) = 8.2 Hz, 1.5 Hz, 2H, bipy), 7.95 (td, J(H,H) = 5.5 Hz, 1.2 Hz, 2H, bipy), 7.67-7.64 (m, 2H, Ph), 7.37-7.31 (m, 3H, Ph). $^{13}C\{^1H\}$ (76 MHz, CD_3CN): 148.32, 145.05, 136.25, 134.94, 130.51, 129.69, 125.86.

7.3.11. [PhSb(bipy)][OTf]$_2$

$PhSbCl_2$ (0.134 g, 0.500 mmol) was dissolved in 3mL of DCM to which solid bipy (0.156 g, 1.00 mmol) to form a bright yellow precipitate, followed by AgOTf (0.257 g, 1.00 mmol) after which the yellow precipitate redissolved. The colourless mixture was left to stir in the dark for 1 hour after which the colourless AgCl was filtered off. The colourless solution was placed in the freezer -30°C resulting in colourless crystals. Yield: 65% (crystalline). M.P. = 146-150 °C. ^{1}H NMR (300 MHz, CD_3CN): δ_H = 9.27-9.29 (d, J(H,H) = 6.4 Hz, 2H, Ar-H, [bipy]), 8.79-8.82 (d, J(H,H) = 8.2 Hz, 2H, Ar-H, [bipy]), 8.58-8.64 (dt, J(H,H) = 7.6 Hz, J(H,H) =

1.5 Hz 2H, Ar-H, [bipy]), 8.06-8.11 (dt, J(H,H) = 6.0 Hz, J(H,H) = 1.2 Hz 2H, Ar-H, [bipy]) 7.50-7.54 (m, 2H, Ph), 7.36-7.41 (m, 3H, Ph). $^{13}C\{^{1}H\}$ (76 MHz, CD_3CN): δ_C = 153.15, 150.60, 149.46, 146.65, 135.27, 132.47, 131.15, 130.93, 127.49.

7.3.12. $PhSbCl_2(dmap)_2$

$PhSbCl_2$ (0.127 g, 0.471 mmol) was dissolved in 3mL of DCM to which solid dmap (0.124 g, 1.02 mmol) was added to form a colourless mixture which was stirred for 1 hour. All volatiles were removed under vacuum, the powder washed with ether and a small portion redissolved in DCM and placed in a freezer at -30°C resulting in colourless crystals. Yield: 89% (powder).^{1}H NMR (300 MHz, CD_2Cl_2): δ_H = 8.03 (d, J(H,H) = 7.0 Hz, 4H, dmap), 7.88-7.85 (m, 2H, Ph), 7.36-7.28 (m, 3H, Ph), 6.60 (d, J(H,H) = 7.0 Hz, 4H, dmap). $^{13}C\{^{1}H\}$ (76 MHz, CD_2Cl_2): 157.39, 156.63, 143.74, 136.32, 128.78, 107.15, 40.04. Elemental Analysis: Calculated (%): C: 46.73, H: 4.90, N: 10.90, Found (%): C: 45.58, H: 5.27, N: 10.53.

7.3.13. $[PhSbCl(dmap)_2][OTf]$

$PhSbCl_2$ (0.138 g, 0.512 mmol) was dissolved in 3 mL of DCM to which solid dmap (0.124 g, 1.02 mmol) followed by AgOTf (0.129 g, 0.502 mmol) was added to form a colourless mixture which was stirred for 1 hour in the dark. All volatiles were removed under vacuum to furnish a colourless powder. The powder was redissolved in a minimum amount of DCM and layered with Et_2O and placed in a freezer at -30 °C to yield colourless crystals. Yield: 57% (crystalline). M.P. = 124-

126. ^{1}H NMR (300 MHz, CD_3CN): δ_H = 8.05 (d, J(H,H) = 7.0 Hz, 4H, dmap), 7.92-7.89 (m, 2H, Ph), 7.38-7.31 (m, 3H, Ph), 6.65 (d, J(H,H) = 7.0 Hz, 4H, dmap), 3.04 (s, 12H, NMe_2). $^{13}C\{^{1}H\}$ (76 MHz, CD_3CN): 156.96, 151.46, 145.87, 136.81, 129.02, 107.81, 39.88.

7.3.14. $[PhSb(dmap)_3][OTf]_2$

$PhSbCl_2$ (0.127 g, 0.471 mmol) was dissolved in 3 mL of DCM to which solid dmap (0.183 g, 1.51 mmol) followed by AgOTf (0.257 g, 1.00 mmol) was added to form a colourless mixture which was stirred for 1 hour in the dark. All volatiles were removed under vacuum to furnish a colourless powder. All attempts to crystallize the compound in various solvent systems and temperatures yielded only microcrystalline or powdery material. Yield: 45% (powder). ^{1}H NMR (300 MHz, CD_3CN): δ_H = 7.94 (d, J(H,H) = 7.3 Hz, 6H, dmap), 7.77-7.73 (m, 2H, Ph), 7.59-7.55 (m, 3H, Ph), 6.63 (d, J(H,H) = 7.3 Hz, 6H, dmap), 3.03 (s, 18H, NMe_2). $^{13}C\{^{1}H\}$ (76 MHz, CD_3CN): 157.00, 150.04, 148.07, 136.32, 128.38, 131.06, 40.09. Elemental Analysis: Calculated (%): C: 40.15, H: 4.53, N: 9.69, Found (%): C: 40.49, H: 4.85, N: 10.29.

7.3.15. $Ph_2SbCl(dmap)$

Ph_2SbCl (0.153 g, 0.491 mmol) was dissolved in 3 mL of DCM to which solid dmap (0.065 g, 0.46 mmol) to form a colourless mixture which was stirred for 1 hour. All volatiles were removed under vacuum to furnish a colourless powder which was washed with 3x0.5 mL of Et_2O. A small amount of solid was redissolved

and placed into a freezer at -30 °C to yield X-ray quality crystals. Yield: 94% (powder). ^{1}H NMR (300 MHz, CD_3CN): δ_H = 7.73 (d, J(H,H) = 7.5 Hz, 2H, dmap), 7.67-7.64 (m, 4H, Ph), 7.44-7.42 (m, 6H, Ph), 6.49 (d, J(H,H) = 7.5 Hz, 2H, dmap), 2.98 (s, 6H, NMe_2). Elemental Analysis: Calculated (%): C: 56.19, H: 5.44, N: 10.08, Found (%): C: 55.98, H: 5.42, N: 9.72.

7.3.16. [$Ph_2Sb(dmap)_2$][OTf]

Ph_2SbCl (0.150 g, 0.482 mmol) was dissolved in 3 mL of DCM to which solid dmap (0.123 g, 1.00 mmol) was added to form a colourless mixture to which AgOTf (0.130 g, 0.506 mmol) was added and left to stirred for 1 hour. The mixture was filtered and all volatiles were removed under vacuum to furnish a colourless powder which was washed with 3x0.5 mL of Et_2O. The solid was redissolved and placed into a freezer at -30 °C to yield X-ray quality crystals. Yield: 82% (crystalline). M.P. = 114-116 °C. ^{1}H NMR (300 MHz, CD_3CN): δ_H = 7.71 (d, J(H,H) = 7.3 Hz, 4H, dmap), 7.67-7.65 (m, 4H, Ph), 7.47-7.45 (m, 6H, Ph), 6.53 (d, J(H,H) = 7.3 Hz, 4H, dmap). 2.98 (s, 12H, dmap). $^{13}C\{^{1}H\}$ (76 MHz, CD_3CN): 157.00, 147.28, 136.97, 131.21, 130.74, 108.63, 40.03.

7.3.17. Attempted synthesis of $Ph_2SbCl(bipy)$

Ph_2SbCl (0.160 g, 0.514 mmol) was dissolved in 3 mL of DCM to which solid bipy (0.123 g, 1.00 mmol) was added to form a colourless mixture which was left to stirred for 1 hour to yield a colourless powder. The mixture was filtered and the powder was washed with 3x0.5 mL of Et_2O. A small amount of solid was

redissolved and placed into a freezer at -30 °C to yield X-ray quality crystals which were determined to be $PhSbCl_2$(bipy). Yield: 30% (crystalline).

7.3.18. Attempted synthesis of [Ph_2Sb(bipy)][OTf]

Ph_2SbCl (0.159 g, 0.511 mmol) was dissolved in 3 mL of DCM to which solid bipy (0.122 g, 1.00 mmol) was added to form a colourless mixture which was left to stirred for 1 hour to yield a colourless powder. The mixture was filtered and the powder was washed with 3x0.5 mL of Et_2O. A small amount of solid was redissolved and placed into a freezer at -30 °C to yield X-ray quality crystals which were determined to be [PhSbCl(bipy)][OTf]. Yield: 37% (crystalline).

7.3.19. Attempted synthesis of Ph_3Sb(dmap)

Ph_3Sb (0.360 g, 1.02 mmol) was dissolved in 5 mL of DCM to which solid dmap (0.129 g, 1.06 mmol) resulting in a clear, colourless solution which was stirred for 1 hour. All volatiles were removed under vacuum to furnish a colourless powder which was washed with 3x0.5 mL of Et_2O. The sample was redissolved and placed in a freezer at -30 °C to yield X-ray quality crystals of free Ph_3Sb and dmap. Yield: 98% (powder). ^{1}H NMR (300 MHz, CD_2CCl_2): δ_H = 10.15 (d, J(H,H) = 7.9 Hz, 4H, dmap), 7.46-7.30 (m, 15H, Ph), 6.88 (d, J(H,H) = 7.9 Hz, 4H, dmap), 3.22 (s, 12H, NMe_2).

Table 7.3.1: Crystallographic details for compounds in Chapter 3

	$SbCl_3(bipy)$	$[SbCl_2(bipy)][OTf]$	$[SbCl(bipy)_2][OTf]_2$
Empirical formula	$C_{10}H_8Cl_3N_2Sb$	$C_{11}H_8Cl_2F_3N_2O_3SSb$	$C_{48}H_{38}Cl_2F_{12}N_{10}O_{12}S_4Sb_2$
Formula weight	384.28	497.90	1617.52
Temperature/K	296.15	273.15	296.15
Crystal system	triclinic	monoclinic	triclinic
Space group	P-1	$P2_1/c$	P-1
a/Å	7.2921(10)	10.3886(4)	7.5470(17)
b/Å	8.4991(11)	8.3656(3)	20.233(4)
c/Å	11.3858(15)	18.0129(7)	21.443(5)
α/°	105.930(3)	90	63.248(3)
β/°	105.707(3)	98.909(2)	81.295(4)
γ/°	102.326(3)	90	85.039(4)
Volume/$Å^3$	620.85(14)	1546.56(10)	2889.6(11)
Z	2	4	2
$\rho_{calc}g/cm^3$	2.056	2.138	1.859
Radiation	MoKα (λ = 0.71073)	MoKα (λ = 0.71073)	MoKα (λ = 0.71073)
Goodness-of-fit on F^2	1.077	1.059	1.041
Final R indexes [I>=2σ (I)]	R_1 = 0.0157, wR_2 = 0.0359	R_1 = 0.0154, wR_2 = 0.0371	R_1 = 0.0302, wR_2 = 0.0624
Final R indexes [all data]	R_1 = 0.0179, wR_2 = 0.0370	R_1 = 0.0166, wR_2 = 0.0376	R_1 = 0.0428, wR_2 = 0.0679

Table 7.3.2: Crystallographic details for compounds in Chapter 3 (cont.)

	$SbCl_3(dmap)_2 \bullet$ ½ CH_3CN	$[SbCl_2(dmap)_2][TMS\text{-}dmap][OTf]_2$	$[SbCl(dmap)_2][OTf]_2$
Empirical formula	$C_{15}H_{21.5}N_{4.5}Cl_3Sb$	$C_{27}H_{24}Cl_2F_6N_6O_6S_2SbSi$	$C_{17}H_{22}Cl_3F_6N_4O_6S_2Sb$
Formula weight	492.97	927.38	784.60
Temperature/K	173.15	173.15	173.15
Crystal system	triclinic	monoclinic	triclinic
Space group	P-1	C2/c	P-1
a/Å	8.6050(11)	12.148(4)	10.8405(4)
b/Å	9.0038(12)	17.670(4)	11.3897(4)
c/Å	13.9347(18)	17.713(5)	12.8357(5)
α/°	106.200(2)	90	93.6830(10)
β/°	90.521(2)	95.410(6)	90.4430(10)
γ/°	103.201(2)	90	114.9880(10)
Volume/$Å^3$	1006.3(2)	3785.3(18)	1432.45(9)
Z	2	4	1
$\rho_{calc}g/cm^3$	1.627	1.627	0.910
Radiation	MoKα (λ = 0.71073)	MoKα (λ = 0.71073)	CuKα (λ = 1.54184)
Goodness-of-fit on F^2	1.095	1.079	1.079
Final R indexes [I>=2σ (I)]	R_1 = 0.0239, wR_2 = 0.0650	R_1 = 0.0413, wR_2 = 0.1099	R_1 = 0.0340, wR_2 = 0.0850
Final R indexes [all data]	R_1 = 0.0260, wR_2 = 0.0659	R_1 = 0.0463, wR_2 = 0.1151	R_1 = 0.0341, wR_2 = 0.0851

Table 7.3.3: Crystallographic details for compounds in Chapter 3 (cont.)

	$[Sb(dmap)_3][OTf]_3$	$PhSbCl_2(dmap)_2$	$Ph_2SbCl(dmap)$
Empirical formula	$C_{28}H_{36}F_9N_8O_9S_3Sb$	$C_{20}H_{25}Cl_2N_4Sb$	$C_{19}H_{20}N_2SbCl$
Formula weight	1017.58	514.09	433.57
Temperature/K	173(2)	296.15	296.15
Crystal system	triclinic	triclinic	monoclinic
Space group	P-1	P-1	$P2_1/n$
a/Å	8.089(3)	9.5414(9)	9.1544(4)
b/Å	12.005(4)	11.0830(11)	22.4842(10)
c/Å	21.472(8)	12.1539(12)	9.2997(4)
α/°	94.789(7)	107.747(2)	90
β/°	99.354(4)	103.603(2)	105.4210(10)
γ/°	91.438(5)	107.706(3)	90
Volume/$Å^3$	2048.6(13)	1087.28(18)	1845.24(14)
Z	2	2	1
$\rho_{calc}g/cm^3$	1.650	1.570	0.390
Radiation	MoKα (λ = 0.71073)	MoKα (λ = 0.71073)	MoKα (λ = 0.71073)
Goodness-of-fit on F^2	1.043	1.050	1.028
Final R indexes [I>=2σ (I)]	R_1 = 0.0423, wR_2 = 0.1067	R_1 = 0.0187, wR_2 = 0.0454	R_1 = 0.0341, wR_2 = 0.0668
Final R indexes [all data]	R_1 = 0.0546, wR_2 = 0.1157	R_1 = 0.0203, wR_2 = 0.0461	R_1 = 0.0527, wR_2 = 0.0725

Table 7.3.4: Crystallographic details for compounds in Chapter 3 (cont.)

	$PhSbCl_2(bipy)$	[PhSbCl(bipy)][OTf]
Empirical formula	$C_{16}H_{13}Cl_2N_2Sb$	$C_{17}H_{13}ClF_3N_2O_3SSb$
Formula weight	425.93	539.55
Temperature/K	173(2)	296.15
Crystal system	triclinic	orthorhombic
Space group	P-1	Pbca
a/Å	8.124(4)	14.036(3)
b/Å	10.762(5)	15.194(3)
c/Å	19.446(9)	17.913(3)
α/°	85.398(7)	90
β/°	78.574(7)	90
γ/°	70.762(7)	90
Volume/$Å^3$	1573.2(13)	3820.1(12)
Z	4	8
$\rho_{calc}g/cm^3$	1.798	1.876
Radiation	MoKα (λ = 0.71073)	MoKα (λ = 0.71073)
Goodness-of-fit on F^2	1.172	1.020
Final R indexes [I>=2σ (I)]	R_1 = 0.0599, wR_2 = 0.1357	R_1 = 0.0262, wR_2 = 0.0595
Final R indexes [all data]	R_1 = 0.0892, wR_2 = 0.1446	R_1 = 0.0363, wR_2 = 0.0647

7.4. Compounds from Chapter 4

7.4.1. $[Me_2HNBH_2(OPyrMe)][OTf]$

$[Ph_2Sb(OPyrMe)_4][OTf]_3$ (0.290 g, 0.250 mmol) was dissolved in 3 mL of DCM to which Me_2HNBH_3 (0.015g, 0.25 mmol) was added and left to stir for 1 hour to afford a yellow solution. The solution was concentrated under vacuum and placed in a freezer at -30 °C to yield colourless crystals. Yield: 89% (crystalline). ^{1}H NMR (300 MHz, CD_2CCl_2): δ_H = 8.62 (d, J(H,H) = 7.0 Hz, 2H, OPyrMe), 7.64 (d, J(H,H)

= 7.0 Hz, 2H, OPyrMe), 6.26 (s, broad, 1H, N-H), 2.60 (s, 3H, $OPyrCH_3$), 2.50 (d, J(H,H) = 5.6 Hz, 6H, NMe_2).

7.4.2. Reaction of $[Ph_2Sb(OPyrMe)_4][OTf]_3$ with dmap

$[Ph_2Sb(OPyrMe)_4][OTf]_3$ was dissolved in a variety of solvents (DCM, CH_3CN, DMSO, DMF, CH_2NO_2) to which solid dmap (4-4.5 equivalents) was added resulting in a pale yellow solution which turned dark red over 10 minutes of stirring in all cases. The reaction was halted at 10 min, 30 min, or 1 hour after which all volatiles were removed under vacuum to yield a red viscous oil. Attempts at several crystallization methods only resulted in colourless crystals identified as [H-dmap][OTf], dmap, OPyrMe, or $[CH_2(dmap)][OTf]_2$ when the reaction was performed in DCM. ^{1}H NMR has not aided in analysis as most resonances are very broad. Attempts to crystallize the antimony containing species are ongoing.

7.4.3. Reaction of $[Ph_2Sb(OPyrMe)_4][OTf]_3$ with PMe_3

$[Ph_2Sb(OPyrMe)_4][OTf]_3$ (0.287 g, 0.247 mmol) was dissolved in 5 mL of DCM to which PMe_3 (104 μL, 1.00 mmol) was added to afford a yellow solution which was left to stir for 5 min. All volatiles were removed under vacuum to furnish a colourless oil which was washed with 3x0.5 mL of Et_2O. The solid was redissolved in a minimum amount of DCM and placed in a freezer at -30 °C to furnish colourless crystals. Yield: 47% (crystalline). $^{31}P\{^1H\}$ NMR: (122 MHz, CD_2Cl_2): 21.6. ^{1}H NMR (300 MHz, CD_3CN): 8.71 (d, broad, J(H,H) = 5.0 Hz, 1H, Ar-H),

7.83 (m, 1H, Ar-H), 7.52 (m, 1H, Ar-H), 2.46 (s, 3H, CH_3), 2.09 (d, J(H,P) = 14.6 Hz, 9H, PMe_3).

7.4.4. Reaction of $[Ph_2Sb(OPyrMe)_4][OTf]_3$ with PEt_3

$[Ph_2Sb(OPyrMe)_4][OTf]_3$ (0.290 g, 0.250 mmol) was dissolved in 5 mL of DCM to which PEt_3 (147 μL, 1.00 mmol) was added to afford a yellow solution which was left to stir for 5 min. All volatiles were removed under vacuum to furnish a colourless oil which was washed with 3x0.5 mL of Et_2O. Attempts at crystallization have, as of yet, been unsuccessful. $^{31}P\{^1H\}$ NMR: (122 MHz, CD_2Cl_2): 35.22.

7.4.5. Reaction of $[Ph_2Sb(OPyrMe)_4][OTf]_3$ with P*n*Pr$_3$

$[Ph_2Sb(OPyrMe)_4][OTf]_3$ (0.290 g, 0.250 mmol) was dissolved in 5 mL of DCM to which P*n*Pr_3 (200 μL, 1.00 mmol) was added to afford a yellow solution which was left to stir for 5 min. All volatiles were removed under vacuum to furnish a colourless oil which was washed with 3x0.5 mL of Et_2O. Attempts at crystallization have, as of yet, been unsuccessful.$^{31}P\{^1H\}$ NMR: (122 MHz, CD_2Cl_2): 28.45.

7.4.6. Reaction of $[Ph_2Sb(OPyrMe)_4][OTf]_3$ with P*i*Pr$_3$

$[Ph_2Sb(OPyrMe)_4][OTf]_3$ (0.290 g, 0.250 mmol) was dissolved in 5 mL of DCM to which P*i*Pr_3 (200 μL, 1.00 mmol) was added to afford a yellow solution which was left to stir for 5 min. All volatiles were removed under vacuum to furnish a colourless oil which was washed with 3x0.5 mL of Et_2O.The oil was redissolved in a minimum amount of DCM, layered with Et_2O and placed in a freezer at -30 °C to

furnish a small amount of crystals. Yield: 3%. $^{31}P\{^{1}H\}$ NMR: (122 MHz, CD_3CN): 42.4.

7.4.7. Reaction of $[Ph_2Sb(OPyrMe)_4][OTf]_3$ with P*t*Bu$_3$

$[Ph_2Sb(OPyrMe)_4][OTf]_3$ (0.290 g, 0.250 mmol) was dissolved in 5 mL of DCM to which P*t*Bu$_3$ (0.116 g, 1.00 mmol) was added to afford a yellow solution which was left to stir for 5 min. All volatiles were removed under vacuum to furnish a colourless oil which was washed with 3x0.5 mL of Et_2O. Attempts at crystallization have, as of yet, been unsuccessful. $^{31}P\{^{1}H\}$ NMR spectroscopy indicates the majority of the reaction mixtures is unreacted P*t*Bu$_3$.

7.4.8. Reaction of $[Ph_2Sb(OPyrMe)_4][OTf]_3$ with PCy_3

$[Ph_2Sb(OPyrMe)_4][OTf]_3$ (0.290 g, 0.250 mmol) was dissolved in 5 mL of DCM to which P*t*Bu$_3$ (0.116 g, 1.00 mmol) was added to afford a yellow solution which was left to stir for 5 min. All volatiles were removed under vacuum to furnish a colourless oil which was washed with 3x0.5 mL of Et_2O. Attempts at crystallization have, as of yet, been unsuccessful. $^{31}P\{^{1}H\}$ NMR: (122 MHz, CD_2Cl_2): 33.5, 28.8.

7.4.9. Reaction of $[Ph_2Sb(OPyrMe)_4][OTf]_3$ with PPh_3

$[Ph_2Sb(OPyrMe)_4][OTf]_3$ (0.290 g, 0.250 mmol) was dissolved in 5 mL of DCM to which P*t*Bu$_3$ (0.116 g, 1.00 mmol) was added to afford a yellow solution which was left to stir for 5 min. All volatiles were removed under vacuum to furnish a colourless oil which was washed with 3x0.5 mL of Et_2O. Attempts at crystallization have, as of yet, been unsuccessful. $^{31}P\{^{1}H\}$ NMR: (122 MHz, CD_2Cl_2): 33.5, 28.8.

7.4.10. Arylation of 4-chlorobenzaldehyde

Reaction was carried out *via* a modified literature procedure.[94] [Me_3P(2,4-methylpyridine)][OTf] (0.048 g 0.15 mmol), 4-chlorobenzaldehyde (0.014 g, 0.10 mmol), and $CsCO_3$ (0.065 g, 0.20 mmol) were all added to a glass pressure reactor under nitrogen with 1 mL of THF. The reaction was heated to 70 °C and left to stir for 17 hours after which the reaction was quenched with 1 mL of 6M HCl. The resulting mixture was extracted with 3 x 1 mL of DCM and dried over $MgSO_4$. After filtration, the solvent was passed through a silica plug and solvent removed under vacuum to yield a colourless powder. Yield: 81%. ^{1}H NMR (300 MHz, CD_2CCl_2): δ_H = 7.30-7.15 (m, 8H, Ar), 5.80 (s, 1H, C-H), 2.30 (s, 3H, CH_3).

Table 7.4.1: Crystallographic details for compounds in Chapter 4

	$[CH_2(dmap)_2][OTf]_2$	$[Me_2HNBH_2OPyrMe][OTf]$	$[Me_3P(2\text{-}4\text{-}methylpyridine)][OTf]$
Empirical formula	$C_{17}H_{22}F_6N_4O_6S_2$	$C_9H_{16}BN_2O_4F_3S$	$C_{10}H_{21}NO_3F_3PS$
Formula weight	556.50	316.11	323.31
Temperature/K	273.15	173.15	273.15
Crystal system	monoclinic	monoclinic	monoclinic
Space group	C2/c	$P2_1/c$	$P2_1/n$
a/Å	19.6972(13)	10.2679(7)	7.9808(4)
b/Å	10.2612(7)	9.5215(7)	10.6995(6)
c/Å	11.3738(8)	15.3867(11)	16.3341(9)
α/°	90	90	90
β/°	91.2750(10)	107.1434(8)	95.101(2)
γ/°	90	90	90
Volume/$Å^3$	2298.3(3)	1437.46(18)	1389.25(13)
Z	4	4	4
$\rho_{calc}g/cm^3$	0.402	1.461	1.546
Radiation	MoKα (λ = 0.71073)	MoKα (λ = 0.71073)	MoKα (λ = 0.71073)
Goodness-of-fit on F^2	1.044	1.062	1.093
Final R indexes [I>=2σ (I)]	R_1 = 0.0401, wR_2 = 0.1055	R_1 = 0.0466, wR_2 = 0.1216	R_1 = 0.0456, wR_2 = 0.1104
Final R indexes [all data]	R_1 = 0.0477, wR_2 = 0.1124	R_1 = 0.0562, wR_2 = 0.1300	R_1 = 0.0546, wR_2 = 0.1141

Table 7.4.2: Crystallographic details for compounds in Chapter 4 (cont.)

	[*i*Pr$_3$P(2-4-methylpyridine)][OTf]	[Ph$_2$Sb(OPyrMe)$_3$(OH)][OTf]$_2$
Empirical formula	$C_{16}H_{27}F_3NO_3PS$	$C_{32}H_{32}F_6N_3O_{10}S_2Sb$
Formula weight	401.41	918.47
Temperature/K	273.15	273.15
Crystal system	triclinic	monoclinic
Space group	P-1	$P2_1/c$
a/Å	8.6699(3)	10.3732(5)
b/Å	10.2428(4)	22.4918(12)
c/Å	11.7099(4)	15.9378(8)
α/°	107.190(2)	90
β/°	96.169(2)	100.162(2)
γ/°	96.166(2)	90
Volume/Å^3	977.02(6)	3660.1(3)
Z	2	4
ρ_{calc}g/cm^3	1.364	1.667
Radiation	MoKα (λ = 0.71073)	MoKα (λ = 0.71073)
Goodness-of-fit on F^2	1.046	1.021
Final R indexes [I>=2σ (I)]	R_1 = 0.0366, wR_2 = 0.0944	R_1 = 0.0478, wR_2 = 0.1104
Final R indexes [all data]	R_1 = 0.0445, wR_2 = 0.0998	R_1 = 0.0877, wR_2 = 0.1276

7.5. Compounds from Chapter 5

7.5.1. Attempted synthesis of $PhSbCl_4$

Reaction was carried out *via* a modified literature procedure.[38] Ph_3Sb and $SbCl_3$ were combined in a 2:1 ratio to form a viscous, golden yellow melt which was left to stir at ambient temperature for three days after which DCM was added. 1 molar

equivalent of 1M SO_2Cl_2 in DCM was added dropwise to the stirred solution and left to stir for 24 hours resulting in a mixture of golden yellow liquid and a colourless powder. A minimum amount of DCM was added to dissolve the powder and this was stored in a freezer at -30 °C to yield colourless crystals which were determined to be Ph_2SbCl_3.

7.5.2. Attempted synthesis of $PhSbCl_2F_2$

$PhSbCl_2$ was dissolved in *ca.* 3 mL of CH_3CN and one equivalent of solid XeF_2 was added resulting in effervescence and a golden yellow solution which was stirred for 30 min. The solution was concentrated under vacuum and placed in a freezer at -25 °C to afford colourless crystals which were characterized as $Ph_2SbCl_3(NCCH_3)$.

7.5.3. Attempted synthesis of $PhSbF_4$

$PhSbCl_2$ was dissolved in *ca.* 3 mL of CH_3CN to which two equivalents of AgOTf was added and let to stir for 30 min in the dark. The *in situ* solution of $PhSb(OTf)_2$ was filtered and two equivalents of CsF added to the filtrate and left to stir for 1.5 hours. The solution was filtered and XeF_2 added to the filtrate containing $PhSbF_2$ to afford a clear, golden brown solution. ^{19}F NMR spectroscopy shows a variety of fluoride containing species with 12 resonances from -102 - -124 ppm.

7.5.4. [$PhPCl_3$][Cl] and $PhPCl_4$

$PhPCl_2$ (2.00 mL, 14.7 mmol) was dissolved in 10 mL of DCM to which solid PCl_5 (3.06 g, 14.7 mmol) was added portion-wise to afford a colourless mixture. After filtration, the solid was washed with cold 3x0.5 mL of DCM while all volatiles were removed from the filtrate under vacuum. Yield: 33% (precipitate, [$PhPCl_3$][Cl]. $^{31}P\{^1H\}$ NMR: (122 MHz, CD_3CN): δ_P = 98.8 ppm. Yield: 64% (filtrate, $PhPCl_4$). $^{31}P\{^1H\}$ NMR: (122 MHz, CD_2Cl_2): δ_P = -33.9 ppm.

7.5.5. $PhPF_4$

Reaction was carried out *via* a modified literature procedure.[104] SbF_3 (8.78 g 49.1 mmol) was added portion-wise to neat $PhPCl_2$ (5.00 mL, 36.8 mmol) in a 50 mL Schleck flask to afford a black slurry. The mixture was heated for 1 hour at 60 °C. $PhPF_4$ was isolated by distillation at ambient pressure with collection of material with boiling point of 134-136 °C. $PhPF_4$ can be stored in a glass vial for several weeks under inert atmosphere at -30 °C. Yield: 90%. $^{31}P\{^1H\}$ NMR: (122 MHz, CD_2Cl_2): δ_P = -50.29 (pentet, J(P,F) = 963.4 Hz). ^{19}F NMR: (282.54 MHz, CD_2Cl_2): δ_F = -54.57 (d, J(F,P) = 963.4 Hz).

7.5.6. [$PhPF_3(dmap)_2$][OTf]

$PhPF_4$ (0.092, 0.50 mmol) was dissolved in 3 mL of DCM to which solid dmap (0.122 g, 1.00 mmol) to form a colourless mixture after which TMSOTf (90.5 µL, 0.500 mmol) was added to form a clear, colourless solution which was left to stir for 1 hour. The solution was concentrated under vacuum and placed in a freezer at

– 30 °C to yield yellow crystals. Yield 27% (crystalline). $^{31}P\{^{1}H\}$ NMR: (122 MHz, CD_2Cl_2): δ_P = -141.9 (td, J(P,F) = 882 Hz, J(P,F) = 742 Hz). ^{19}F NMR: (282.54 MHz, CD_2Cl_2): δ_F = -78.9 (s, 3F, OTf), - 67.2 (dd, J(F,P) = 882 Hz, J(F,F) = 38 Hz, 2F), -38.1 (dt, J(F,P) = 742 Hz, J(F,F) = 38 Hz, 1F).

7.5.7. $PhPF_4(PMe_3)$

$PhPF_4$ (0.092, 0.50 mmol) was dissolved in 2 mL of DCM to which PMe_3 (52.0 µL, 0.500 mmol) to form a fuming colourless solution from which colourless crystals immediately started to grow. The mixture was left to sit for 16 hours after which the crystals were isolated. Yield 83% (crystalline). $^{31}P\{^{1}H\}$ NMR: (122 MHz, CD_2Cl_2): δ_P =broad 23-4 (apparent dt centered at 14.7, J(P,P) = 772 Hz, J(P,F) = 258 Hz, $PhPF_4$(**P**Me_3)), -135.4 (pentet of doublets, broad, J(P,P) = 778 Hz, J(P,F) = 947, Ph**P**F_4(PMe_3)). ^{19}F NMR: (282.54 MHz, CD_2Cl_2): δ_F = -39.1 (dd, broad, J(F,P) = 953 Hz, 222 Hz). ^{1}H NMR (300 MHz, CD_2Cl_2): δ_H = 7.47-7.36 (m, 2H, Ph), 7.12-7.08 (m, 3H, Ph), 1.5-0.5 (broad, PMe_3).

7.5.8. *t*$BuPF_2$

Solid SbF_3 (8.48 g 47.4 mmol) was added to solid *t*$BuPCl_2$ (5.00 g, 31.5 mmol) in a 50 mL Schleck flask and left to stir for 24 hours to afford a mixture of pale yellow liquid and orange solid. The liquid was isolated and analyzed to be *t*$BuPF_2$ with trace amounts of *t*$BuPF_4$. Yield: 60%. $^{31}P\{^{1}H\}$ NMR: (122 MHz, CD_2Cl_2): δ_P = 229 (t, J(P,F) = 1176 Hz, *t*$BuPF_2$), -30.4 (p, J(P,F) = 1033 Hz, *t*$BuPF_4$). ^{19}F NMR:

(282.54 MHz, CD_2Cl_2): δ_F = -109.9 (d. J(F,P) = 1175 Hz, *t*BuPF$_2$), -57.9 (d, J(F,P) = 1033 Hz, *t*BuPF$_4$).

7.5.9. Attempted synthesis of *t*BuPF$_4$

Route A: Solid SbF_3 and solid *t*BuPCl$_2$ were combined in a 1.5:1 ratio in a 50 mL Schleck flask and heated to 100 °C for 24 hours. The resulting yellow liquid was collected and determined to be *t*BuPF$_2$ with only trace amounts of *t*BuPF$_4$.

Route B: A solution of *t*BuPF$_2$ was added dropwise over the course of 2 hours to a solution of $SeCl_4$ in CH_3CN. The reaction is very exothermic and produces red fumes and a black precipitate. Upon complete addition of *t*BuF$_2$, a solution of SbF_3 was added dropwise over the course of 1 hour. Again, the reaction is highly exothermic. The resulting mixture was heated at 60 °C for 1 hour after which collection of *t*BuPF$_4$ was attempted by distillation. However, no distillate could be collected. $^{31}P\{^1H\}$ spectroscopy indicates many phosphorus containing species. Attempts to perform the reaction at -78 °C resulted in the same outcome.

Route C: Solid XeF_2 was added portion wise to *t*BuPF$_2$, however, immediately upon addition a small fire started. Attempts to perform the reaction at low temperature (at -30 °C and -78 °C) and low concentration also resulted in fires.

7.5.10. $SbCl_5$(dmap)

$SbCl_5$ (63.4 μL, 0.500 mmol) was dissolved in 3 mL DCM to which solid dmap (0.061 g, 0.50 mmol) was added to form an orange solution which was left to stir

for 1 hour. The solution was concentrated under vacuum and placed in a freezer at -25 °C to yield orange crystals. Yield: 67% (crystalline). M.P. = 167-170 °C. δ_H = 8.8 (borad, s, 2H, dmap), 7.6 (d, J(H,H) = 7.7 Hz, 2H, dmap), 3.2 (s, 6H, NMe_2). $^{13}C\{^1H\}$ (76 MHz, CD_3CN): 156.9, 142.9, 105.9, 40.6.

7.5.11. $SbCl_5$(OPyrMe)

$SbCl_5$ (63.4 μL, 0.500 mmol) was dissolved in 3 mL DCM to which solid OPyrMe (0.060 g, 0.55 mmol) was added to form a yellow mixture which was left to stir for 30 min. The yellow solid was isolated and washed with 3x0.5 mL of cold DCM. A small amount of solid was redissolved in a minimum amount of CH_3CN and crystals were obtained from vapour diffusion with Et_2O. Yield: 92% (powder). ^1H NMR (300 MHz, CD_3CN): δ_H = 8.5 (d, J(H,H) = 7.0 Hz, 2H, OPyrMe), 7.6 (d, J(H,H) = 7.0 Hz, 2H, OPyrMe), 2.6 (s, 3H, CH_3). $^{13}C\{^1H\}$ (76 MHz, CD_3CN): 154.0, 140.5, 129.1, 22.0.

7.5.12. Attempted synthesis of $[PCl_4(OPyrMe)_2][OTf]$

PCl_5 (0.104 g, 0.499 mmol) was dissolved in 3 mL of CH_3CN to which solid OPyrMe (0.109 g, 1.00 mmol) followed by AgOTf (0.129 g, 0.502 mmol) which was left to stir for 1 hour. The resulting yellow mixture was filtered and the filtrate analyzed by $^{31}P\{^1H\}$ spectroscopy to reveal several phosphorus containing species. Purification and isolation attempts are ongoing. $^{31}P\{^1H\}$ NMR: (122 MHz, CD_3CN): δ_P = -117.9 (s, 0.12 P), -130.6 (s, 0.14 P), -145.4 (s, 0.70 P), -157.6 (s, 1.00 P).

7.5.13. Attempted synthesis of $[PCl_3(OPyrMe)_3][OTf]_2$

PCl_5 (0.104 g, 0.499 mmol) was dissolved in 3 mL of CH_3CN to which solid OPyrMe (0.164 g, 1.50 mmol) followed by AgOTf (0.257 g, 1.00 mmol) which was left to stir for 1 hour. The resulting yellow-orange mixture was filtered and the filtrate analyzed by $^{31}P\{^1H\}$ spectroscopy to reveal several phosphorus containing species. Purification and isolation attempts are ongoing. $^{31}P\{^1H\}$ NMR: (122 MHz, CD_3CN): δ_P = -117.9 (s, 0.83 P), -119.2 (s, 0.11 P) -130.6 (s, 1.00 P), -145.4 (s, 0.20 P), -157.6 (s, 0.32 P).

7.5.14. Attempted synthesis of $[PCl_2(OPyrMe)_4][OTf]_3$

PCl_5 (0.104 g, 0.499 mmol) was dissolved in 3 mL of CH_3CN to which solid OPyrMe (0.218 g, 2.00 mmol) followed by AgOTf (0.385 g, 1.50 mmol) which was left to stir for 1 hour. The resulting orange-red mixture was filtered and the filtrate analyzed by $^{31}P\{^1H\}$ spectroscopy to reveal several phosphorus containing species. Purification and isolation attempts are ongoing. $^{31}P\{^1H\}$ NMR: (122 MHz, CD_3CN): δ_P = -4.1 (s, 0.26 P), -117.9 (s, 0.25 P), -119.2 (s, 0.20 P), -130.6 (s, 1.00 P).

7.5.15. Attempted synthesis of $[PCl(OPyrMe)_5][OTf]_4$

PCl_5 (0.104 g, 0.499 mmol) was dissolved in 3 mL of CH_3CN to which solid OPyrMe (0.273 g, 2.50 mmol) followed by AgOTf (0.512 g, 2.00 mmol) which was left to stir for 1 hour. The resulting red mixture was filtered and the filtrate analyzed by $^{31}P\{^1H\}$ spectroscopy to reveal several phosphorus containing species. Purification and isolation attempts are ongoing. $^{31}P\{^1H\}$ NMR: (122 MHz,

CD_3CN): δ_P = -4.1 (s, 0.22 P), -119.2 (s, 1.00 P), -123.4 (s, 0.32 P), -130.6 (s, 0.31 P).

7.5.16. Attempted synthesis of $[P(OPyrMe)_6][OTf]_5$

PCl_5 (0.104 g, 0.499 mmol) was dissolved in 3 mL of CH_3CN to which solid OPyrMe (0.327 g, 3.00 mmol) followed by AgOTf (0.644 g, 2.50 mmol) which was left to stir for 1 hour. The resulting red-brown mixture was filtered and the filtrate analyzed by $^{31}P\{^1H\}$ spectroscopy to reveal several phosphorus containing species. Purification and isolation attempts are ongoing. $^{31}P\{^1H\}$ NMR: (122 MHz, CD_3CN): δ_P = -4.1 (s, 0.67 P), -119.2 (s, 1.00 P), -123.4 (s, 0.13 P), -130.6 (s, 0.31 P).

7.5.17. Attempted synthesis of $[PCl_4(O_2\text{-bipy})][OTf]$

PCl_5 (0.104 g, 0.499 mmol) was dissolved in 3 mL of CH_3CN to which solid O_2-bipy (0.096 g, 0.50 mmol) followed by AgOTf (0.129 g, 0.502 mmol) which was left to stir for 1 hour. The resulting yellow mixture was filtered and the filtrate analyzed by $^{31}P\{^1H\}$ spectroscopy to reveal a single phosphorus containing species. Purification and isolation attempts are ongoing. $^{31}P\{^1H\}$ NMR: (122 MHz, CD_3CN): δ_P = -147.2.

7.5.18. Attempted synthesis of $[PCl_2(O_2\text{-bipy})_2][OTf]_3$

PCl_5 (0.104 g, 0.502 mmol) was dissolved in 3 mL of CH_3CN to which solid O_2-bipy (0.192 g, 1.00 mmol) followed by AgOTf (0.385 g, 1.50 mmol) which was left to stir for 1 hour. The resulting yellow mixture was filtered and the filtrate analyzed

by $^{31}P\{^{1}H\}$ spectroscopy to reveal several phosphorus containing species. Purification and isolation attempts are ongoing. $^{31}P\{^{1}H\}$ NMR: (122 MHz, CD_3CN): δ_P = -0.17 (s, 0.76 P), -74.9 (s, 0.12 P), -94. (s, 0.22 P), -99.4 (s, 0.31 P), -101.4 (s, 0.40), -125.6 (s, 1.00 P), -127.4 (s, 0.80 P).

7.5.19. Attempted synthesis of $[P(O_2\text{-bipy})_3][OTf]_5$

PCl_5 (0.104 g, 0.502 mmol) was dissolved in 3 mL of CH_3CN to which solid O_2-bipy (0.283 g, 1.50 mmol) followed by AgOTf (0.644 g, 2.50 mmol) which was left to stir for 1 hour. The resulting yellow-brown mixture was filtered and the filtrate analyzed by $^{31}P\{^{1}H\}$ spectroscopy to reveal several phosphorus containing species. Purification and isolation attempts are ongoing. $^{31}P\{^{1}H\}$ NMR: (122 MHz, CD_3CN): δ_P = -0.17 (s, 1.00 P), -74.9 (s, 0.13 P), -94. (s, 0.31 P), -99.4 (s, 0.29 P), -101.4 (s, 0.50), -125.6 (s, 0.67 P), -127.4 (s, 0.81 P).

7.5.20. Crystallographic Information

Table 7.5.1: Crystallographic details for compounds in Chapter 5

	$[PhPF_3(dmap)_2][OTf]$	$SbCl_5(OPyrMe)$	$SbCl_5(dmap)$
Empirical formula	$C_{23}H_{29}Cl_4F_6N_4O_3PS$	$C_6H_7NOCl_5Sb$	$C_7H_{10}Cl_5N_2Sb$
Formula weight	728.33	408.13	421.17
Temperature/K	173.15	193.15	188.15
Crystal system	monoclinic	orthorhombic	monoclinic
Space group	C2/c	$P2_12_12_1$	$P2_1/c$
a/Å	17.3865(3)	7.5170(3)	9.9892(14)
b/Å	12.0616(2)	8.2302(4)	11.4091(16)
c/Å	17.1043(3)	20.1934(9)	12.7875(18)
α/°	90	90	90
β/°	116.6925(8)	90	110.179(2)
γ/°	90	90	90
Volume/$Å^3$	3204.67(10)	1249.29(10)	1367.9(3)
Z	4	4	4
$\rho_{calc}g/cm^3$	1.510	2.170	2.045
Radiation	CuKα (λ = 1.54178)	MoKα (λ = 0.71073)	MoKα (λ = 0.71073)
Goodness-of-fit on F^2	1.029	1.048	1.119
Final R indexes [I>=2σ (I)]	R_1 = 0.0474, wR_2 = 0.1272	R_1 = 0.0213, wR_2 = 0.0518	R_1 = 0.0162, wR_2 = 0.0416
Final R indexes [all data]	R_1 = 0.0493, wR_2 = 0.1296	R_1 = 0.0224, wR_2 = 0.0525	R_1 = 0.0180, wR_2 = 0.0427

Table 7.5.2: Crystallographic details for compounds in Chapter 5 (cont.)

	$PhPF_4(PMe)_3$
Empirical formula	$C_9H_{14}F_4P_2$
Formula weight	260.14
Temperature/K	173.15
Crystal system	orthorhombic
Space group	$Pna2_1$
a/Å	15.3690(6)
b/Å	6.5078(2)
c/Å	11.6675(4)
α/°	90
β/°	90
γ/°	90
Volume/Å^3	1166.96(7)
Z	4
ρ_{calc}g/cm^3	1.481
Radiation	CuKα (λ = 1.54178)
Goodness-of-fit on F^2	1.070
Final R indexes [I>=2σ (I)]	R_1 = 0.0203, wR_2 = 0.0528
Final R indexes [all data]	R_1 = 0.0204, wR_2 = 0.0530

Bibliography

[1] D. Seyferth, *Organometallics* **2001**, *20*, 1488–1498.

[2] C. Jones, G. A. Koutsantonis, *Aust. J. Chem.* **2013**, *66*, 1163–1170.

[3] A. H. Cowley, *J. Organomet. Chem.* **2000**, *600*, 168–173.

[4] K. S. Pitzer, *J. Am. Chem. Soc.* **1948**, *70*, 2140–2145.

[5] R. S. Mulliken, *J. Am. Chem. Soc.* **1950**, *72*, 4493–4503.

[6] R. West, M. J. Fink, J. Michl, *Science.* **1981**, *214*, 1343–1344.

[7] M. Yoshifuji, I. Shima, N. Inamoto, K. Hirotsu, T. Higuchi, *J. Am. Chem. Soc.* **1981**, *103*, 4587–4589.

[8] G. Becker, G. Gresser, W. Uhl, *Z. Naturforsch* **1981**, *36b*, 16–19.

[9] A. G. Brook, F. Abdesaken, B. Gutekunst, G. Gutekunst, R. K. Kallury, *J. Chem. Soc. Chem. Commun.* **1981**, 191–192.

[10] T. A. Engesser, M. R. Lichtenthaler, M. Schleep, I. Krossing, *Chem. Soc. Rev.* **2016**, *45*, 789–899.

[11] B. D. Ellis, C. L. B. Macdonald, *Coord. Chem. Rev.* **2007**, *251*, 936–973.

[12] C. Jones, A. Stasch, in *Alkaline-Earth Met. Compd. Top. Organomet. Chem.* **2013**, pp. 285–381.

[13] R. C. Fisher, P. P. Power, *Chem. Rev.* **2010**, *110*, 3877–3923.

[14] H. Schnöckel, *Chem. Rev.* **2010**, *110*, 4125–4163.

[15] P. P. Power, *Nature* **2010**, *463*, 171–177.

[16] H. Braunschweig, R. D. Dewhurst, F. Hupp, M. Nutz, K. Radacki, C. W. Tate, A. Vargas, Q. Ye, *Nature* **2015**, *522*, 327–330.

[17] G. H. Spikes, J. C. Fettinger, P. P. Power, *J. Am. Chem. Soc.* **2005**, *127*, 12232–

12233.

[18] Y. Peng, M. Brynda, B. D. Ellis, J. C. Fettinger, E. Rivard, P. P. Power, *Chem. Commun.* **2008**, 6042.

[19] Z. Zhu, X. Wang, Y. Peng, H. Lei, J. C. Fettinger, E. Rivard, P. P. Power, *Angew. Chemie. Int. Ed.* **2009**, *48*, 2031–2034.

[20] G. C. Welch, R. R. San Juan, J. D. Masuda, D. W. Stephan, *Science* **2006**, *314*, 1124–6.

[21] D. Himmel, I. Krossing, A. Schnepf, *Angew. Chem. Int. Ed.* **2014**, *53*, 370–374.

[22] G. Frenking, *Angew. Chem. Int. Ed.* **2014**, *53*, 6040–6046.

[23] D. Himmel, I. Krossing, A. Schnepf, *Angew. Chem. Int. Ed.* **2014**, *53*, 6047–6048.

[24] J. R. Rumble, in *CRC Handbook of Chemistry and Physics, 98th Ed.*, **2018**.

[25] R. Jambor, L. Dostal, *Organometallic Pincer Chemistry*, **2013**.

[26] C. Jones, *Coord. Chem. Rev.* **2010**, *254*, 1273–1289.

[27] J. L. Dutton, P. J. Ragogna, *Coord. Chem. Rev.* **2011**, *255*, 1414–1425.

[28] P. A. Gray, N. Burford, *Coord. Chem. Rev.* **2016**, *324*, 1–16.

[29] N. Menschutkin, *Z. Phys. Chem.* **1890**, *5*, 589.

[30] I. S. Ke, M. Myahkostupov, F. N. Castellano, F. P. Gabbaï, *J. Am. Chem. Soc.* **2012**, *134*, 15309–15311.

[31] M. Hirai, M. Myahkostupov, F. N. Castellano, F. P. Gabbaï, *Organometallics* **2016**, *35*, 1854–1860.

[32] M. Hirai, F. P. Gabbaï, *Chem. Sci.* **2014**, *5*, 1886–1893.

[33] A. Kumar, M. Yang, M. Kim, F. P. Gabbaï, M. H. Lee, *Organometallics* **2017**, *36*, 4901–4907.

[34] A. M. Christianson, F. P. Gabbaï, *Chem. Commun.* **2017**, *53*, 2471–2474.

[35] A. P. M. Robertson, N. Burford, R. McDonald, M. J. Ferguson, *Angew. Chem. Int. Ed.* **2014**, *53*, 3480–3483.

[36] A. P. M. Robertson, S. S. Chitnis, H. a. Jenkins, R. McDonald, M. J. Ferguson, N. Burford, *Chem. A Eur. J.* **2015**, *21*, 7902–7913.

[37] Yang, M.; Gabbaï, F. P. *Inorg. Chem.* **2017**, *56* (15), 8644–8650.

[38] D. M. Nunn, Michael, Sowerby, Brian D. Wesolek, *J. Organomet. Chem.* **1983**, *251*, C45–C46.

[39] A. P. M. Robertson, S. S. Chitnis, H. A. Jenkins, R. McDonald, M. J. Ferguson, N. Burford, *Chem. Eur. J.* **2015**, *21*, 7902–7913.

[40] K. Singhal, R. Kant, R. N. P. Yadav, P. C. Pandey, P. Raj, *Synth. React. Inorg. Met. Chem.* **2004**, *34*, 459–468.

[41] M. J. Begley, D. B. Sowerby, *Acta Crystallogr. Sect. C Cryst. Struct. Commun.* **1993**, *49*, 1044–1046.

[42] A. Polynova, T. N., Porai-Koshits, M., *Zhurnal Strukt. Khimii* **1967**, *8*, 112.

[43] V. I. Zdanovich, D. N. Kursanov, V. N. Setkina, *J. Organomet. Chem.* **1972**, *37*, 297–301.

[44] V. Gutmann, *Coord. Chem. Rev.* **1976**, *18*, 225–255.

[45] U. Mayer, V. Gutmann, W. Gerger, *Monatshefte für Chemie* **1975**, *106*, 1235–1257.

[46] I. B. Sivaev, V. I. Bregadze, *Coord. Chem. Rev.* **2014**, *270–271*, 75-88.

[47] D. G. Hendershot, J. C. Pazik, C. George, A. D. Berry, *Organometallics* **1992**, *11*, 2163–2168.

[48] S. S. Chitnis, N. Burford, J. J. Weigand, R. McDonald, *Angew. Chem. Int. Ed. Engl.* **2015**, *54*, 7828–32.

[49] S. S. Chitnis, A. P. M. Robertson, N. Burford, J. J. Weigand, R. Fischer, *Chem. Sci.* **2015**, *6*, 2559–2574.

[50] J. Bader, B. Neumann, H.-G. Stammler, N. Ignat'ev, B. Hoge, *Chem. Eur. J.* **2018**, *24*, 6975–6982.

[51] R. Kleinmaier, S. Arenz, A. Karim, A. C. C. Carlsson, M. Erdélyi, *Magn. Reson. Chem.* **2013**, *51*, 46–53.

[52] V. H. L. Wong, A. J. P. White, T. S. A. Hor, K. K. Hii, *Adv. Synth. Catal.* **2015**, *357*, 2485–2491.

[53] M. Lehmann, A. Schulz, A. Villinger, *Eur. J. Inorg. Chem.* **2012**, 822–832.

[54] C. Hering, J. Rothe, A. Schulz, A. Villinger, *Inorg. Chem.* **2013**, *52*, 7781–7790.

[55] P. Pyykkö, M. Atsumi, *Chem. Eur. J.* **2009**, *15*, 186–197.

[56] A. P. M. Robertson, P. A. Gray, N. Burford, *Angew. Chem. Int. Ed.* **2014**, *53*, 6050–6069.

[57] P. Pyykko, M. Atsumi, *Chem. Eur. J.* **2009**, *15*, 186–197.

[58] M. Mantina, A. C. Chamberlin, R. Valero, C. J. Cramer, D. G. Truhlar, *J. Phys. Chem. A.* **2009**, *113*, 5806–5812.

[59] S. S. Chitnis, N. Burford, R. McDonald, M. J. Ferguson, *Inorg. Chem.* **2014**, *53*, 5359–5372.

[60] K. L. Bamford, A. P. M. Robertson, H. A. Jenkins, B. O. Patrick, N. Burford, *Can. J. Chem.* **2015**, *379*, 375–379.

[61] T. Chu, G. I. Nikonov, *Chem. Rev.* **2018**, *118*, 3608–3680.

[62] S. S. Chitnis, A. P. M. Robertson, N. Burford, B. O. Patrick, R. Mcdonald, M. J. Ferguson, *Chem. Sci.* **2015**, *6*, 6545–6555.

[63] A. Swidan, R. Suter, C. L. B. Macdonald, N. Burford, *Chem. Sci.* **2018**, DOI: 10.1039/c8sc01682h.

[64] J. M. Bayne, D. W. Stephan, *Chem. Soc. Rev.* **2015**, *45*, 765–774.

[65] J. Carreras, M. Patil, W. Thiel, M. Alcarazo, *J. Am. Chem. Soc.* **2012**, *134*, 16753–16758.

[66] A. R. J. Genge, N. J. Hill, W. Levason, G. Reid, *J. Chem. Soc. Dalon Trans.* **2001**, 1007–1012.

[67] N. Burford, M. D'Eon, P. J. Ragogna, R. McDonald, M. J. Ferguson, *Inorg. Chem.* **2004**, *43*, 734–738.

[68] W. Clegg, M. R. J. Elsegood, N. C. Norman, N. L. Pickett, *J. Chem. Soc., Dalton Trans* **1994**, 1753–1757.

[69] J. T. Price, M. Lui, N. D. Jones, P. J. Ragogna, *Inorg. Chem.* **2011**, *50*, 12810–12817.

[70] J. W. Wielandt, N. L. Kilah, A. C. Willis, S. B. Wild, *Chem. Commun.* **2006**, 3679–3680.

[71] N. L. Kilah, S. Petrie, R. Stranger, J. W. Wielandt, A. C. Willis, S. B. Wild, *Organometallics* **2007**, *26*, 6106–6113.

[72] S. S. Chitnis, B. Peters, E. Conrad, N. Burford, R. McDonald, M. J. Ferguson, *Chem. Commun. (Camb).* **2011**, *47*, 12331–3.

[73] E. H. Lizarazo-Jaimes, P. G. Reis, F. M. Bezerra, B. L. Rodrigues, R. L. Monte-Neto, M. N. Melo, F. Frézard, C. Demicheli, *J. Inorg. Biochem.* **2014**, *132*, 30–36.

[74] A. Lipka, H. Wunderlich, *Zeitschrift fur Naturforschung, B Chem. Sci.* **1980**, 1548–1551.

[75] M. Nunn, M. J. Begley, D. B. Sowerby, I. Haiduc, *Polyhedron* **1996**, *15*, 3167–3174.

[76] H. Althaus, H. J. Breunig, E. Lork, *Organometallics* **2001**, *20*, 586–589.

[77] A. Lipka, *Zeitschrift fur Naturforschung, B Chem. Sci.* **1983**, *38*, 341.

[78] S. S. Chitnis, N. Burford, M. J. Ferguson, *Angew. Chemie Int. Ed.* **2013**, *52*, 2042–2045.

[79] S. S. Chitnis, A. P. M. Robertson, N. Burford, B. O. Patrick, R. McDonald, M. J. Ferguson, *Chem. Sci.* **2015**, 6545–6555.

[80] R. Suter, H. Sinclair, N. Burford, *Dalton Trans.* **2017**, *46*, 7681–7685.

[81] P. P. Power, *Chem. Rev.* **1999**, *99*, 3463–3504.

[82] Y. Mizuhata, T. Sasamori, N. Tokitoh., *Chem. Rev.* **2009**, *109*, 3479–3511.

[83] E. Welz, I. Krummenacher, B. Engels, H. Braunschweig, *Science.* **2018**, *900*, 896–900.

[84] G. Linti, H. Schnöckel, *Low Valent Aluminum and Gallium Compounds - Structural Variety and Coordination Modes to Transition Metal Fragments*, **2000**.

[85] R. G. Hicks, *Org. Biomol. Chem.* **2007**, *5*, 1321.

[86] P. P. Power, *Chem. Rev.* **2003**, *103*, 789–809.

[87] L. Balázs, H. J. Breunig, I. Ghesner, E. Lork, *J. Organometalic Chem.* **2002**, *648*, 33–38.

[88] G. Ferguson, *Acta Crystallogr. Sect. C Cryst. Struct. Commun.* **1987**, *C43*, 2078–2081.

[89] S. Pankaj, N. Rosas, G. Espinosa-Pérez, A. Cabrera, *Acta Crystallogr. Sect. C Cryst. Struct. Commun.* **1996**, *C52*, 889–891.

[90] H. J. Breunig, E. Lork, O. Moldovan, C. I. Raţ, *J. Organomet. Chem.* **2008**, *693*, 2527–2534.

[91] J. A. Bilbrey, A. H. Kazez, J. Locklin, W. D. Allen, *J. Comput. Chem.* **2013**, *34*, 1189–1197.

[92] M. C. Hilton, R. D. Dolewski, A. McNally, *J. Am. Chem. Soc.* **2016**, *138*, 13806–13809.

[93] A. McNally, in *101st CCCE - Sel. Funct. Pyridines, Diazines Pharm.*, **2018**.

[94] Z. Deng, J. H. Lin, J. C. Xiao, *Nat. Commun.* **2016**, *7*, 1–8.

[95] X. Zhang, A. McNally, *Angew. Chem. Int. Ed.* **2017**, *56*, 9833–9836.

[96] R. G. Anderson, B. M. Jett, A. McNally, *Tetrahedron* **2018**, *74*, 3129–3136.

[97] C. Patel, M. Mohnike, M. C. Hilton, A. McNally, *Org. Lett.* **2018**, *20*, DOI acs.orglett.8b00813.

[98] R. D. Dolewski, P. J. Fricke, A. McNally, **2018**, DOI 10.1021/jacs.8b04530.

[99] J. L. Koniarczyk, D. Hesk, A. Overgard, I. W. Davies, A. McNally, *J. Am. Chem. Soc.* **2018**, *140*, 1990–1993.

[100] E. Vitaku, D. T. Smith, J. T. Njardarson, *J. Med. Chem.* **2014**, *57*, 10257–10274.

[101] B. Bone, Stephen, P. Sowerby, D., *J. Chem. Soc., Dalton Trans* **1979**, 1430–1433.

[102] J. C. S. Dalton, B. K. Dillon, R. N. Reeve, T. C. Waddington, **1977**, 1318–1323.

[103] Y.-R. Luo, *Handbook of Bond Dissociation Energies in Organic Compounds*, **2002**.

[104] R. Schmutzler, *Inorg. Chem.* **1963**, *473*, 410–415.

[105] W. S. Sheldrick, *J. Chem. Soc.*, *Dalton Trans* **1974**, 1402.

[106] A. P. M. Robertson, S. S. Chitnis, S. Chhina, H. J. Cortes S., B. O. Patrick, H. A. Jenkins, N. Burford, *Can. J. Chem.* **2016**, *94*, 424–429.

[107] B. M. Fild, R. Schmutzler, *J. Chem. Soc. A* **1970**, 2359–2364.

[108] H. D. Hausen, W. Schwarz, G. Rajca, J. Weidlein, *Zeitschrift fur Naturforschung ,B Chemical Sci.* **1986**, *41*, 1223.

[109] SAINT: Version 8.34A Bruker AXS Inc., Madison, Wisconsin, USA. (1997-2013).

[110] SADABS: Bruker AXS Inc., Madison, Wisconsin, USA. (1997-2012).

[111] G. M. Sheldrick, *Acta Cryst* **2008**, *A64*, 112–122.

[112] G. M. Sheldrick, *Acta Cryst* **2008**, *A64*, 112–122.